Aus dem Institut für medizinische Physik und Biophysik der Medizinischen Fakultät Charité – Universitätsmedizin Berlin

Dissertation

The quaternary structure of rhodopsin and its implications for rhodopsin function.

zur Erlangung des akademischen Grades
Doctor medicinae (Dr. med.)

vorgelegt der Medizinischen Fakultät
Charité – Universitätsmedizin Berlin

von

Verena Gramse

aus Potsdam

Gutachter: 1. Priv.-Doz. Dr. O. Ernst

2. Prof. Dr. P. Hegemann

3. Prof. Dr. med. Mi. Schaefer

Datum der Disputation: 19.5.2008

Parts of the results of this thesis were published in:

Ernst, O.*, Gramse, V.*, Kolbe, M.*, Hofmann, K.P., Heck, M., "Monomeric GPCR rhodopsin in solution activates its G protein transducin at the diffusion limit." Proc Natl Acad Sci U S A, June 26, 2007, vol.104, no.26, p.10859-10864.

*these authors contributed equally

ABSTRACT

The present work focuses on the quaternary structure of rhodopsin and its possible implications for the function of the receptor as a light transducer. Rhodopsin is a prototypical G protein-coupled receptor (GPCR) that is found in high concentrations in the discs of the outer segment of rod photoreceptor cells. Its physiological function is the transduction of light into a biological relevant signal under dim light conditions.

There is growing evidence that GPCRs form and might even function as oligomers in membranes (Milligan, Ramsay et al. 2003; Milligan 2006). Oligomers were also reported for rhodopsin by atomic force microscopy (Fotiadis, Liang et al. 2003), chemical cross-linking (Jastrzebska, Maeda et al. 2004; Medina, Perdomo et al. 2004; Jastrzebska, Fotiadis et al. 2006), blue native electrophoresis (Jastrzebska, Maeda et al. 2004) and FRET studies (Kota, Reeves et al. 2006; Mansoor, Palczewski et al. 2006). This view is challenged by early biophysical and biochemical studies suggesting that rhodopsin is monomeric (Cone 1972; Poo and Cone 1974; Chabre 1975; Chabre and le Maire 2005). However, it remains to be elucidated whether its quaternary structure is of any physiological significance for visual signal transduction.

In the present thesis, I investigated rhodopsin's propensity to oligomerize in the plasma membrane of HEK293 and COS-1 cells using bimolecular fluorescence complementation (BiFC) and fluorescence resonance energy transfer (FRET) as techniques. As possible interaction domains for rhodopsin oligomers, helices IV and V (Liang, Fotiadis et al. 2003) as well as helices I, II and VIII (Salom, Lodowski et al. 2006) have been proposed so far. In my thesis, I also tried to verify possible interaction domains using FRET competition experiments. Furthermore, I was interested in investigating whether a change in rhodopsin's quaternary structure alters its ability of binding or activating its G protein transducin (G_t). For this question I used purified, solubilized rhodopsin and rhodopsin fusion proteins in 0.01% DM to measure FRET as well as G_t activation rates.

I found that BiFC yields fluorescing cells upon coexpression of several unrelated membrane and non-membrane proteins with opsin. This suggests that it is not a suitable test for specific membrane protein interaction. Furthermore, I found that opsin shows very high FRET efficiency in the plasma membranes of HEK293 and COS-1 cells. The FRET competition data confirms the idea of helix IV/V as part of the oligomerization interface. When detergent is added to purified membranes as well as to HEK293 cells *in vivo*, FRET efficiency decreases significantly. In

purified, solubilized samples (0.01% DM), no FRET could be measured at all. Under the chosen experimental conditions, solubilized rhodopsin therefore appears to be present as a monomer. Nevertheless, measurements of G_t activation revealed that monomeric rhodopsin efficiently activates its cognate G protein at high rates (V_{max} of 40 G_t/s, K_M of 3.3 µM). Monomeric rhodopsin therefore works with a specificity constant of $1.3 \cdot 10^{-7} M^{-1} s^{-1}$, which is close to the diffusion limit (Berg and von Hippel 1985) and can thus be called a 'perfect enzyme'.

ZUSAMMENFASSUNG

In der hier vorliegenden Doktorarbeit wurde die Quartärstruktur von Rhodopsin und ihre Rolle für die Weiterleitung von Lichtsignalen an das G-Protein Transducin untersucht. Rhodopsin ist ein prototypischer G-Protein-gekoppelter Rezeptor (GPCR), der in hohen Konzentrationen in den Membranen der Disks der Stäbchenaußensegmente vorkommt. Seine physiologische Funktion ist die Übersetzung von Licht in ein biologisch verwertbares Signal unter Dämmerlicht Bedingungen.

Es gibt zunehmend Hinweise, dass GPCRs oligomere Strukturen bilden, die möglicherweise auch ihre funktionellen Einheit darstellen (Milligan, Ramsay et al. 2003; Milligan 2006). Mit Hilfe von Techniken wie *atomic force microscopy* (Fotiadis, Liang et al. 2003), *cross-linking* (Jastrzebska, Maeda et al. 2004; Medina, Perdomo et al. 2004; Jastrzebska, Fotiadis et al. 2006), *blue native gel electrophoresis* (Jastrzebska, Maeda et al. 2004) und *fluorescence resonance energy transfer* (FRET) (Kota, Reeves et al. 2006; Mansoor, Palczewski et al. 2006) wurden auch für Rhodopsin Oligomere als Quartärstruktur postuliert. Diese Experimente stehen aber im Widerspruch zu Resultaten aus früheren biophysikalischen und biochemischen Experimenten, in denen keinerlei Evidenz für eine dimere/oligomere Quartärstruktur zu finden war (Cone 1972, Poo und Cone 1974; Chabre 1975; Chabre und le Maire 2005). Weiterhin bleibt zudem unklar, ob eine Oligomerisierung relevant für die physiologische Funktion von Rhodopsin als Licht Rezeptor *in vivo* ist.

In der hier präsentierten Arbeit wurde die Dimerisierung von Rhodopsin in der Plasmamembran von HEK293 und COS-1 Zellen mit Hilfe von *bimolecular fluorescence complementation assay* (BiFC) und FRET untersucht. Als mögliche Interaktionsdomainen der Oligomerbildung von Rhodopsin wurden bisher Helices IV und V (Liang, Fotiadis et al. 2003) als auch Helices I, II, und VII (Salom, Lodowski et al. 2006) postuliert. In der vorliegenden Arbeit wurden mögliche Interaktionsdomainen der Rhodopsin Oligomerbildung mit Hilfe von FRET untersucht. Weiterhin sollte untersucht werden, ob eine Änderung der Quartärstruktur auch zu einer Änderung in der Katalyseeffizienz der G-Protein Aktivierung führt. Für diese Frage wurde solubilisiertes Rhodopsin und entsprechende Rhodopsin-Fluorophor Fusionsproteine in 0,01% DM präpariert, um G-Protein Aktivierungsraten als auch FRET zu messen.

Es zeigt sich, dass die Koexpression von komplementären Opsin-BiFC Fusionsproteinen zu einem starken Fluoreszenzsignal *in vivo* führte. Die Tatsache, das auch die Koexpression von

verschiedener anderer -membranständiger als auch zytoplasmatischer- Proteine als BiFC Konstrukte mit einem komplementären Opsin-BiFC Konstrukt Fluoreszenz zeigten, legt allerdings nahe, dass BiFC kein spezifischer Marker für intermolekulare Interaktion von Membranproteinen ist.

FRET Experimente mit geeigneten Opsin-Fluorophor Fusionsproteinen ergaben eine hohe FRET Effizienz in der Plasmamembran von transfizierten HEK293 and COS-1 Zellen. Die FRET Kompetitionsexperimente unterstrichen weiterhin die Theorie, dass Helices IV and V eine Rolle bei der Oligomerisierung spielen. Wenn das Detergens Dodecylmaltosid (DM) zu gereinigten COS-1 Membranen oder HEK293 Zellen *in vivo* gegeben wurde, verringerte sich die FRET Effizienz signifikant. In aufgereinigten, solubilisierten Proben (0,01% DM) konnte überhaupt kein FRET Signal mehr gemessen werden. Daraus kann geschlussfolgert werden, dass Rhodopsin in 0,01% DM als Monomer vorliegt. Unter denselben experimentellen Bedingungen wurde auch die katalytische G-Protein Aktivierungskapazität von gereinigtem Rhodopsin bestimmt.

Es zeigte sich, dass monomeres Rhodopsin sehr effizient in der Lage ist Transducin zu aktivieren (V_{max} = 40 G_t/s, K_M = 3,3 µM). Daraus folgt, dass monomeres Rhodopsin mit einer Spezifizitätskonstante von $1{,}3 \cdot 10^{-7}$ $M^{-1}s^{-1}$ nahe am theoretisch möglichen Diffusionslimit arbeitet, (Berg und von Hippel 1985) und somit als so genanntes ‚perfektes Enzym' beschrieben werden kann.

CONTENTS

1 FIGURES

2 ABBREVIATIONS

Aa	amino acid
AFP	auto fluorescent proteins
BiFC	bimolecular fluorescence complementation
BTP	1,3-bis-[tris(hydroxymethyl)methylamine]-propane
DM	n-dodecyl-β-D-maltosid
DEAE-dextran	diethylamine-dextran
DMEM	Dulbecco Modified Eagle's medium
DTT	1,4-dithio-DL-threitol; (reducing agent)
ECFP	enhanced cyan fluorescent protein
EDTA	ethylenediaminetetraacetic acid
EGFP	enhanced green fluorescent protein
EYFP	enhanced yellow fluorescent protein
FCS	fetal calf serum
FRET	fluorescence resonance energy transfer
GDP, GTP, (c)GMP	guanosine-5'diphosphate, guanosine-5'triphosphate, (cyclic) guanosine-5'monophosphate
GPCR	G protein-coupled receptor
G protein	guanine-nucleotide binding regulatory protein
G_t	G protein transducin
$G_t\beta\gamma$	βγ-subunit of G_t
GTPγS	guanosine-5'[γ-thio]-triphospate, (non-hydrolysable)
$G_t\alpha$	A-subunit of G_t
kDa	kilo Dalton
LB	Luria Bertani broth
Meta-I/Meta-II	Metarhodopsin-I, Metarhodopsin-II
OD	optical density
PBS	phosphate buffered saline
PDE	cGMP-phosphodiesterase
PMSF	phenylmethanesulphonylfluoride (serine protease inhibitor)
R, R*	rhodopsin, active form of rhodopsin

R-ECFP	rhodopsin fused with ECFP
RIS	rod inner segment
ROS	rod outer segment
R-venus	rhodopsin fused with venus
Tris-HCl	tris(hydroxymethyl)aminomethane
w/v	weight/volume

3 INTRODUCTION

3.1 Vision

Rods and cones constitute the light sensitive cell layer of the retina. At their basal end they form synapses with bipolar cells, and at their apical end they are connected to pigment epithelia cells. Cones are responsible for color vision and are present primarily in the *fovea centralis*, the area of most precise vision. The density of cones drops rapidly with a diameter of 5 mm around the *fovea*. The rest of the retina is dominated by rods (30:1 at their peak density of 160000 m^{-2}), which constitute about 95% of all photoreceptor cells. Rod cells are responsible for vision under dim light conditions (scotopic vision). The following work will focus exclusively on rods and their photoreceptor rhodopsin. However, photoreceptors found in cones are closely related to rhodopsin, thus most probably they share the same functional mechanisms.

A simplified outline of the visual pathways will be given in the following chapter, more extensive coverage is provided by several excellent textbooks on the visual system (e.g. Rodieck 1998).

Light entering the eye is focused by the lens and the cornea to the back of the eyeball. Its innermost layer is constituted by the retina, which contains the first three neuronal cell layers of the visual pathway as well as pigment epithelia cells and different glial cells (Figure 1). Entering light encounters light-sensitive photoreceptor cells of the retina, triggering a cascade of enzymatic reactions that finally leads to a hyperpolarization of the photoreceptor cell. Photoreceptor cells are primary sensory cells and form synapses onto bipolar cells. Hyperpolarization of the photoreceptor cell results in a graded decrease of inhibitory glutamate exocytosis into the synaptic cleft with its bipolar cell. The resulting depolarization of the (on-midget) bipolar cells leads to higher frequency firing, which is detected by the corresponding ganglion cells. At this stage, a gradual change is encoded into a change of firing frequency. The visual information leaves the eyeball and enters the brain in the bundled axons of ganglion cells, the optic nerve. Until this point, the initial light signal has already been integrated to improve signal contrast and to enable complex analysis of movements, pattern and color further upstream. The gain of contrast is achieved by the diverging pathways of on- and off-midget cells and the lateral forward inhibition of horizontal and amacrine cells of the retina.

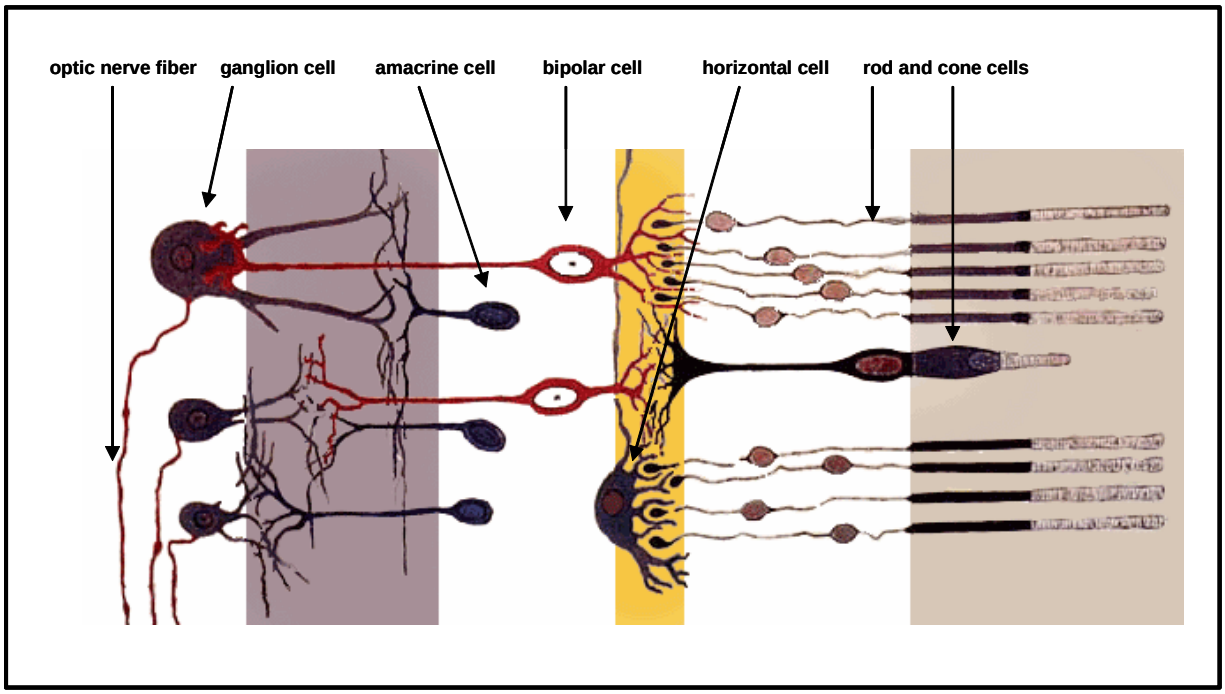

Figure 1: Cell layers of the retina

Figure adapted from Ramón y Cajal, “Structure of the Mammalian Retina”, 1900.

Fibers of the optic nerve coming from the nasal parts of the retina cross sides at the optic chiasma and join uncrossed fibers from the temporal part of the ipsilateral retina (Figure 2). The crossing of nasal fibers leads to a contralateral representation of the visual fields in the brain and is also necessary for spatial vision. From the optic chiasm, information travels via the optic tract to the lateral geniculate body of the thalamus, where ganglion cell synapse onto the fourth neurons of the visual pathway. These thalamic neurons project to the primary visual cortex in the back of the occipital lobe. In the primary visual cortex as well as in the adjacent secondary visual cortex and other related areas, visual information is further processed. This enables us to establish an internal neuronal correlate of our visual environment and to recognize and interpret what we are seeing. Apart from the main visual information processing pathway that was just described, visual information is also projected directly to the brainstem for coordinative function of the oculomotoric and vestibular system.

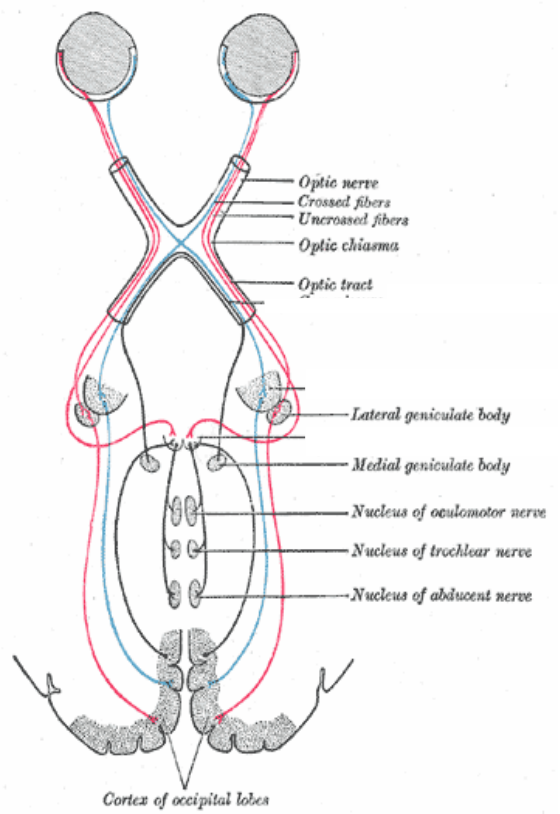

Figure 2: Visual pathway

Figure adapted from 'Gray's Anatomy of the Human Body' (online edition of 20th U.S. edition).

3.2 Photoreceptor cells

Rods are very long stretched cells that have a peculiar but highly ordered structure (Figure 3).The cells are divided by a cilium into the rod inner segment (RIS) and the rod outer segment (ROS). The RIS contains all the machinery responsible for cell metabolism and forms a synapse onto bipolar cells at its most basal end. The ROS is about 25 µm long with a diameter of 2 µm and contains a stack of about 1000 discs. The discs are made up of invaginations of cell membrane at the basal end of the ROS; each disc has a life span of about two weeks and shifts during its life towards the apical end of the rod. Old discs are shed off in stacks of about 10 discs and are metabolized by the retinal epithelia cells. Rhodopsin is produced in the RIS and shuttled into the ROS via rhodopsin-bearing transport carriers (RTCs). It is inserted into the plasma membrane at the bottom part of the ROS, which then invaginates forming new discs. Rhodopsin occupies about 50% of the disc area, with a molar ratio of 1:60 comparing rhodopsin to phospholipids (Palczewski 2006). Amazingly, rods can reliably detect single photons (high sensitivity), but also

produce relatively little noise (high specificity). The noise is temperature-dependent and occurs statistically every 160 s at 37°C (Rodieck 1998). It looks exactly like the signal of a single photon in size and duration of the voltage drop (-1.7 mV). Keeping in mind the amplification steps of the visual cascade (see 3.3-3.4), the most probable cause of the noise therefore lies in the very first step of the visual cascade: the formation of the enzymatically active form of rhodopsin (R*). Taking into account that each rod has about $1.4*10^8$ rhodopsin molecules sitting in its ROS, each rhodopsin molecule has a statistical probability of R* formation in absolute darkness of once per 760 years (Rodieck 1998).

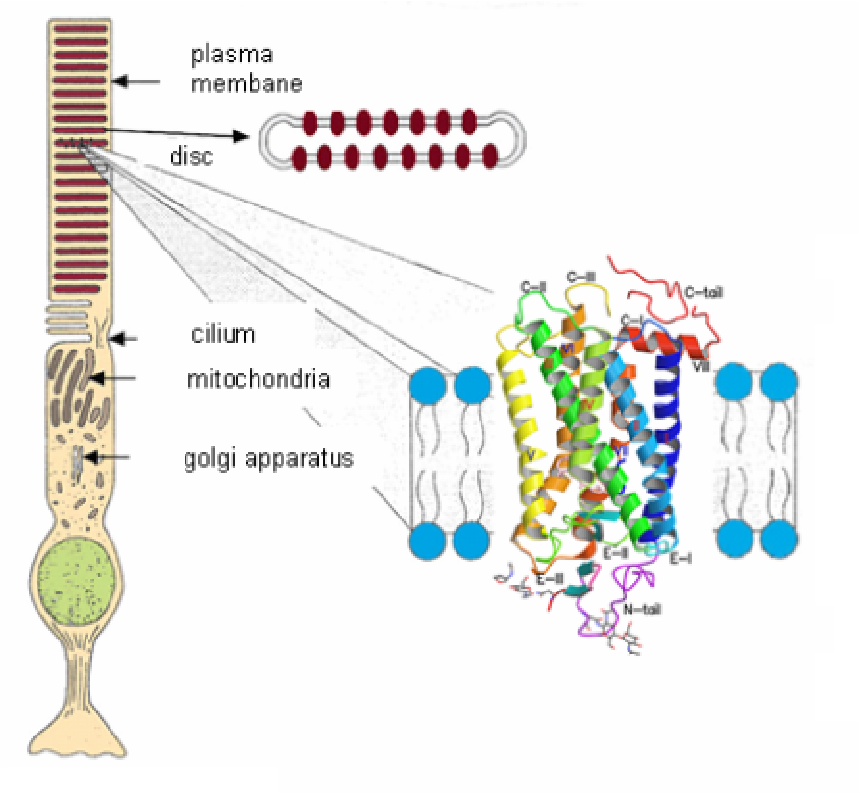

Figure 3: Rod photoreceptor cell
Figure modified from (Hargrave, Hamm et al. 1993).

3.3 Rhodopsin

Rhodopsin is an integral membrane protein and belongs to the large class A of GPCRs. So far, it is the only GPCR whose crystal structure has been successfully solved (Palczewski, Kumasaka et

al. 2000). Rhodopsin has 348 amino acids and a protein mass of 40 kDa (Figure 4); post-translational modifications include palmitoylation, acylation of the N-terminus, glycosylation and a disulfide bond (Palczewski 2006). It forms seven α-helices that span the membrane and a short 8th α-helix that lies parallel to the cytoplasmic surface. Its extracellular N-terminus points towards the inner part of the disc, whereas the C-terminal region is located in the cytoplasm. In its dark state, rhodopsin is bound to its inverse agonist 11-*cis*-retinal, a vitamin A derivative, by means of a protonated Schiff base with Lys^{296}. The positive charge of this bond is counteracted by a negatively charged counterion, Glu^{113}, in close neighborhood. The absorption spectrum of rhodopsin in its inactive dark state shows a maximum at 498 nm. The binding of 11-*cis*-retinal stabilizes the receptor in its inactive state and thus increases receptor specificity. When a photon hits rhodopsin, the energy is absorbed in about two thirds of all cases and used for isomerization of 11-*cis*-retinal to all-*trans*-retinal (Rodieck 1998).

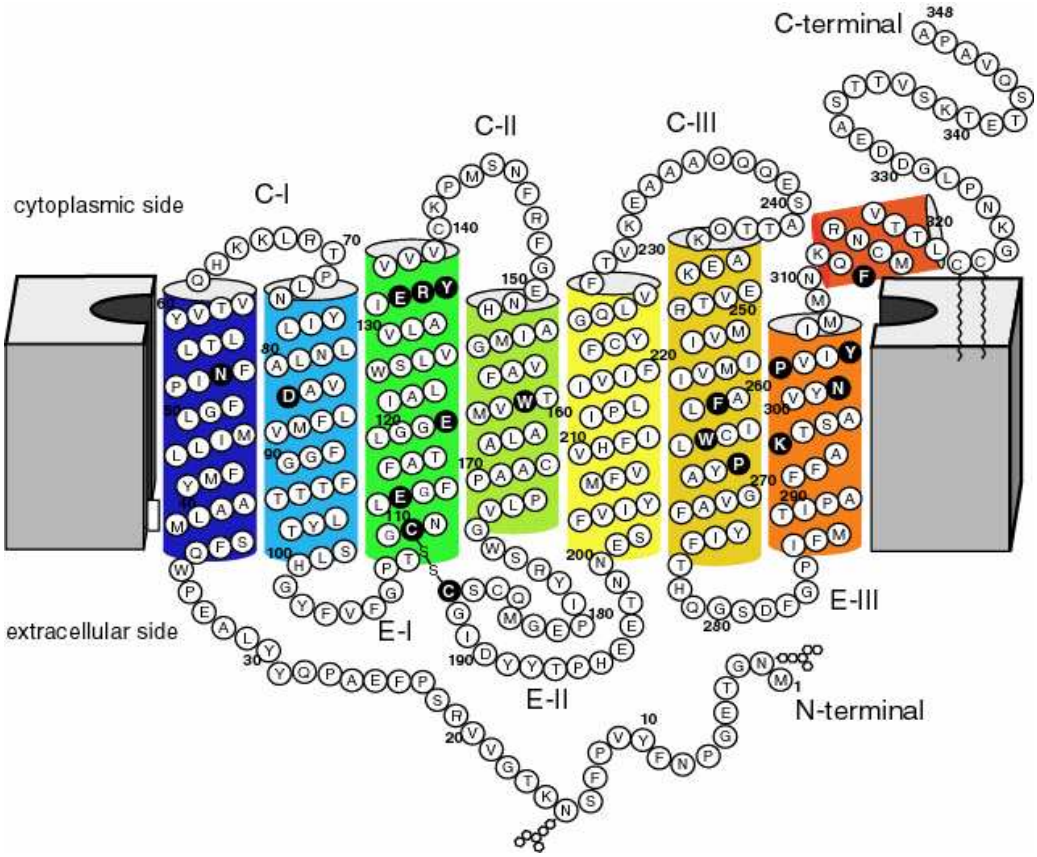

Figure 4: Rhodopsin

Figure adapted from Palczewski et al (Palczewski, Kumasaka et al. 2000). Amino acids in black are especially important for rhodopsin function and highly conserved throughout class A GPCRs.

The isomerization of 11-*cis*-retinal to all-*trans*-retinal induces a series of changes in the receptor conformation; several short-term intermediates (Lumi- and Bathorhodopsin) are followed by the more stable intermediate Metarhodopsin-I (Meta-I). In Meta-I, the chromophore is bound to opsin in its all-*trans* conformation but the absorption maximum has shifted from 498 nm (inactive form in the dark) to 480 nm. Meta-I is in equilibrium with Metarhodopsin-II (Meta-II), which under physiological conditions is strongly favoured. This can be measured as a shift in the absorption maximum from 480 nm to 380 nm. Meta-II can be subdivided into Meta-IIa and Meta-IIb. In Meta-IIa, the Schiff base is deprotonated and Glu^{113} is protonated. Meta-IIb is characterized by a further proton uptake at the cytoplasmic site, which most likely leads to the protonation of the counterion Glu^{134}. Meta-IIb is the enzymatically active form of rhodopsin and is often called R*. By random lateral diffusion through the disc membrane, R* encounters and binds transducin (G_t). Transducin belongs to the large group of heterotrimeric G proteins and consists of subunits Gα and Gβγ (see 3.4). During the existence of the R*G_t complex, Gα bound GDP is exchanged against GTP. As a result, the subunits dissociate into the enzymatically active GTP bound Gα (Gα*) subunit and Gβγ. R* has a mean lifetime of 100 ms and produces around 700 Gα* during that time. Rhodopsin deactivates due to the hydrolysis of the protonated Schiff bond with its agonist all-*trans*-retinal. All-*trans*-retinal diffuses out of rhodopsin and is recycled by the retinal epithelia cells to 11-*cis*-retinal. It is then shuttled back into the rods, where it binds again to the apoprotein opsin forming a new functional inactive molecule of rhodopsin.

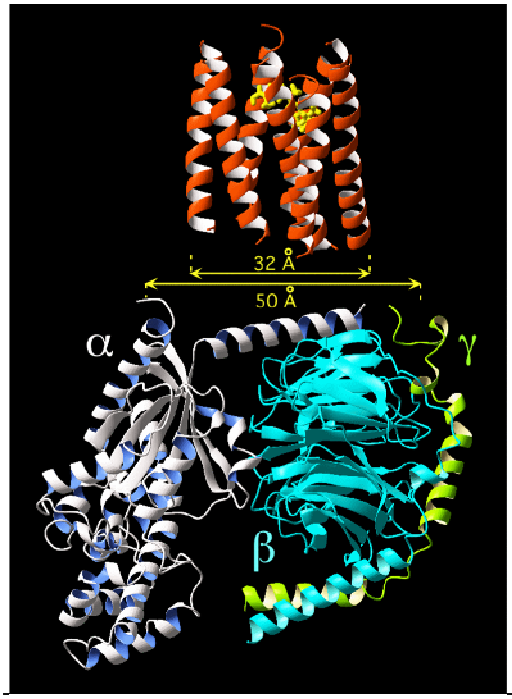

Figure 5: Size comparison of rhodopsin and its G protein transducin

red: rhodopsin, *blue* and *green*: G Protein subunits

Figure modified from Palczewski et al. (Palczewski, Kumasaka et al. 2000) and Lambright et al. (Lambright, Sondek et al. 1996; Sondek, Bohm et al. 1996).

If we consider the actual interaction between G_t and rhodopsin, it becomes obvious that the interaction interface of the two partners differs in size by almost a factor of two (Figure 5).
Under dim light conditions, which are physiological conditions for rods, the probability that two photons hit adjacent rhodopsin molecules is very low. Furthermore, it is known that a single photon can trigger the stereotypical response pattern of -1.7 mV. This means that a single R* must be able to activate the size superior G_t. However, the interaction domains of both proteins lie at opposite ends (Gα and Gγ subunits), which leads to the interesting question how a single R* can activate G_t. Mainly, three different strategies are thinkable:

1. Upon activation and binding, rhodopsin and G_t undergo conformational changes, thus enabling simultaneous interaction of the binding domains described.
2. Rhodopsin dimerizes forming a R*R unit for G_t interaction.
3. The interaction occurs in a sequential fashion, where G_t kind of sweeps along rhodopsin.

There have been several pieces of evidence for all of the three theories. In the early ‘70s, work by Cone (Cone 1972) and Chabre (Chabre and Cavaggioni 1975) showed that the rotational and lateral diffusion constant as well as diffraction patterns of the disc membrane were in accordance

with rhodopsin monomers. Hermann et al. (Herrmann, Heck et al. 2004) proposed a sequential fit model, where rhodopsin first interacts with one portion of the G_t and later with a second interaction interface in a sliding through manner. Support for rhodopsin dimers comes from work of the group around Palczewski. Using atomic force microscopy (Fotiadis, Liang et al. 2003; Liang, Fotiadis et al. 2003), they show that rhodopsin forms long rows of dimers in native disk preparation mounted on mica support. In a follow-up paper, the authors (Filipek, Krzysko et al. 2004) use molecular modeling and argue that the functional unit of a rhodopsin is a tetramer with a dimer interface between helices IV/V. They propose that for G_t activation only one rhodopsin of the dimeric complex needs to be activated, whereas the second serves as some sort of anchor for G_t binding and thus aids in the efficient catalysis (Fotiadis, Jastrzebska et al. 2006). Furthermore, it has been known for a long time that rhodopsin aggregates to oligomers on SDS-PAGE. More systematic studies using chemical cross linking (Jastrzebska, Maeda et al. 2004; Medina, Perdomo et al. 2004), blue native gel electrophoresis (Jastrzebska, Maeda et al. 2004), size exclusion chromatography (Medina, Perdomo et al. 2004) and fluorescence resonance energy transfer conclude that rhodopsin dimers are not only present in disc membranes and cytoplasmic membranes of COS-1 cells but also in artificially reconstituted asolectin liposomes and solubilized samples (Kota, Reeves et al. 2006; Mansoor, Palczewski et al. 2006). However, it remains to be further elucidated if the quaternary structure of rhodopsin is functionally relevant during signal transduction.

3.4 G protein transducin and the visual cascade

Like all trimeric guanine-nucleotide regulatory proteins (G proteins), G_t consists of the subunit Gα and Gβγ. G_t undergoes post-translational modifications - myristoylation of the Gα subunit, farnesylation of the Gγ subunit - which enable it to anchor to the disc membrane. When activated by R*, Gα bound GDP is exchanged against GTP (Figure 6). This leads to the dissociation of the GTP bound active Gα* subunit and Gβγ. Gα* can now bind its substrate, the phosphodiesterase (PDE), and thus exposes its catalytical site. Each PDE has two catalytical sites that can be activated separately by Gα*. Once Gα* binds, the PDE hydrolyzes cyclic GMP (cGMP) to GMP about 100 times more efficiently. In the dark, cGMP is present in 4 µM concentration in the ROS. It functions as a second messenger by binding and opening Na^+/Ca^{2+} selective channel in the plasma membrane of the ROS. One R* results in a cleavage of about 1400 cGMP molecules.

This is 0.7% of all cGMP contained in the ROS. A reduction of cGMP concentration leads to a decreased probability of cGMP binding to the cation channel while the k_{diss} stays constant. Since each cGMP-dependent ion channel needs at least three of the four cGMP binding sites occupied to remain open, roughly 2% of all ion channels (0.7% * 3) close due to decreased cGMP concentration. This translates into an approximate drop of –1.7 mV in membrane potential. The hyperpolarization leads to a graded reduction of glutamate release at the synaptic terminal of the rod. The bipolar cells sense this reduction and transmit it mainly to amacrine and ganglion cells (see 3.1.). The visual cascade is turned off at different levels: Rhodopsin loses its agonist all-*trans*-retinal and is phosphorylated by rhodopsin kinase. Gα bound GTP is cleaved GDP which in turn leads to the dissociation of the PDE-Gα complex and a 100-fold reduction in cGMP hydrolysis. The resulting rise in cGMP concentration leads to more open channels, which restores the equilibrium between Na^+/Ca^{2+} influx (ROS), K^+ outflux (RIS) and active transport (Na^+/Ca^{2+}, K^+ exchanger, Na^+/K^+ pump) and thus the dark membrane potential.

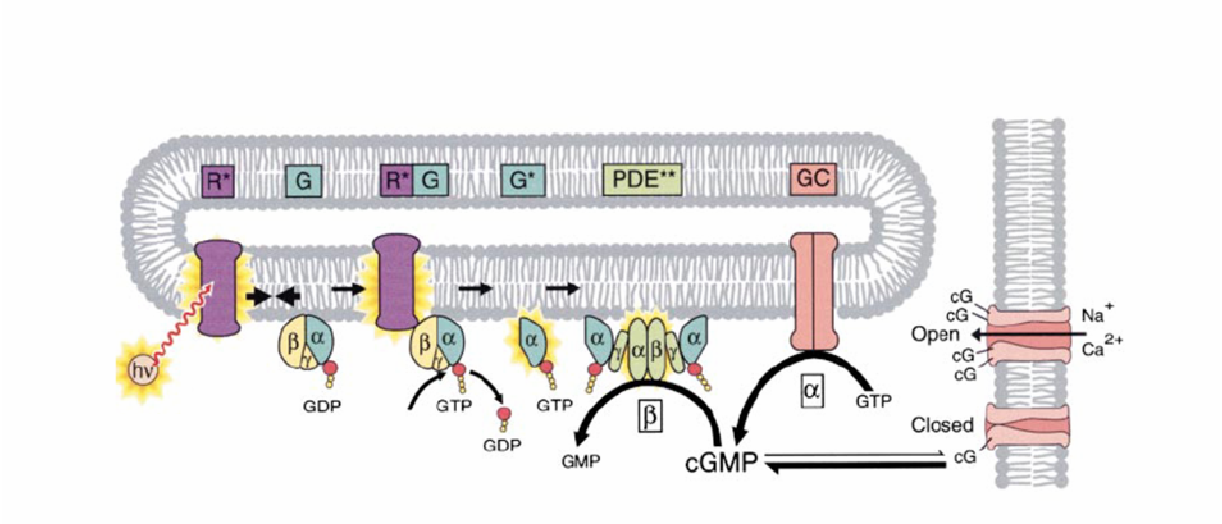

Figure 6: The visual cascade in rods

Figure modified from Leskov and Arshavsky, (Leskov, Klenchin et al. 2000).

3.5 The GPCR family

Rhodopsin research has long been at the forefront of GPCR research, mainly because rhodopsin can be isolated fairly easily and in big quantities from fresh bovine eyes obtained from the local slaughterhouse. Furthermore, the activation of the receptor can be easily induced and measured due to its light-sensitive ligand. Even though rhodopsin is as receptor specialized for visual signal

transduction, several functionally important motifs (e.g. D(E)RY in transmembrane helix III and NPxxY in transmembrane helix VII; see Figure 4) have theirs homologues in other class A GPCRs, suggesting similar functional mechanisms. Since rhodopsin is currently the only GPCR with a solved crystal structure for its inactive, dark state (Palczewski, Kumasaka et al. 2000), it has been the base for extensive molecular modelling for the whole GPCR family (Zhang, Devries et al. 2006).

With the availability of the information of the Human Genome Project, about 900 putative GPCRs have been identified so far. It has been estimated that 5% of all human genes code for GPCRs (Zhang 2006). They are involved in a wide range of physiological signal transduction systems (odorants, light, metals, biogenic amines, fatty acids), which make them very interesting targets for therapeutic interventions. At the moment, an estimated 30% of all prescription drugs target GPCRs (Jacoby, Bouhelal et al. 2006). A precise understanding of the exact mechanism of GPCR activation and signal transduction might be of great value not only for basic science but also for a better understanding of the underlying pathophysiology of several diseases linked to GPCR and G protein malfunctioning (e.g. Retinitis Pigmentosa, high blood pressure, heart failure, several endocrine diseases). Furthermore, it will be a valuable tool for designing more specific and efficient drugs (Jacoby, Bouhelal et al. 2006; Milligan 2006).

GPCRs all feature seven transmembrane (TM) domains; most of them bind heterotrimeric G proteins upon activation. G proteins can be composed of a range of different versions of the subunits; so far, 16 Gα, 5 Gβ, and 12 Gγ were identified (Milligan and Kostenis 2006). Depending on the specific composition of the G protein, the extracellular signal can be transduced to different effectors: Gs stimulates adenylyl cyclase, Gq activates phospholipase Cβγ, G12 binds to guanine nucleotide exchange factors, and Gi inhibits the adenylyl cyclase or activates inward rectifying GIRK channels.

GPCRs were historically grouped into three classes according to sequence homology (within each class 20% sequence homology). Recently, GPCRs were reclassified into the GRAFS system, which groups them according to phylogenetic lineage into five main families: Glutamate, Rhodopsin, Adhesion, Frizzled/Taste2, and Secretin (Fredriksson, Lagerstrom et al. 2003; Schioth and Fredriksson 2005). However, in this thesis, it will be referred to the historical GPCR classification into classes A through C.

Class A: The large Rhodopsin-like receptor group comprises roughly 700 receptors, many of which are odorant receptors of the olfactory epithelia but also other physiologically important receptors such as the β_2-adrenergic receptor and the dopamine D_2 receptor belong to class A.
Class B: The secretin-like group contains about 25 receptors such as the calcitonin receptor and many gastrointestinal peptide hormone receptors (e.g. secretin and glucagon).
Class C: This small group contains the metabotropic glutamate receptors (mGluRs) as well as the $GABA_B$ receptor. Class C GPCRs have long N-termini that are important for ligand binding and the formation of their quaternary structure.

There is a growing pool of evidence that GPCRs form oligomeric structures, which might be important for proper receptor functioning. So far, dimerization/oligomerization has been linked to proper posttranslational receptor maturation in the endoplasmatic reticulum (Fotiadis, Jastrzebska et al. 2006). This is well established for class C GPCRs, which form constitutive hetero/homodimers during biosynthesis. For $GABA_B$ receptors, heterodimerization between subtypes $GABA_BR$-1 and $GABA_BR$-2 has been shown to be required for proper receptor targeting. $GABA_BR$-1 (necessary for GABA binding) needs to heterodimerize with $GABA_BR$-2 to reach the cell surface (Marshall, White et al. 1999).
There are also indications that hetero/homo dimerization might be functionally important for class A GPCRs: Expression of rhodopsin mutants linked to Retinitis Pigmentosa (RP) with *wt* rhodopsin has been shown to lead to the retention of the *wt* form in the ER (Rajan et al. 2005). Furthermore, heterodimerization between the closely related α_{1d}-adrenergic receptor and the α_{1B}-adrenergic receptor has been shown to be necessary for cell surface expression (Hague, Uberti et al. 2004). Also, coexpression of class A dopamine receptors D1 and D2 was shown to result in a change of downstream signaling: instead of an inhibition (D2) or activation (D1) of adenylate cyclase, phospholipase C - mediated Ca^{2+} influx was stimulated (Lee et al. 2004). There have been several other studies using coimmunoprecipitation, fluorescence resonance energy transfer, bioluminescence resonance energy transfer, blue native gel electrophoresis and atomic force microscopy as techniques, which showed evidence for class A hetero/homo dimerization (Bulenger, Marullo et al. 2005; Milligan 2006). So far though, conclusive experimental data linking the quaternary structure to the functional output of GPCRs in their target compartment remains rare. It has been speculated that homo dimerization might be important for specificity

and efficiency of signal transduction, whereas heterodimers might be able to diversify signalling through GPCRs (Fotiadis, Jastrzebska et al. 2006).

3.6 Aim of this thesis

In this thesis, I was interested in examining rhodopsin's quaternary structure and its implications on G_t activation. To study rhodopsin's quaternary structure *in vivo* in HEK293 and COS-1 cells, bimolecular fluorescence complementation (BiFC) and fluorescence resonance energy transfer (FRET) were used as assays. BiFC technique is based on the idea that complementing fragments of autofluorescent proteins like yellow fluorescent protein (YFP) can reassociate to form functional fluorophores when fused to interacting proteins (Hu, Chinenov et al. 2002). To examine opsin with BiFC, fusion proteins of opsin and several control proteins with complementing fragments of the YFP variant venus (Nagai, Ibata et al. 2002) were prepared and coexpressed. For FRET, donor and acceptor fusion proteins were prepared by fusing venus as acceptor and enhanced cyan fluorescent protein as donor to the C-terminal end of rhodopsin, respectively. FRET efficiency as a measure of intermolecular proximity of the fusion proteins was determined with an acceptor bleach protocol. A FRET competition assay was used to explore possible dimerization interfaces of opsin *in vivo*.

Furthermore, I was interested in the use of FRET to test rhodopsin's propensity to form oligomeric structures in 0.01% dodecyl maltoside, a standard amount of detergent for solubilizing rhodopsin. Many structure-function studies of rhodopsin - especially mutagenesis studies - are carried out in its solubilized state rather than in its native disc membrane environment (see e.g.: Fritze, Filipek et al. 2003; Xie, Gross et al. 2003). It would therefore be interesting to know whether the detergent environment changes the native quaternary structure of rhodopsin and interferes with its function. Previously, it has been suggested that rhodopsin's functional unit for G_t activation is at least a dimer and that the monomeric state of rhodopsin has no catalytic activity (Park and Palczewski 2005; Jastrzebska, Fotiadis et al. 2006). Apart from atomic force microscopy studies, which do not answer functional questions, this has been mainly concluded from experiments comparing the catalytic activity of monomeric and oligomeric rhodopsin preparations in detergent (Jastrzebska, Fotiadis et al. 2006). However, experimental data has not been very conclusive so far, which is due to the fact that different detergent conditions strongly

influence the chosen G_t activation assays and thus data from different conditions cannot be compared without accounting for these differences.

In my thesis, I was also interested in determining whether receptor monomers are really functionally inactive, which would mean that oligomers are the functional unit for G protein activation. To answer that question, I measured maximal G protein activation rates of *wt* rhodopsin under the same detergent conditions as in the described fluorescence resonance energy transfer experiments.

4 MATERIALS AND GENERAL METHODS

4.1 Materials

1D4 Antibody	National Cell Culture Center, Minneapolis, USA
all-*trans*-retinal	Sigma-Aldrich, Taufkirchen
ampicillin	Roche, Mannheim
Biorad (Bradford) Reagent	Biorad, München
buffer A	pH 7.0, 40 mM K_2HPO_4, 26 mM KH_2PO_4, 1 mM $Mg(CH_3COO)_2$, 0.1 mM EDTA, 1 mM DTT, 0.1 mM PMSF, 10 mM glucose
buffer E	20 mM Tris-HCl, pH 6.8, 150 mM NaCl, 1 mM $MgCl_2$, 1 mM $CaCl_2$, 10 mM EDTA, 0.1 mM PMSF
buffer C	20 mM BTP, pH 7.1, 130 mM NaCl, 1 mM $MgCl_2$ and 2 mM DTT
buffer D	10 mM Tris-HCl, pH 6.8, 1 mM EDTA, 1 tablet Complete™-Protease inhibitor/50 ml buffer
buffer P	20 mM BTP, 120 mM KCl, 0.2 mM $MgCl_2$, 5 mM DTT, pH 6.9
buffer Q	5 mM Tris-HCl, 5 mM DTT, pH 6.9
cell culture roller bottle (850 cm^2)	Falcon, Greiner
Centricon YM-10 concentrators	Millipore, Eschborn
chloroquine	Sigma-Aldrich, Taufkirchen
Complete™-Protease inhibitor	Roche, Mannheim
Concanavalin-A (Con-A) sepharose	Amersham Pharmacia Biotech, Freiburg
COS-1 cells	American Type Cell Collection, Rockeville, USA (ATCC#CRL-1650)
n-dodecyl-β-D-maltoside (DM)	Biomol, Hamburg
DEAE-dextran	Sigma-Aldrich, Taufkirchen
Dulbecco's modified Eagle's medium (DMEM)	Gibco Invitrogen, Karlsruhe
DMEM/F12 medium	Gibco Invitrogen, Karlsruhe
DNA standard	Roche, Mannheim
DNA-Mini/Mega/Giga-Prep Kit	QUIAGEN, Hilden
EB buffer (elution buffer)	1.25 M NaCl, 50 mM Tris-HCl, pH 8.5, 15% isopropanol; Qiagen, Hilden
EDTA	Sigma-Aldrich, Taufkirchen
fetal calf serum (FCS)	Gibco Invitrogen, Karlsruhe
FRET buffer	128 mM NaCl, 6 mM KCl, 1 mM $MgCl_2$, 5.5 mM glucose, 10 mM Hepes, 1 mM $CaCl_2$, 0.2% BSA, pH 7.4-7.6
FuGene Transfection Kit	Roche
glutamine	Gibco Invitrogen, Karlsruhe
HEK293 cells	Prof. Dr. Michael Schäfer, FU Berlin
Luria-Bertani (LB) medium	10 g/l Bacto™ Trypton, 5 g/l yeast extract, 5 g/l NaCl, 1 mM NaOH, pH 7.0; Becton-Dickinson, Augsburg
medium A	DMEM with 1% glutamine, 1% penicillin, 1%

	streptavidin, 10% FCS, 1.5 g/l NaHCO3, 4.5 g/l glucose
medium B	DMEM with 1% L-glutamine, 1% penicillin, 1% streptavidin, 1.5 g/l NaHCO3, 4.5 g/l glucose
N3 buffer (neutralization)	3 M K-acetate, pH 5.5; QUIAGEN, Hilden
P1 buffer (resuspension)	50 mM Tris-HCl, pH 8.0, 10 mM EDTA, 100 µg/ml RNAse A; QUIAGEN, Hilden
P2 buffer (lysis)	200 mM NaOH, 1% SDS; QUIAGEN, Hilden
phosphate buffered saline (PBS)	137 mM NaCl, 2.7 mM KCl, 8.1 mM Na_2HPO_4, 1.5 mM KH_2PO_4, pH 7.4; Gibco Invitrogen, Karlsruhe
PE buffer (washing)	1 M NaCl, 50 mM Tris-HCl, pH 7.0, 15% Isopropanol; QUIAGEN, Hilden
penicillin / streptomycin	Gibco Invitrogen, Karlsruhe
phenylmethanesulphonylfluoride (PMSF)	Sigma-Aldrich, Taufkirchen
QuikChange Site-Directed Mutagenesis Kit	Stratagene, La Jolla, USA
restriction endonucleases	New England BioLabs
Tris-HCl (1 M, pH 7.4)	Sigma-Aldrich, Taufkirchen
trypsin	Gibco Invitrogen, Karlsruhe

4.1.1 COS-1 cells

COS-1 cells were used for transient expression of rhodopsin, rhodopsin fusion proteins as well as other control fusion proteins. COS-1 cells (Gluzman 1981) were derived from green monkey kidney cells. The cell line was created by transfecting CV1 cells with the origin defective simian virus SV40. COS-1 cells carry a single integrated copy of an origin defective SV40, which codes for wild type tumor antigen (T-antigen). T-antigen is a DNA helicase, which is important for the replication and transcription of plasmids carrying a SV40 origin such as the pMT4 plasmid. COS-1 cells were grown in Dulbecco's modified Eagle's medium (DMEM) with 4 mM L-glutamine, 1.5 g/l $NaHCO_3$, 4.5 g/l glucose, 10% fetal bovine serum at 37°C and 5% CO_2.

4.1.2 HEK293 cells

HEK293 cells were used for transient expression of rhodopsin, rhodopsin fusion proteins as well as other control fusion proteins. HEK293 cells were derived by permanently transforming human embryonic kidney cells with sheared adenovirus (Graham, Smiley et al. 1977). HEK293 cells express various adenovirus-specific proteins such as the viral T-antigen, which is important for replication and transcription of plasmid DNA. Interestingly, HEK293 cells were probably not derived from kidney cells but from neuronal cells of the kidney, which explains why they express many neuronal proteins such as neurofilaments and retinal synthesis machinery (Brueggemann, Sullivan et al. 2002). HEK293 cells were grown in DMEM/F12 medium with 10% fetal bovine serum and 4 mM L-glutamine at 37°C and 5% CO_2.

4.2 Molecular biology procedures

All centrifugation steps were carried out with an Eppendorf 5417C centrifuge unless stated otherwise.

4.2.1 pMT4 vector

All cloning work in this thesis was done in the mammalian cell expression vector pMT4 (Figure 7). The plasmid pMT4 carries an artificial opsin gene (Oprian, Molday et al. 1987) and has been generated via insertion of an EcoRI/NotI opsin fragment into the pMT3 vector (Franke et al. 1988; Oprian 1993).

All molecular biology procedures were carried out following standard procedures unless stated otherwise (for further reference see: Ausubel et al, 3rd edition, "Short protocols in molecular biology", 1995).

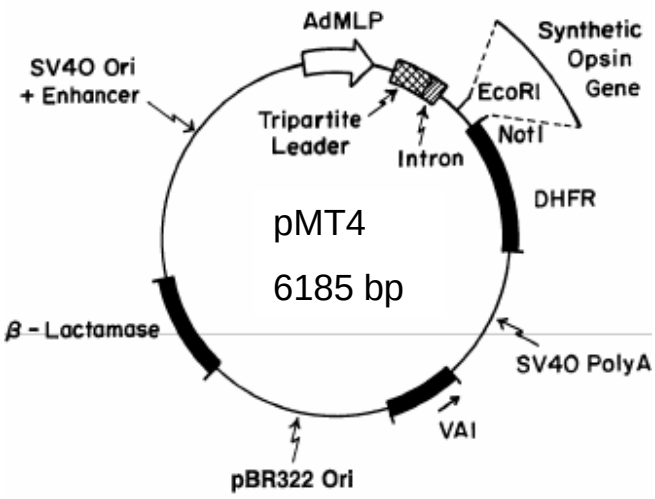

Figure 7: pMT4 expression vector

The vector pMT4 was created by inserting the artificial rhodopsin gene into the pMT3 vector at a EcoRI site (N-terminal) and a NotI site (C-terminal). Ori: origin of replication, DHFR: gene coding for dihydrofolate reductase, AdMLP: adenovirus major late promoter, Poly A: polyadenylation signal, VAI: virus associated gene.

4.2.2 Restriction endonuclease digests

For preparative digests, 2-4 µg plasmid DNA was mixed with 5 µl of the restriction endonuclease, 30 µl appropriate 10X buffer, 10 µg/ml BSA (if required), and deionized water up to a final volume of 300 µl. Analytical digests of plasmid DNA were performed with 0.5 µg DNA and 0.5 µl enzyme in a final volume of 10 µl. Preparative digests were incubated for 4-6 hours, analytical digests for 60 min; the temperature was chosen according to the manufacturer's suggestion for the respective endonuclease (New England Bio Labs, NEB). Double-digest reactions were left to incubate overnight. The digested DNA was subjected to gel electrophoresis. The band of interest was checked for expected size and strengths, cut out of the agarose gel and purified.

4.2.3 Gel electrophoresis

Different sized DNA fragments can be separated using gel electrophoresis due to the fact that their migration speed towards the positive electrode is proportional to their lengths. 1% agarose gels were prepared by heating agarose in TAE buffer (40 mM triacetate, 20 mM sodium acetate, 1 mM EDTA, pH 7.2) until it dissolved. The solution was left to cool before ethidium bromide (~1 µg/ml final concentration) was added and the gel was poured into the chamber. The solid gel was transferred into the running chamber and covered with TAE buffer. The DNA was mixed with 10X running buffer (50% glycerol, 50 mM EDTA, 0.25% bromphenol blue, pH 8.0) and filled into the gel slots. The gels were run at about 80 V until the buffer front was close to the positive electrode. An appropriate DNA ladder was used as size standard (100 bp or 1 kb, NEB). All gels were imaged under UV light, for preparative digests, the DNA band was excised as small as possible with a scalpel.

4.2.4 DNA fragment extraction from agarose gels

The DNA extraction was carried out using the *QIAquick* Gel-Extraction Kit (QIAGEN).
The gel slice was weighed into a 2 ml tube and three times the volume QG buffer was added. The gel was left to dissolve completely on a shaking device at 50°C. If the solution turned orange or violet, 10 µl sodium acetate was added. One volume of isopropanol was added if the DNA

fragment was below 500 bp or above 4 kb. The dissolved DNA mix was applied to a *QIAquick* spin column, centrifuged (14,000 rpm, 1 min) and the flow-through was discarded. 0.5 ml QG buffer was added to the column to remove traces of agarose. After centrifugation (14,000 rpm, 1 min), the flow-through was discarded and 0.75 ml PE buffer was added. After 2 min, the column was centrifuged (14,000 rpm, 1 min), the flow-through was discarded and the column centrifuged for an additional minute. The column was now inserted into a new 1.5 ml tube and 50 µl EB buffer was applied to the center of the membrane. After one minute, the column was centrifuged (14,000 rpm, 1 min) and the eluted DNA stored at -20°C.

4.2.5 PCR procedure

For all polymerase chain reactions (PCR), the QuikChange site-directed mutagenesis kit (Stratagene) was used. For the reaction, 5 µl 10X reaction buffer, 5-50 ng dsDNA template, 125 ng oligonucleotide 1 (forward primer), 125 ng oligonucleotide 2 (reverse primer), 1 µl dNTP mix, and deionized water to a final volume of 50 µl were mixed. 1 µl Pfu Turbo DNA polymerase was added after the reaction mix had incubated for 1 min at 95°C. PCRs were run in 15-20 cycles of 95°C for 30 s (melting of dsDNA), 50-65°C for 1 min (primer annealing, temperature depended on the primer used) and 68-72°C for 1 min/1 kb (elongation). The PCR product was stored at 4°C until purification of the DNA.

4.2.6 5'-Dephosphorylation with calf intestine phosphatase (CIP)

Before ligating DNA fragments into an appropriate vector, the vector was treated with alkaline phosphatase (CIP) to remove 5'-phosphate groups and thus reduce the amount of self-ligation between two vector ends. About 1-2 µg DNA was mixed with 10 µl 10X CIP buffer, 1 µl CIP and deionized water to a final volume of 100 µl. The reaction was incubated for 1 h at 37°C. The phosphatase was then denatured for 10 min at 65°C. The DNA was purified before ligation.

4.2.7 DNA purification

QIAquick PCR Purification Kit (QIAGEN) was used to purify DNA after PCR or alkaline phosphatase treatment. The reaction was diluted fivefold with PE buffer and mixed. The mixture was applied to a *QIAquick* spin column, which was placed in its collection tube. The column was

centrifuged (14,000 rpm, 1 min) and the flow-through was discarded. The column was centrifuged for another minute and placed into a new 1.5 ml tube. 30 to 50 µl EB buffer was applied to the center of the membrane and left to incubate for 1 min. The column was centrifuged (14,000 rpm, 1 min) to recover the DNA in the flow-through.

4.2.8 Ligation

To create a phosphodiester bond between 5'-phosphate and 3'-hydroxy ends, the Quick Ligation Kit (New England Bio Labs) was used. 50 ng vector was mixed with a threefold molar excess of the insert, 10 µl 2X Quick ligation buffer, 1 µl Quick T4 DNA ligase and deionized water to a final volume of 20 µl. The ligation was incubated for 20 min at room temperature and then used to transform *E. coli* cells (or stored at –20°C). As a negative control, the vector on its own was subjected to a ligation reaction to estimate the amount of self-ligation.

4.2.9 Transformation of E. coli with plasmid DNA

Competent XL1Blue *E. coli* cells (Stratagene, LaJolla, CA, USA) were kept at –80°C and removed 30 min before transformation to slowly thaw on ice. Plasmid DNA from a ligation (10 µl of the ligation reaction) or any other source (~50 ng) was added to 50 µl competent XL1Blue cells. Cells were left on ice for another 5 min. They were then heat-shocked for 2 min at 42°C. After the heat-shock, cells were left at room temperature for another 2 min. 500 µl LB medium was added to the cells, which were then incubated at 37°C and gently shaken for 45 min. 100 µl of the *E. coli* culture was applied to the center of LB-ampicillin agar plates (ampicillin 100 µg/ml). The cell solution was spread on the agar surface with a sterilized metal stick. The plates were incubated overnight at 37°C. If the number of colonies was very high, one colony was picked and streaked on a new agar plate. The colonies were used to inoculate LB-medium for quantitative DNA extraction.

For cultivation of *E.coli* cells, 5 ml LB medium (Ampicillin 100µg/ml) was inoculated with one freshly grown transformed *E.coli* colony. The culture was incubated at 37°C and shaken for 8-12 hours. The grown culture was used for DNA minipreps or as a starter culture for DNA megapreps.

4.2.10 Isolation of plasmid DNA from E. coli

For purification of small quantities of plasmid DNA *QIAprep* Spin Miniprep Kit (QIAGEN) was used. The kit uses alkaline lyses of bacterial cells. The DNA is then adsorbed to a silica-gel membrane. The bound DNA can be washed and finally eluted of the membrane.
E. coli from overnight culture were collected by centrifugation at 14,000 rpm for 1 min. The supernatant was discarded and the pellet was resuspended in 250 µl P1 buffer. After adding 250 µl P2 buffer, the reaction was gently shaken. 350 µl N3 buffer were added and the solution was carefully mixed. The tube was now centrifuged for 10 min at 14,000 rpm. The supernatant was applied to a *QIAprep* column. The column was centrifuged for 1 min and the flow-through was discarded. The column was washed with 0.5 ml PB buffer and centrifuged (14,000 rpm, 1 min). After discarding the flow-through, 0.75 ml PE buffer was added and the column centrifuged again (14,000 rpm, 1 min). The flow-through was discarded and the column centrifuged again (14,000 rpm, 1 min), the column was inserted into a new 1.5 ml tube and 50 µl EB buffer was applied. After 1 min, the tube was centrifuged (14,000 rpm, 1 min) and the eluted DNA collected.

4.2.11 DNA megapreparation

For higher amounts of DNA, *QIAprep* Spin Megaprep Kit (QUIAGEN) was used.
The overnight *E. coli* culture was diluted into 600 ml LB-ampicillin medium (100 µg ampicillin/ ml) and grown overnight at 37°C on a shaking device. The cell density was checked to be around 10^9 cells/ml. Cells were harvested by centrifuging the culture for 30 min at 3,100 rpm and 10°C. The supernatant was discarded and the pellet resuspended in 50 ml P1 buffer. 50 ml P2 buffer was added and the solution was gently shaken 4-6 times. The lyses was not allowed to proceed more than 5 min. Then, 50 ml of P3 buffer was added and after shaking the solution 4-5 times, it was applied onto a sterile *QIAfilter* cartridge, which had previously been adjusted to a sterile 500 ml glass filtration flask. The supernatant was left to incubate for 10 min, after which it was filtrated by applying a vacuum to the flask. By applying 35 ml QBT buffer, a QIAGEN-tip 2500 column was equilibrated. The filtered supernatant was applied to the column and left to drain. The column was washed with 100 ml QC buffer. The DNA was then eluted with 35 ml QF buffer into a sterile 35 ml flask. To precipitate the DNA, 24.5 ml isopropanol were added and after

mixing, the solution was divided into centrifugation tubes and centrifuged immediately for 30 min (11,000 rpm, 4°C, Beckmann JA 25-50). The supernatant was discarded and the pellets were washed with 8 ml 70% ethanol each and centrifuged again (10 min, 11,000 rpm, 4°C, Beckmann JA 25-50). The supernatant was discarded and the pellet left to air-dry for 10 min. It was then resuspended in 750 µl TE buffer. The DNA was transferred into 2 ml Eppendorf tubes and the centrifugation tube was washed with another 500 µl TE buffer to recover remaining DNA.

4.2.12 DNA concentration

The purified plasmid DNA was diluted 50 fold with water and the OD (optical density) at 260 nm, 280 nm and 325 nm was measured (Eppendorf, Bio-Photometer). The concentration was determined from the OD_{260} via c [µg/ml] = OD_{260}/0.02 (at d = 1 cm). As a measure of DNA purity, the quotient of OD_{260}/OD_{280} was calculated (~1.8) and OD_{325} had to be below 0.02.

4.2.13 DNA sequencing

All cloned DNA constructs were sequenced at a facility of the Humboldt University (Dr. Martin Meixner, Institute of Genetics, Humboldt University Berlin).

4.3 Biochemical methods

4.3.1 Expression and purification of wild type rhodopsin and rhodopsin fusion proteins

Rhodopsin, rhodopsin fusion proteins and venus-ECFP fusion proteins were transiently expressed in COS-1 cells using a DEAE-dextran transfection procedure (McCutchan and Pagano 1968). DEAE is a polycation and forms complexes with DNA. When the DEAE/DNA mix is applied to cells, DEAE interacts with the plasma membrane, resulting in an increased endocytosis of the DNA.

For one 850 cm^2 roller bottle, the following transfection protocol was applied: 150 µg DNA, 6 ml 1 M Tris-HCl, 48 ml medium B, and 6 ml DEAE-dextran were added into a sterile 75 ml flask. The flask was warmed up to 37°C in a water bath. The cells were checked under the microscope

to be at about 80% confluence, and their medium was removed. The transfection cocktail was added to the cells and incubated for 5.5 h at 37°C and 5% CO_2. In a second sterile 75 ml flask, 7.5 ml chloroquine (0.1 mM) and 67.5 ml medium A were mixed. The DNA transfection cocktail was removed and 75 ml chloroquine/medium A mix was added. The cells were then incubated for another 1.5 h at 37°C and 5% CO_2. The chloroquine/medium A mix was removed and the cells were washed twice with medium B. Finally, 250-300 ml medium A was added to the cells and they were incubated at 37°C and 5%CO_2.

Cells were harvested 72 h after transfection and the expressed proteins were purified using a 1D4-sepharose immunoaffinity matrix procedure (Oprian, Molday et al. 1987). The 1D4 antibody binds to the C-terminus of rhodopsin and is linked covalently to a sepharose matrix.
The cells were washed twice with PBS and then incubated for 10 min with 30 ml EDTA-PBS (1 mM EDTA in PBS) at 37°C and 5% CO_2 The roller bottle was carefully shaken to remove all adhered cells from the wall and 5 ml PBS with 1 tablet Complete^{TM} Protease Inhibitor (Roche) was added. The cell suspension was collected and centrifuged (2 min, 3500 rpm, EEC-centra CL2, 1568 G). The pellet was washed twice with 30 ml PBS and then resuspended in 15 ml EDTA-PBS.

All following procedures were carried out under dim red light conditions. For reconstitution, the cell suspension was incubated with 30 µM 11-*cis*-retinal on a shaking device for 4 h (or overnight) at 4°C. At this point, cells were either frozen at -20°C or subject to protein purification.
Cells were solubilized for 2 h at 4°C in 1% (w/v) n-dodecyl-β-D-maltosid (DM) in a 50 ml Falcon tube by using a 10% DM stock solution. N-dodecyl-β-D-maltosid is a non-ionic detergent with a molar mass of 510.63 g/mol and a critical micelle concentration (CMC) of 120 µM (Rosevear, VanAken et al. 1980). The solubilized cell suspension was then centrifuged (2 min, 3500 rpm, EEC-centra CL2, 1568 G) and the supernatant transferred onto 250 µl 1D4-sepharose gel (binding capacity: ~1 µg/µl). The gel was washed once with 40 ml PBS and centrifuged (4 min, 3500 rpm, EEC-centra CL2, 1568 G) before addition of the solubilized protein. The mixture was incubated overnight at 4°C. The gel material was centrifuged (4 min, 3500 rpm, EEC-centra CL2, 1568 G) and the supernatant was discarded. To remove excess 11-*cis*-retinal, the gel material was washed three times with 30 ml DM-PBS buffer (0.03% DM in PBS, pH 7.4)

and once with 50 ml DM-BTP buffer (0.03% DM, 10 mM BTP, pH 6.0). During each washing step, the gel was incubated 2 min on a shaking device before being centrifuged (4 min, 3500 rpm, EEC-centra CL2, 1568 G). The washed gel material was resuspended in 1 ml DM-BTP buffer and transferred into a 2 ml Eppendorf tube. The tube was centrifuged for 10 s (16,100 rpm, Eppendorf 5417C) and the supernatant was discarded. The 1D4-bound proteins were eluted from the sepharose gel by incubating the gel with 1 ml elution buffer (100 µM 1D4 peptide, 10 mM BTP, pH 6.0, 0.03% DM) for 2 h at 4°C. The 1D4 peptide corresponds to the last C-terminal 18 amino acids of rhodopsin (DEASTTVSKTETSQVAPA). The supernatant was separated from the gel by centrifugation (10 s, 16100 rpm, Eppendorf 5417C) and subsequent ultracentrifugation (60,000, 15 min at 4°C, Beckmann TL 100.3). The elution procedure was repeated twice with 0.8 ml and 0.5 ml elution buffer. To quantify the concentration of the expressed protein, UV/Vis absorption spectra were taken of all three elutions. Purified proteins were stored at -20°C.

4.3.2 Preparation of rod outer segments

The ROS preparation followed a protocol published by Papermaster et al. (Papermaster 1982).
Under dim red light, retinas were isolated from bovine eyes obtained from a local slaughterhouse. The retinas were cut off at the optic nerve and directly dropped into 45% sucrose in buffer A (pH 7.0, 40 mM K_2HPO_4, 26 mM KH_2PO_4, 1 mM $Mg(CH_3COO)_2$, 0.1 mM EDTA, 1 mM DTT, 0.1 mM PMSF, 10 mM glucose) on ice. Until further use, retinas were stored at -80°C.
For ROS preparation, retinas were thawed, resuspended and then vigorously shaken for 2 min to break off the ROS at the cilium. Consecutively, the suspension was centrifuged (5,000 rpm, 5 min, 4°C, Beckmann JS-13.1) and filtered through a cotton cloth. Buffer A was added 1:1 to the filtered solution and the solution was centrifuged again (10,000 rpm, 10 min, 4°C, Beckmann JS-13.1). The pellet was resuspended in 45% sucrose in buffer A and added carefully on top of a discontinuous sucrose gradient (1.11, 1.13 and 1.15 g/cm^3). After centrifugation, ROS was extracted from the uppermost boundary layer with a syringe. The extract was washed with buffer A and centrifuged (10,000 rpm, 10 min, 4°C, Beckmann JS-13.1). The pellet was stored at -40°C or directly used to extract transducin.

4.3.3 Preparation of G_t holoprotein

Transducin was prepared from bovine rod outer segments (ROS) following a published procedure (Kühn 1982) in a modified form (Heck and Hofmann 1993).

Purified ROS of about 100 retinas were resuspended in isotonic buffer P (20 mM BTP, 120 mM KCl, 0.2 mM $MgCl_2$, 5 mM DTT, pH 6.9), which contained 1 tablet Complete^{TM}-Protease inhibitor (Roche) per 250 ml buffer. The suspension was homogenized with a glass homogenizer and diluted to 1 mg rhodopsin/ml with buffer P and $MgCl_2$ (final concentration 5 mM). The solution was stored on ice and bleached for 10 min with orange light (filter Schott OG-550) to bind G_t to the activated rhodopsin. The solution was centrifuged (28,000 rpm, 30 min, 4°C, Beckmann JA-30.50) and the pellet resuspended in hypotonic buffer Q (5 mM Tris-HCl, 5 mM DTT, pH 6.9). The solution was centrifuged again (28,000 rpm, 30 min, 4°C, Beckmann JA-30.50), the pellet resuspended in buffer Q with 150 µM GTP and 50 µM $MgCl_2$ (rhodopsin concentration ~3 mg/ml) and incubated for 9 min. At this step, G_t exchanges GDP against the present GTP and dissociates from rhodopsin and the disc membrane.

The suspension was centrifuged again (28,000 rpm, 30 min, 4°C, Beckmann JA-30.50) and the supernatant removed and stored. The step was repeated and the resulting supernatant was added to the first supernatant. To remove remaining membrane impurities, the G_t solution was centrifuged (40,000 rpm, 15 min, 4°C, Beckmann 50.2) and the supernatant concentrated via ultrafiltration (Amicon YM-10) to 3 ml. The concentrated G_t preparation was then dialyzed (pore size <12 kDa) overnight against buffer C (20 mM BTP, pH 7.1, 130 mM NaCl, 1 mM $MgCl_2$ and 2 mM DTT).

To remove traces of rhodopsin, the dialyzed G_t preparation (~8-15 ml volume) was then applied to a Concanavalin-A column (~1 ml ConA sepharose) at a flow rate of 0.1 ml/min in buffer C at 6°C. Remaining rhodopsin binds to the ConA sepharose via its sugar modifications. The resulting G_t preparation was further concentrated by ultrafiltration (Centricon YM-10) and stored on ice. Protein concentration was determined with the Bradford assay (see 4.4.2). To exactly determine the amount of functional G protein, G_t was further quantified by titrating it with exact amounts of GTPγS (100 nM) using 10 nM rhodopsin as catalyst in a final volume of 1000 µl while subjecting it to constant stirring (Ernst, Bieri et al. 2000).

GTPγS concentration was determined by UV/Vis absorption spectroscopy with ε_{253}= 13700 $M^{-1}cm^{-1}$ (Bock et al. 1956). G_t concentrations ranged between 30-40 µM. Interestingly, only one third of the G_t protein pool determined by Bradford assay could be activated. This could be an effect of G_t agglomeration due to the high concentrations achieved during ultrafiltration or else due to the suboptimal quality of the retinas and/or G_t preparation. However, all calculated activation rates in this work refer to the amount of functional G_t as determined by GTPγS titration.

4.3.4 Membrane preparation of COS-1 cells

The protocol for 1 roller bottle (850 cm^2) was adapted from Han and Sakmar (Han and Sakmar 2000). Cells were harvested in 15 ml PBS (pH 7.4) into a 50 ml Falcon tube. They were centrifuged (2 min, 3500 rpm, EEC-centra CL2, 1568 G) and the supernatant was discarded. The cell pellet was resuspended in 11 ml hypotonic buffer D (10 mM Tris-HCl, pH 6.8, 1 mM EDTA, 1 tablet Complete™-Protease inhibitor/50 ml buffer). The suspension was homogenized 5x with a glass/glass homogenizer and then pulled twice through a 26-gauge cannula attached to a syringe. To separate the membrane fraction, the lysate was applied onto 10 ml of 37.7% saccharose in buffer E (20 mM TrisHCl, pH 6.8, 150 mM NaCl, 1 mM $MgCl_2$, 1 mM $CaCl_2$. 10 mM EDTA, 0.1 mM PMSF) into a centrifuge tube and centrifuged at 24,000 rpm (20 min, 4°C, rotor Ti 50.2). The membrane fraction was extracted with a syringe from the boundary layer between the sucrose layer and the hypotonic buffer. The membranes were diluted with 30 ml buffer E and centrifuged (45,000 rpm 60 min, 4°C, rotor Ti 50.2). The pellet was washed with 30 ml buffer E and centrifuged again (45,000 rpm, 60 min, 4°C, rotor Ti 50.2). The pellet was homogenized in 7.5 ml buffer E with a 26-gauge cannula attached to a syringe. Aliquots of 1.5 ml were frozen in liquid nitrogen and stored at -40°C.

4.3.5 HEK293 cell transfection

HEK293 cells were grown up to about 80% confluence in 10 cm^2 round tissue culture plates which contained a 9 cm^2 round coverslip (*in vivo* FRET experiments) or in 8-well coverslips (BiFC experiments). The serum-free DMEM/F12 medium was warmed up to 37°C. For transfection, the FuGene transfection reagent (Roche) was used according to the manufacturer's

suggestions. For 10 cm^2 tissue plates, 4 µl FuGene per plate was preincubated with 100 µl serum-free medium for 5 min. The mix was then added to the DNA (0.2 $\mu g/cm^2$) and left to incubate for another 20 min after careful mixing. The DNA mix was added to the cells and distributed by gently shaking the plates. Cells were left to incubate 24 h before fluorescence microscopy experiments.

4.4 Biophysical methods

4.4.1 Fluorescence spectroscopy assay for G_t activation

The inactive, GDP-bound G_t is in equilibrium between soluble and micelle-bound (*in vivo*: disc membrane bound) fractions (1). The micelle-bound fraction of inactive, GDP-bound G_t can form a complex with active rhodopsin. Complex formation with rhodopsin induces conformational changes in G_t, which lead to the release of its bound GDP (2). In a next step, empty G_t now binds GTP, which leads to a dissociation of the R*•G_t complex (3). The active G_t species (G_t*) G_t•GTP dissociates into $G_t\alpha$•GTP and $G_t\beta\gamma$, which leave the membrane. In the presence of PDE, active G_t•GTP, especially $G_t\alpha$, does not dissociate from the membrane. G_t bound GTP is hydrolyzed to GDP and P_i due to intrinsic GTPase of G_t (4). This step occurs *in vivo* within seconds, under *in vitro* conditions the timescale is minutes.(Hofmann 1993).

1) $G_{t,sol} \cdot GDP \rightleftarrows G_{t,mb} \cdot GDP$
2) $G_{t,mb} \cdot GDP + R^* \rightleftarrows R^* \cdot G_{t(empty)} + GDP$
3) $R^* \cdot G_{t(empty)} + GTP \rightarrow [R^* \cdot G_t \cdot GTP] \rightarrow R^* + G_{t,sol} \cdot GTP$
4) $G_{t,sol} \cdot GTP \rightarrow G_{t,sol} \cdot GDP + P_i$

G_t activation was measured here using intrinsic fluorescence dequenching of $G_t\alpha$ (Trp^{207}) upon exchange of GDP against GTP, which was first described by Higashijima (Higashijima, Ferguson et al. 1987). Even though there are several additional tryptophans present in Gα (2), Gβγ (8) and rhodopsin (5), the fluorescence increase due to G_t activation leads to a 25-30% increase in detectable fluorescence in the sample. This G_t activation assay was first described by Phillips et al. (Phillips and Cerione 1988), for experiments described here, a modified version as described in (Ernst, Bieri et al. 2000; Bartl et al. 2005) was applied.

To measure activation kinetics without an overlay of GTP hydrolysis, a non-hydrolysable GTP, GTPγS, was used. All measurements were carried out at 20°C. For G_t activation assay, settings

were λ_{ex} = 300 nm, and λ_{em} = 345 nm with an integration time of 0.5-2 s. Basal fluorescence levels were recorded for about 15 s before activation of rhodopsin was triggered with orange light (480 nm longpass filter, GG495 Schott, Mainz, Germany). Activation of the whole G_t pool was achieved by adding 50 nM rhodopsin to the cuvette. The slope of the initial rise in fluorescence emission (F/t) was quantified by linear regression. Since the maximal amplitude of fluorescence after addition of excess rhodopsin accounts for the total amount of G_t, the change in fluorescence (F/t) could be transferred into G_t*/t. All data was analyzed with Sigma Plot 2000.

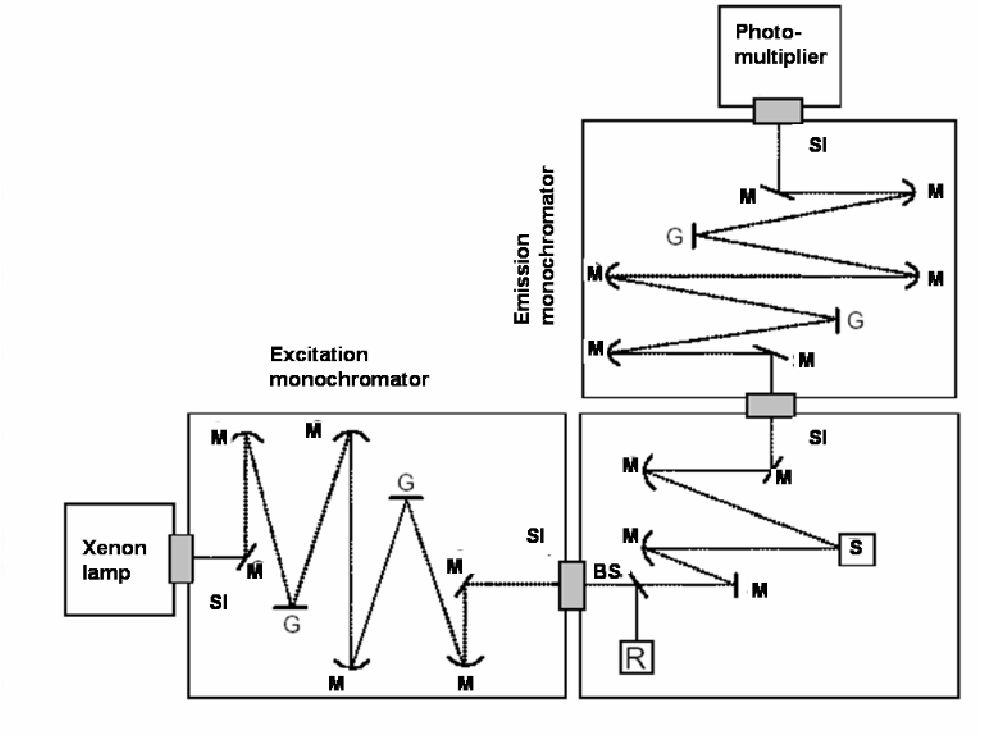

Figure 8: Setup for measurements of fluorescence emission spectra *in vitro*

Experiments were carried out with a fluorescence spectrometer (SPEX, Fluorolog II) equipped with a 450W xenon arc lamp. Abbreviations: M: mirror, Sl: slit, R: reference, BS: beam splitter, S: sample chamber, G: grater.

4.4.2 Bradford assay

The Bradford assay (Bradford 1976) is a spectroscopic assay to determine the concentration of a protein in solution. It is based on the fact that the dye Coomassie changes its absorbance when it binds to arginine and hydrophobic amino acid residues. In its anionic, bound state Coomassie

absorbs mainly at 595 nm. The absorbance at 595 nm is linearly proportional to the amount of protein, typically in the range of 2 µg/ml to 120 µg/ml. Due to the fact that different proteins do not have the same amino acid composition and thus also differ in the percentage of hydrophobic amino acid residues and arginines, the protein standard used has to be similar to the measured protein.

G_t concentrations were measured with the Bradford assay using BioRad protein reagent. 10 µl of the sample was diluted in 790 µl buffer and 200 µl BioRad protein reagent. After 5 min incubation, the absorption was measured at 595 nm. To calibrate the Bradford assay, bovine serum albumin was used as standard.

4.4.3 UV/visible spectroscopy

UV/Vis absorption spectra were taken at 20°C with a Varian Cary 50 UV/visible spectrometer with a resolution of 2 nm. Rhodopsin samples were normally measured in BTP-DM elution buffer (100 µM 1D4 peptide, 10 nM BTP, pH 6.0, 0.03% DM), the same buffer was also used to record basic absorption spectra. For the illuminated ("bleached") rhodopsin spectra, the samples were illuminated for 15 s with a 150 W fiber optic light source equipped with a 480 nm longpass filter (GG495 Schott, Mainz, Germany) and a heat protection filter.

For each sample, absorption spectra between 250 nm and 650 nm were taken for the dark and the illuminated state. Rhodopsin concentration was determined via $E = \varepsilon \cdot c \cdot d$ with E = absorption at $\lambda = 498$ nm, $\varepsilon = 40600\ M^{-1}cm^{-1}$ and d = 1cm (Kropf, Whittenberger et al. 1973) in the dark spectra. In the case of fusion proteins consisting of rhodopsin and fluorescent proteins, difference spectra (spectrum after illumination subtracted from corresponding spectrum in the dark) were used to determine rhodopsin concentration.

5 BIMOLECULAR FLUORESCENCE COMPLEMENTATION

5.1 Method

Bimolecular fluorescence complementation analysis (BiFC) was introduced as a qualitative assay for monitoring molecular interactions of proteins *in vivo*. (Hu, Chinenov et al. 2002; Hu and Kerppola 2003). The authors cut yellow fluorescent protein (YFP) at different non-conserved amino acids in loop region of its β-barrel structure and fused the resulting fragments to the basic region leucine zipper (bZip) domains of the transcription regulatory proteins Jun (bJun) and Fos (bFos), respectively. The bZip domains of Jun and Fos are known to interact with each other. Upon coexpression of the resulting bJun and bFos fusion proteins in *E. coli* or COS-1 cells, fluorescence emission could be measured (Figure 9).

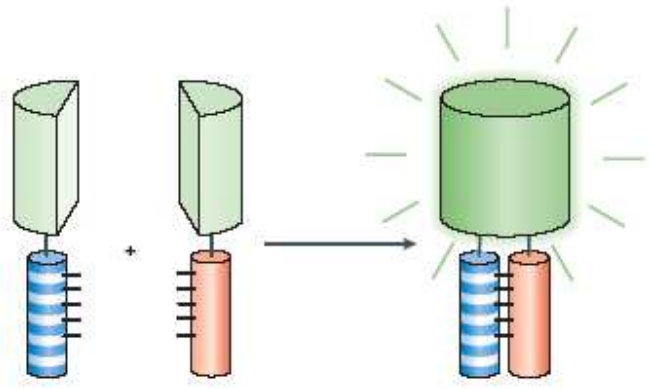

Figure 9: BiFC complementation

Cartoon of fluorophore fragments (*pale green*) fused to interacting proteins bJun and bFos, which upon coexpression lead to BiFC of the fragments (complemented fluorophore: *green*).

Figure adapted from Kerppola (2006).

As a negative control the authors showed that none of the fragments fluoresces on its own, and that coexpression of corresponding fragments lacking the interacting bZip domain yielded no fluorescence emission. The authors also studied fluorophore complementation *in vitro* by denaturing (5 min at 95°C) a mixture of complementing fragments, which were either coexpressed and copurified or mixed after purification. After leaving denaturing conditions, fluorescence emission slowly increased to reach a level comparable to intact fluorophores after several hours. Furthermore, the authors showed that BiFC could be suppressed by the addition of

wild type bZip domains, which strongly suggests that initiation of fluorescence complementation is not driven by the attraction of the fluorophore fragments to each other. However, the addition of competing wild type bZip domains had to occur within seconds after denaturation, which indicates that once complementation is completed the process is not reversible. Thus, the authors claim that BiFC is a valuable tool for monitoring spatially close protein-protein interaction during protein complex formation. But they also say that it is not as suitable to monitor shifts in equilibrium after complex formation due to the irreversible fluorophore formation. However, one main advantage of BiFC over FRET is that fluorescence is only visible if protein interactions occur, which makes it a potentially easy-to-use tool for determining new protein-protein interaction.

So far, BiFC has been mainly used for soluble proteins like bZip domains and the G protein subunits Gβ and Gγ (Hu and Kerppola 2003; Hynes, Tang et al. 2004; Walter, Chaban et al. 2004; Cole, McLaughlin et al. 2007). In my thesis, I was interested in the use of BiFC to investigate membrane protein interactions. For that purpose, fusion proteins between fluorophore fragments and several different proteins such as the GPCR rhodopsin, the tyrosine kinase epidermal growth factor receptor (EGFR), the class A GPCR β_2-adrenergic receptor (β_2-AR), the cation selective ion channel transient receptor potential protein TRPV3 (Xu, Ramsey et al. 2002), the *E. coli* specific outer membrane protein OmpA (Wang and Kim 2002) as well as the soluble maltose binding protein (MBP) were created.

For fluorescence microscopy, fusion protein constructs were transiently expressed in HEK293 cells using FuGene as transfection medium. The cells were imaged 24 h post transfection using an upright, widefield microscope (DMR, Leica, Bensheim, Germany) equipped with a mercury lamp (HBO 50W, Osram) and a Plan-Apochromat 63x/1.4 objective (Leica, Bensheim, Germany). Venus fluorescence emission was filtered and recorded with a cooled CCD camera (C 5985-10, Hamamatsu, Herrsching, Germany). Settings for venus were λ_{exc} = 490 nm, λ_{em} = 535-580 nm (band pass filter). For further characterization, fusion proteins were expressed in COS-1 cells, purified by means of 1D4-immunoaffinity chromatography and characterized via UV/Vis absorption spectroscopy. Rhodopsin fusion proteins were also functionally characterized using the described G_t activation assay (see 4.4.1, data not shown).

5.1.1 BiFC fusion protein constructs

For all fusion protein constructs, pMT4 was modified by standard cloning and PCR procedures (see section 4.2). Codons corresponding to the 1D4-tag followed by a stop codon were added to the C-terminal end of all fusion proteins. The 1D4-tag is a sequence of 9 amino acids at the C-terminal end of rhodopsin. It functions as epitope tag for the monoclonal anti-rhodopsin 1D4 antibody, which was used to immunopurify resulting fusion proteins. Fluorophore fragments of EYFP/venus were generated using previously published split sites (Hu, Chinenov et al. 2002) (Figure 10).

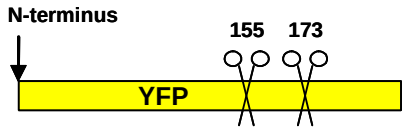

Figure 10: BiFC split sites in YFP

Green fluorescent protein-derived fluorophores have a β-barrel structure, which is constituted by 11 strands surrounding a central α-helix. Both split sites are in loop regions which connect strands forming the β-barrel structure. For C-terminal opsin constructs, the opsin gene was followed by bases GGATCAACCGGT and the gene corresponding to the respective EYFP fragment and codons corresponding to the amino acid sequence GTETSQVAPA (1D4-tag) (Figure 11 A). In N-terminal EYFP-opsin constructs, codons corresponding to opsin amino acids 1-21 were followed by bases ACCGGT, the gene of the respective EYFP fragment, and codons corresponding to opsin amino acids 3-348.

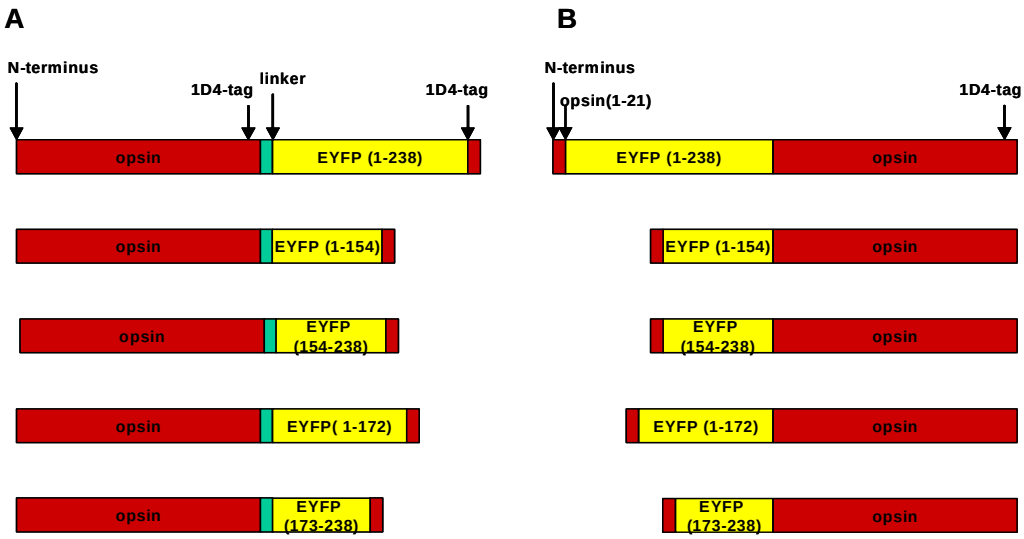

Figure 11: Fusion protein constructs between EYFP and opsin

A: C-terminal fusion protein constructs between opsin and EYFP. **B**: N-terminal fusion protein constructs between opsin and EYFP.

To further optimize the resulting BiFC constructs, EYFP was exchanged against venus in all C-terminal BiFC constructs (Figure 12) (see 5.2). The yellow variant 'venus' is *Aequorea victoria* GFP with mammalian codons and the following additional mutations: F46L, F64L, S65G, V68L, S72A, M153T, V163A, S175G, T203Y, H231L and a Val-1a insertion (Nagai, Ibata et al. 2002) (see 6.1.1 for amino acid alignment). Venus has enhanced maturation properties due to enhanced folding and accelerated formation of the chromophore, which is the rate limiting step of maturation. The resulting opsin-venus fusion proteins were named as follows:

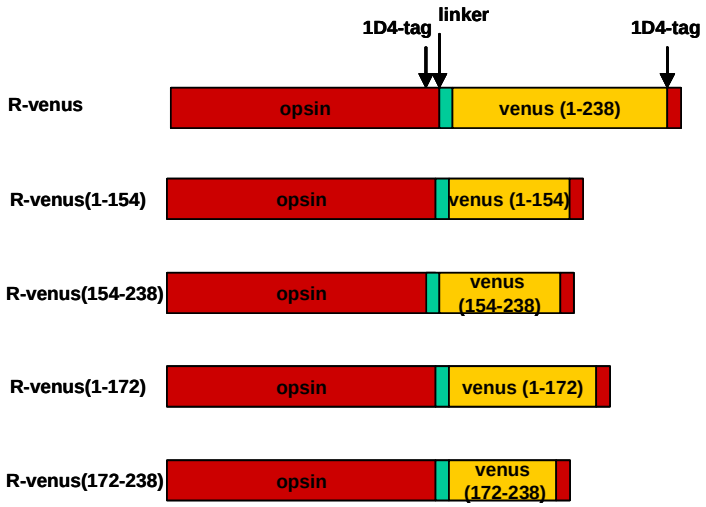

Figure 12: C-terminal fusion proteins constructs between opsin and venus

To investigate BiFC between opsin and other membrane proteins as well as other soluble proteins, the following additional BiFC constructs with venus (fragments) were created (Figure 13).

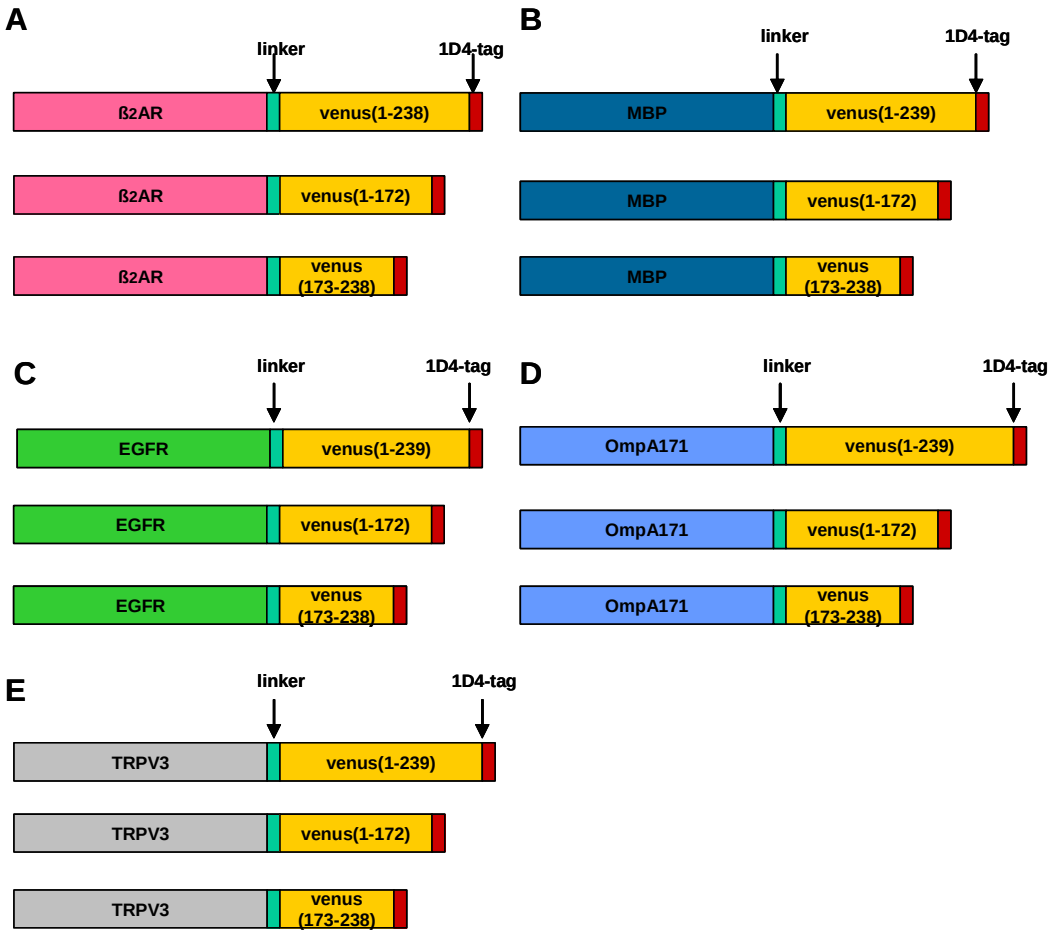

Figure 13: C-terminal fusion proteins constructs between BiFC control proteins and venus

A β_2-AR-venus(1-238): β_2-adrenergic receptor fused to venus(1-238); β_2-AR-venus(1-172): β_2-adrenergic receptor fused to venus(1-172); β_2-AR-venus(173-238): β_2-adrenergic receptor fused to venus(173-238); **B** MBP-venus(1-238): maltose binding protein fused to venus(1-238); MBP-venus(1-172): maltose binding protein fused to venus(1-172); MBP-venus(173-238): maltose binding proteins fused to venus(173-238); **C** EGFR-venus(1-238): epidermal growth factor receptor fused to venus(1-238); EGFR-venus(1-172): epidermal growth factor receptor fused to venus(1-172); EGFR-venus(173-238): epidermal growth factor receptor fused to venus(173-238); **D** OmpA171-venus(1-238): OmpA171 fused to venus(1-238); OmpA171-venus(1-172): OmpA171 fused to venus(1-172); OmpA171-venus(173-238): OmpA171 fused to venus(173-238); **E** TRPV3-venus(1-238): TRPV3 receptor fused to venus(1-238); TRPV3-venus(1-172): TRPV3 receptor fused to venus(1-172); TRPV3-venus(173-238): TRPV3 receptor fused to venus(173-238).

For EGFR constructs, codons corresponding to EGFR were followed by bases TGCTCGAGCATGCATCTAGAG, the gene of the respective fluorophore (or fluorophore fragment) and codons corresponding to the 1D4-tag (amino acids GTETSQVAPA). For MBP constructs, codons corresponding to MBP were followed by bases GGATCAACCGGT, the gene of the respective fluorophore (or fluorophore fragment), and codons corresponding to the 1D4-tag. For OmpA171 constructs, codons corresponding to OmpA171 were followed by bases CCTGCAGGATCAACCGGT, the gene of the respective fluorophore (or fluorophore fragment), and codons corresponding to the 1D4-tag. For TRPV3 constructs, codons corresponding to TRPV3 were followed by bases CTAGATACCGGT, the gene of the respective fluorophore (or fluorophore fragment), and codons corresponding to the 1D4-tag. For β_2-AR constructs, codons corresponding to β_2-AR were followed by bases ACCGGT, the gene of the respective fluorophore (or fluorophore fragment), and codons corresponding to the 1D4-tag.

protein	**abbreviation**	**Genbank entry Swiss-Prot entry**	**amino acids**	**comment/reference**
opsin (bovine)	R	M12689 OPSD_BOVIN	1-348	synthetic gene (Ferretti 1987), modified by (Sakmar 1989)
β_2-adrenergic receptor (human)	β_2AR	P07550 ADRB2_HUMAN	1-413	(Kobilka et al. 1987)
transient receptor potential receptor V3 (murine)	TRPV3	Q8K424 TRPV3_MOUSE	1-790	(Xu, Ramsey et al. 2002) (Peier et al. 2002)
epidermal growth factor receptor (human)	EGFR	P00533 EGFR_HUMAN	1-3205	(Lin et al 1984)
β-barrel of specific outer membrane protein OmpA (*E. coli*)	OmpA171	P0A910 OMPA_ECOLI	22-192	fragment constituting β-barrel (Wang and Kim 2002) gene: (Beck, Bremer 1980)
maltose binding protein	MBP	P0AEX9 MALE_ECOLI	1-387	(Quiocho 1997)

5.2 Results

To determine which complementing fusion protein constructs were most suitable, two different sets of previously published fluorophore fragments, EYFP(1-172)/EYFP(173-238) and EYFP(1-154)/EYFP(155-238) (Hu, Chinenov et al. 2002) were used to generate fusion proteins with opsin as described. The four complementing fragments were fused to the N-terminal as well as to the C-terminal site of opsin, leading to 8 different constructs (Figure 11). All constructs were sequenced and amplified. Fusion proteins were expressed in COS-1 cells, regenerated with 11-*cis*-retinal and purified as described above. Only constructs carrying the fluorophore fragment at the C-terminal site of opsin could be successfully expressed and purified. However, not all C-terminal constructs were expressed equally well (data not shown).

One probable reason for low expression levels are folding distortions. To facilitate folding, fusion proteins were optimized using venus, a maturation-optimized EYFP variant (Nagai, Ibata et al. 2002). The so-derived fusion proteins R-venus(1-154), R-venus(1-172), R-venus(154-238) and R-venus(173-238) (Figure 12) could be successfully expressed in COS-1 and HEK293 cells and purified as shown by UV absorption spectroscopy (Figure 14).

When expressed on their own, R-venus(1-154), R-venus(1-172), R-venus(154-238) and R-venus(173-238) showed typical absorption features of rhodopsin for dark conditions as well as after bleaching (Figure 14). When R-venus(1-154) and R-venus(1-172) were coexpressed with R-venus(154-238) and R-venus(173-238), respectively, the absorption spectra showed an additional absorption peak at $\lambda = 515$ nm, which is typical for R-venus (Figure 15). Both coexpressed samples still showed a normal Meta-II absorption shift (380 nm) of rhodopsin after illumination. Comparing the amount of rhodopsin with venus by means of their extinction coefficients (rhodopsin: $\varepsilon_{498} = 40{,}600\ M^{-1}cm^{-1}$: venus $\varepsilon_{515nm} = 92{,}200\ M^{-1}cm^{-1}$), it turned out that the relation of rhodopsin:venus is not exactly 2:1 (two rhodopsin fusion proteins are needed for one complementing venus) but roughly 3:1. However, Western blot experiments with coexpressed fusion proteins revealed that coexpressed R-FC2 with R-FC4 run as a single band at about the size of two *wt* rhodopsin and one venus (data not shown). This suggests that not all complemented fluorophores actually mature to be fully functional even though they complement.

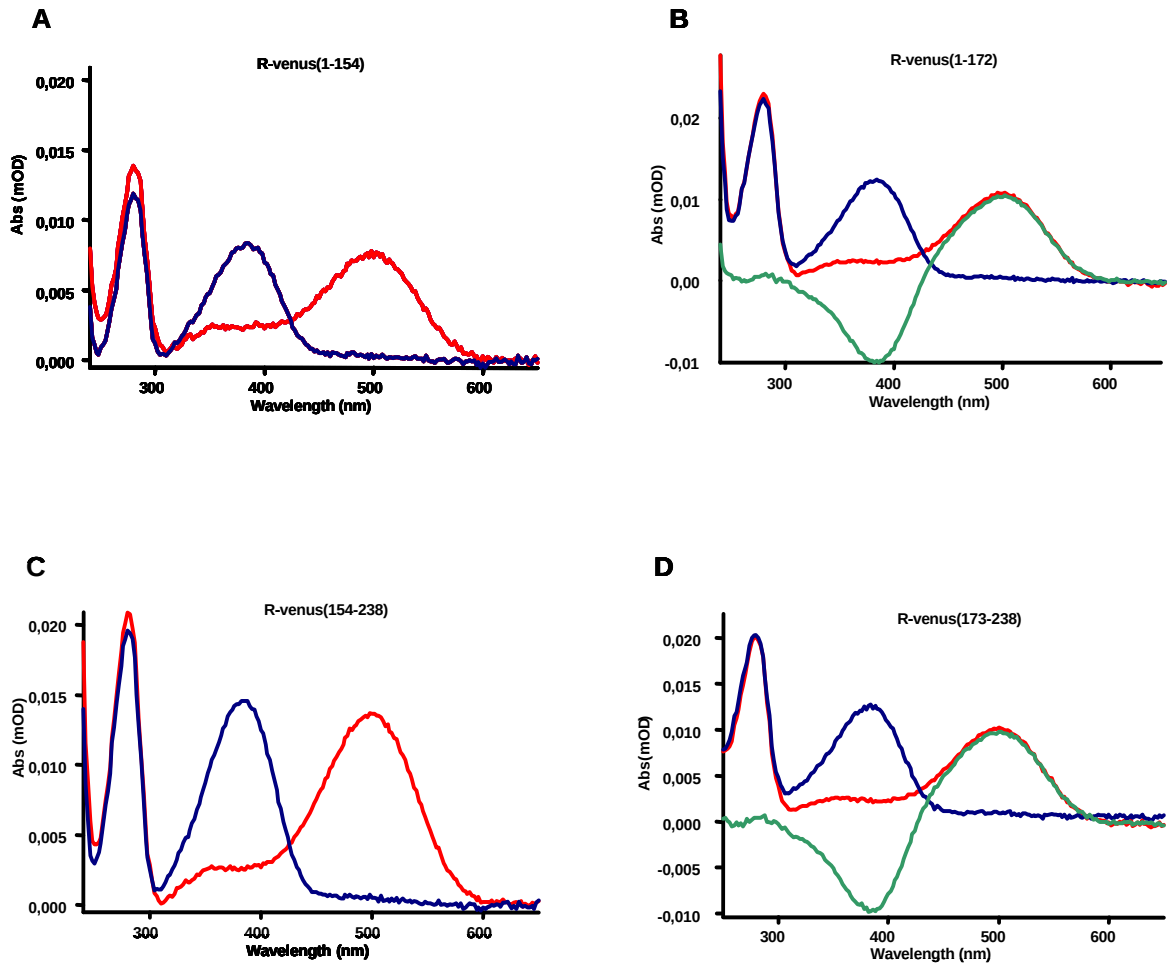

Figure 14: UV/Vis spectra of fusion proteins

A–D: Fusion protein constructs were expressed in COS-1 cells, regenerated with 11-*cis*-retinal and purified as described. All spectra were taken of the purified sample. *Red curves*: spectra taken in the dark, *blue curves*: spectra taken after illumination of the sample for 15 s with orange light, *green curve:* difference spectra of dark-light spectra. After illumination, the absorption maximum shifts from 498 nm to 380 nm, which is typical for *wt* rhodopsin. None of the spectra has an absorption peak at 515 nm, which would be typical for venus absorption.

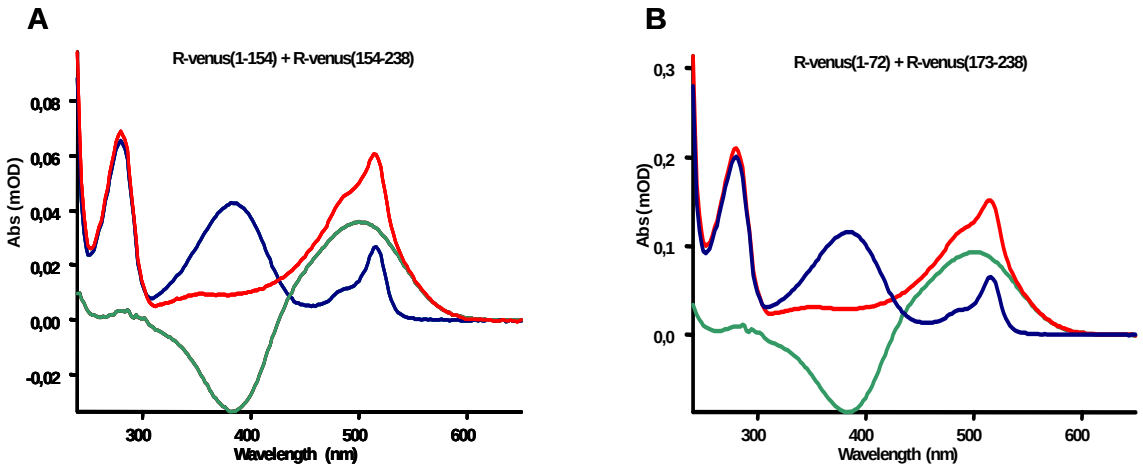

Figure 15: UV/Vis spectra of coexpressed fusion proteins

E–F: Fusion protein constructs were coexpressed in COS-1 cells, regenerated with 11-*cis*-retinal and purified as described. All spectra were taken of the purified sample. *Red curves*: spectra taken in the dark, *blue curves*: spectra taken after illumination of the sample for 15 s with orange light, *green curves:* difference spectra of dark-light spectra. The blue curves show a shift of the maximum absorption from 498 nm (*green*) to 380 nm, which is typical for *wt* rhodopsin. Both red curves show a maximal absorption at 515 nm, which is typical for venus absorption.

The UV/Vis spectra of coexpressed fusion proteins (Figure 15) show that they must come close enough to enable fluorophore fragments to interact and complement to a fluorescing holo protein. COS-1 and HEK293 cells expressing R-venus(1-172), R-venus(173-238) and R-venus(1-172) together with R-venus(173-238) were imaged with fluorescence microscopy. There was no significant fluorescence detectable in cells only expressing R-venus(1-172) or R-venus(173-238) (Figure 16A and B), whereas cells coexpressing both constructs showed strong fluorescence signals (Figure 16 C). Fluorescence was mainly localized in the plasma membrane but also present in intracellular compartments such as the endoplasmatic reticulum (ER) and the Golgi apparatus. This suggests that bimolecular fluorescence complementation occurs during biosynthesis of the fusion proteins. The formed fluorescing protein complex is then shuttled to the plasma membrane.

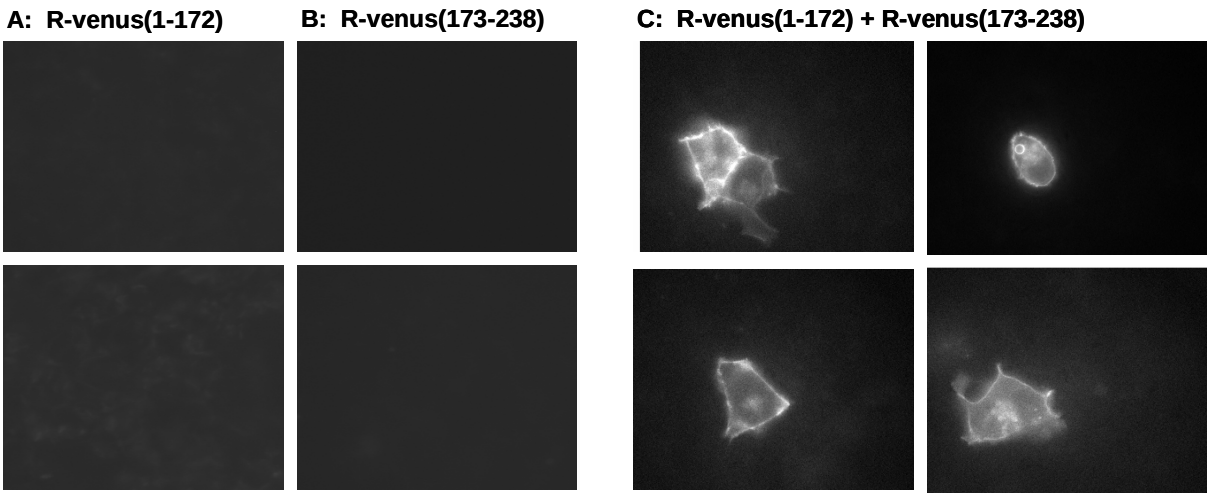

Figure 16: Expression of opsin BiFC constructs in HEK293 cells

All HEK293 cells were imaged 24 h post transfection with FuGene using a 63x/1.4 objective (Leica), λ_{exc} = 490 nm, λ_{em} = 535-580 nm; **A:** R-venus(1-172), no significant fluorescence detectable; **B:** R-venus(173-238), no significant fluorescence detectable; **C:** Coexpression of R-venus(1-172) and R-venus(173-238), strong fluorescence emission localized mainly in the plasma membrane as well as in intracellular compartments such as the ER and the Golgi

To verify that detected fluorescence emission upon coexpression of complementing fragments R-venus(1-172) with R-venus(173-238) is due to specific interaction of opsin with itself, several other proteins were fused to venus fragments and coexpressed with opsin fusion proteins (Figure 17). All control fusion proteins were cloned as described under 5.1.1 (Figure 13) and sequenced. Control BiFC experiments were carried out exactly like coexpression of R-venus(1-172) with R-venus(173-238). Surprisingly, all negative control constructs showed positive BiFC upon expression with opsin fusion protein (Figure 17A-E). Even though the level of fluorescence was not as strong as when coexpressing R-venus(1-172) and R-venus(173-238), it was still clearly detectable in all cases.

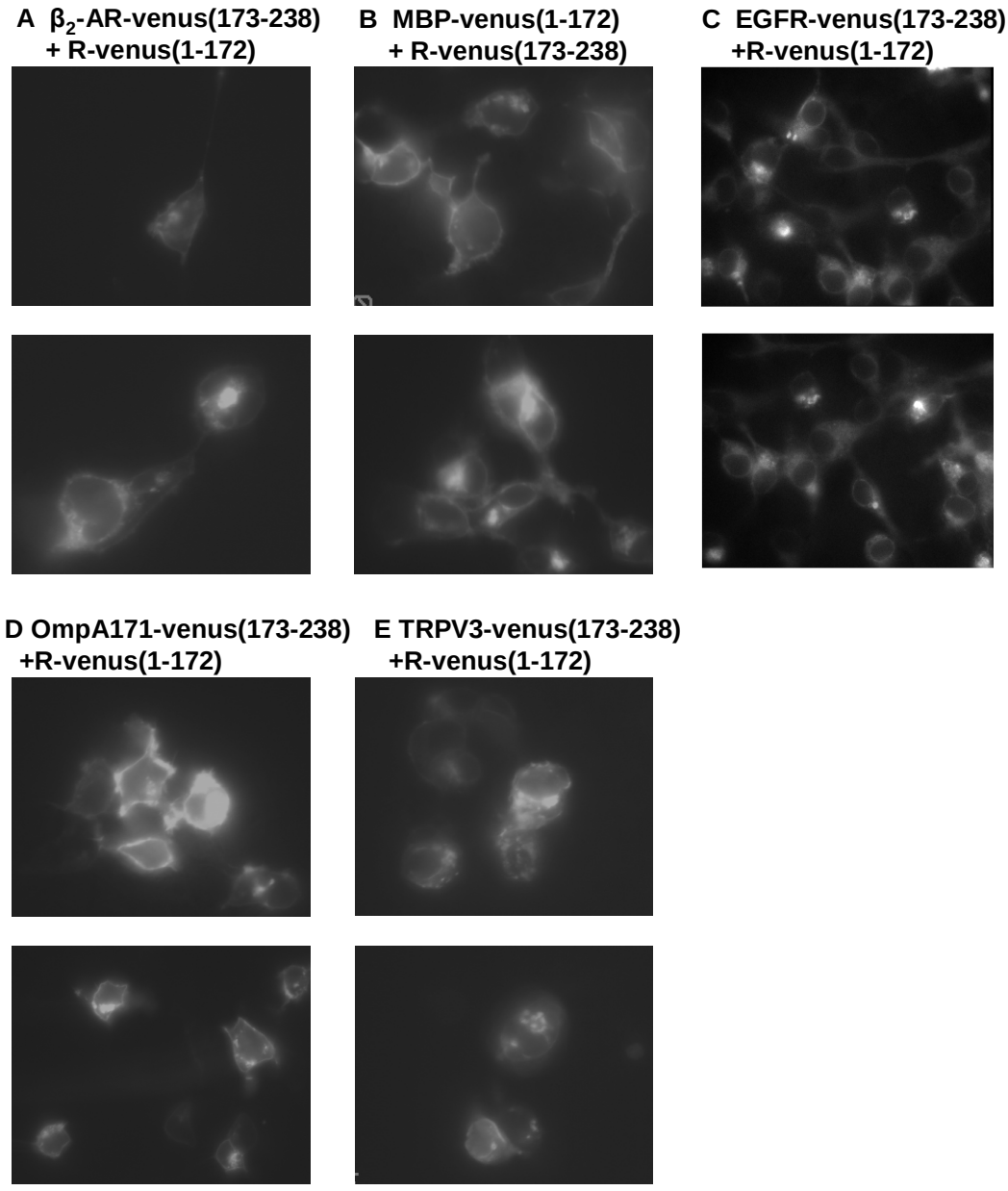

Figure 17: BiFC between opsin and several different control proteins upon coexpression

All HEK293 cells were imaged 24 h post transfection with FuGene using a 63x/1.4 objective (Leica), λ_{exc} = 490 nm, λ_{em} = 535-580 nm; **A:** Coexpression of β_2-adrenergic receptor fused to venus(173-238) with R-venus(1-172) shows strong fluorescence localized mainly in intracellular compartments like the ER but also in the plasma membrane; **B:** Coexpression of maltose binding protein fused to venus(1-172) with R-venus(173-238) shows strong fluorescence localised in the plasma membrane as well as in intracellular compartments (ER); **C:** Coexpression of EGFR-venus(173-238) with R-venus(1-172) shows homogeneous fluorescence in the cytoplasm, the nuclear and plasma membrane as well as in the ER; **D:** Coexpression of OmpA171-venus(173-238) with R-venus(1-172) shows fluorescence mainly in intracellular compartments as well as in the plasma membrane; **E**: Coexpression of TRPV3-venus(173-238) with R-venus(1-172) shows fluorescence mainly in intracellular compartments like the ER.

The fluorescence signal of all control BiFC experiments (Figure 17) is slightly lower than in cells coexpressing of R-venus(1-172) and R-venus(173-238). But this does not necessarily mean that BiFC efficiency is lower, it could also reflect lower expression levels of the control fusion proteins. Moreover, BiFC is a qualitative assay for protein-protein interaction and differences in fluorescence emission cannot be reliably quantified.

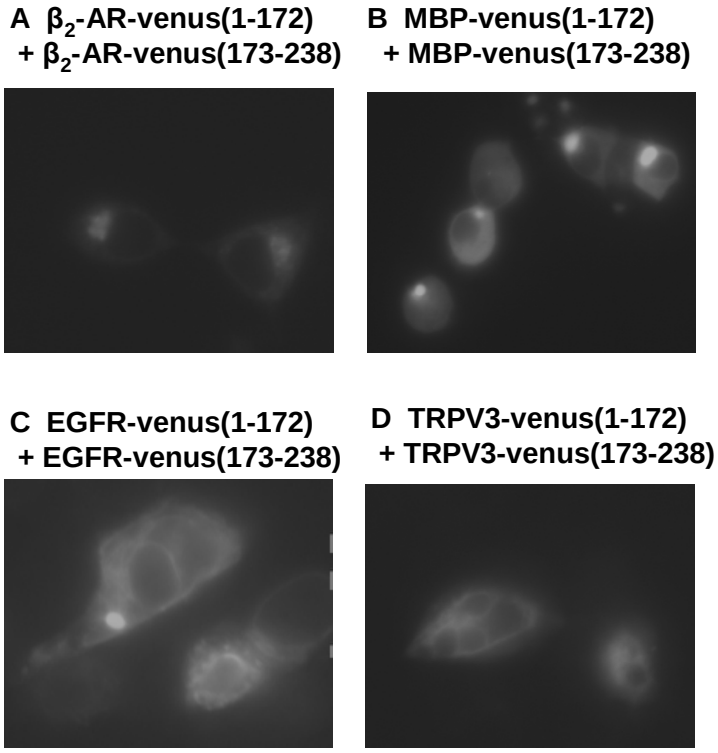

Figure 18: BiFC between control fusion constructs

All HEK293 cells were imaged 24 h post transfection with FuGene using a 63x/1.4 objective (Leica), λ_{exc} = 490 nm, λ_{em} = 535-580 nm. Positive BiFC upon coexpression of control fusion proteins with themselves (see labeling) could be recorded in all cases. **A**: Fluorescence is mainly restricted to intracellular compartments, little fluorescence can be detected in the plasma membrane; **B**: Fluorescence is homogenously distributed in the cytoplasm as well but seems to be higher concentrated in some intracellular compartment, probably due to degradation; **C**: Fluorescence is mainly visible in intracellular compartments like ER and Golgi but also in the plasma membrane; **D**: Fluorescence is mainly localized in intracellular membranes, as well as in the plasma membrane.

BiFC was also tested for control fusion proteins with themselves (Figure 18). As shown, all control fusion proteins exhibit positive BiFC when coexpressed with their respective complementing fusion protein. In the case of EGFR, it is known that upon binding its ligand EGF, the tyrosin kinase dimerizes and is internalized. However, EGF should not be present in

HEK293 cell culture but BiFC between EGFR-venus(1-172) and EGFR-venus(173-238) is nevertheless positive (Figure 18 C). For MBP and TRPV3, homo dimerization has not been reported at all. However, both of them show positive BiFC (Figure 18B, D).

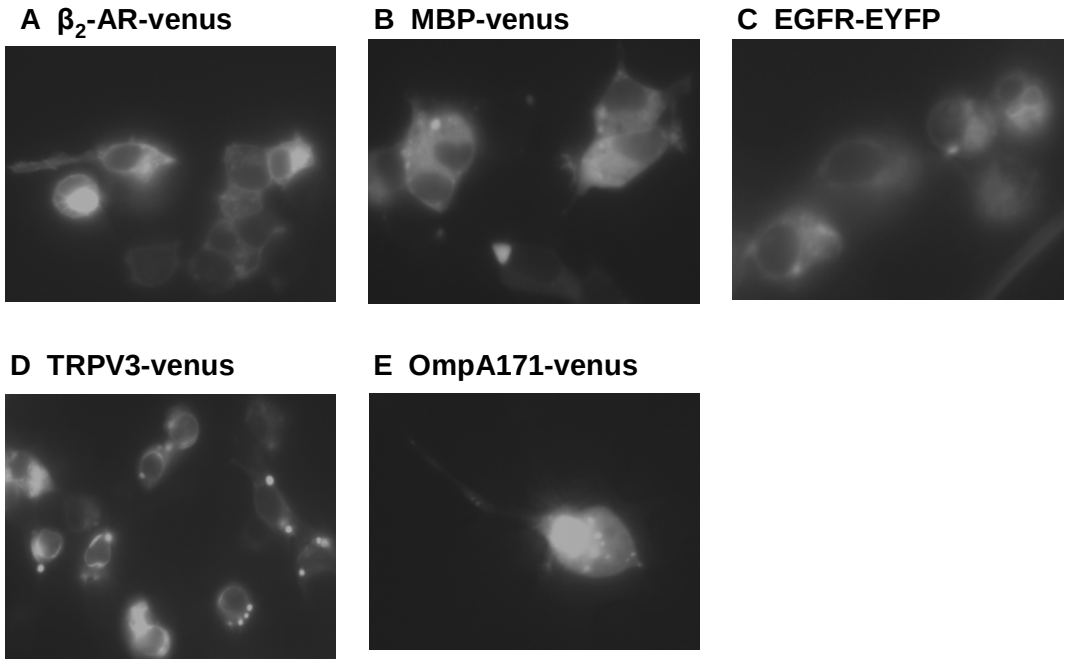

Figure 19: Expression of control proteins fused to venus

All HEK293 cells were imaged 24 h post transfection with FuGene using a 63x/1.4 objective (Leica), λ_{exc} = 490 nm, λ_{em} = 535-580 nm. **A**: Fluorescence is mainly present in intracellular membranes (ER) but also in the plasma membrane, **B**: Fluorescence is homogenously distributed in the cytoplasm, **C**: Fluorescence is mainly visible in intracellular compartments like ER and Golgi, **D**: Fluorescence is mainly localized in intracellular membranes, as well as in the plasma membrane, **E:** Strong fluorescence is present in intracellular compartments (nucleus) and the cytoplasm.

5.3 Discussion

Positive BiFC between R-venus(1-172) and β_2-AR-venus(173-238) is not as surprising as with all of the other fusion proteins. The class A GPCR β_2-AR shares a high sequence homology with rhodopsin and is therefore also structurally very similar. It is thus not too surprising to see fluorescence emission due to successful BiFC between R-venus(1-172) and β_2-AR-venus(173-238) (Figure 17A) and between β_2-AR-venus(173-238) and β_2-AR-venus(1-172) (Figure 18A).

EGFR is a typical tyrosine kinase involved in cell proliferation and cell growth. It does not share many structural features with rhodopsin but nevertheless solid BiFC signals are detectable for coexpression of EGFR-venus(173-238) and R-venus(1-172) (Figure 17C). It is known that crosstalk between GPCRs and EGFR signaling pathways occurs, but so far, none of these interactions were reported to be directly between GPCR and EGFR (Thomas et al. 2006; Fischer, Hart et al. 2003). Fluorescence is not only localized around the plasma membrane but also in the cytoplasm, the ER and the nuclear membrane. This could be due to mistargeting or misfolding of the protein complex. Another possibility is that BiFC already occurs when fusion proteins are expressed, perhaps due to their close localization in the ER upon overexpression.

Especially unexpected was BiFC between opsin and OmpA171, MPB and TRPV3 fusion proteins (Figure 17 B, D, E). TRPV3R is a cation selective ion channel which primarily responds to noxious heat signals in different tissues (skin, tongue, spinal cord and brain) (Xu, Ramsey et al. 2002). It is known to form heterotrimeric channels with TRPV1 but until now, no protein interactions between TRPV3 and GPCRs have been reported. OmpA, the outer membrane protein A of *E. coli*, can act as a porin with low permeability for small solutes, it is also known to be implicated in the stabilization of mating aggregates during conjugation (Wang and Kim 2002).It is known to form homodimers Here, only 171 amino acids which form its 8-stranded transmembrane β-barrel domain were used to generate the described OmpA171-fluorophore fusion proteins. So far, no interaction between GPCRs and OmpA has been reported. The maltose binding protein, MBP, is a soluble plasma protein of *E. coli* involved in the trafficking of maltose. So far, no interactions with rhodopsin have been reported.

To summarize, it can be said that BiFC does not represent an unambiguous tool for monitoring specific interaction of membrane proteins. This might be due to the restriction of membrane proteins to 2-dimensional compartments. However, even unrelated, soluble proteins such as MBP show positive BiFC with opsin.

Also, fluorescence emission is almost always also detectable in intracellular compartments like the ER. This could be an effect of mistargeting or misfolding of the protein complex. An alternative explanation is that fluorescence complementation occurs before the protein complex is shuttled to its target compartment. Kerppola et al. (Hu, Chinenov et al. 2002) showed that once the BiFC complex has assembled, it is very stable due to irreversible fluorophore formation (see 5.1). Thus, fluorescence which can be traced to the Golgi and the ER does not necessarily mean

that proteins specifically interact in their target compartment, e.g. the cell membrane. Positive BiFC could therefore also be a result of close proximity during expression, post-translational modification and transport.

Overall, it can be said that BiFC does not allow for a meaningful interpretation of fluorescence as specific membrane protein interactions. However, it might be a potentially useful technique for linking proteins together. Using complementing fusion protein with strong transport qualities could be a feasible approach for shuttling target proteins to specific cell compartments. In the case of coexpression of R-venus(173-239) with MBP-venus(1-172), for example, the protein complex was mainly located in plasma membrane (Figure 17B), whereas MBP-venus on its own was localized in the cytoplasm (Figure 19B). Furthermore, BiFC linked rhodopsin does not differ significantly in its G protein activation capacity from wild type rhodopsin (experiment was performed as described in 4.4.1, data not shown), which suggests that BiFC linked proteins might be totally functional. BiFC therefore could be used for coupling potential interaction partners to each other and measuring gain or loss of function. Both of these potential applications for BiFC remain to be further investigated.

6 FLUORESCENCE RESONANCE ENERGY TRANSFER *in vivo*

6.1 Method

6.1.1 Construction of opsin-venus, opsin-ECFP and venus-ECFP fusion plasmids

In my thesis, I was especially interested in looking at the quaternary structure of rhodopsin in the cytoplasmic membrane *in vivo*. To do so, it was necessary to choose a protein donor/acceptor pair for FRET instead of labeling purified rhodopsin with chemically derived fluorophores. I used a set of fluorophores, which were derived from the green fluorescent protein (GFP). As acceptor/donor pair, the yellow GFP variant venus and the cyan GFP variant ECFP were employed, respectively.

The vector pMT4 was modified by standard cloning and PCR procedures such that the opsin gene was followed by bases GGATCAACCGGT, then followed by the gene corresponding to ECFP or venus and codons corresponding to the amino acid sequence GTETSQVAPA (1D4-tag) (Figure 20).

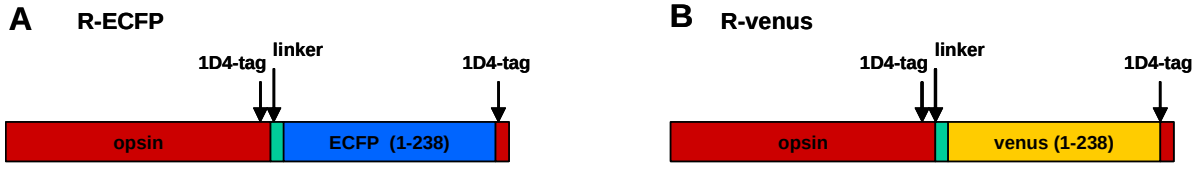

Figure 20: FRET constructs

A: R-ECFP construct consists of the gene for opsin followed by a 12 bp linker and bases coding for the full length ECFP; **B**: R-venus construct consists of the gene for opsin followed by a 12 bp linker and bases coding for the full length venus.

Rhodopsin's C-terminal sequence ETSQVAPA is recognized by the rho-1D4 antibody used for immuno purification of the fusion proteins. The cyan variant 'ECFP' is *Aequorea victoria* GFP with mammalian codons and the following additional mutations: K26R, F64L, S65T, Y66W, N146I, M153T, V163A, N164H, H231L and a Val-1a insertion ((Griffin, Nandi et al. 1998) and Clontech Laboratories) (Figure 21). The yellow variant 'venus' is *Aequorea victoria* GFP with mammalian codons and the following additional mutations: F46L, F64L, S65G, V68L, S72A, M153T, V163A, S175G, T203Y, H231L and a Val-1a insertion (Nagai, Ibata et al. 2002)(Figure

21). The control construct venus-ECFP was cloned by replacing the EcoRI-SalI Fragment of opsin-ECFP with the venus gene. The gene product corresponds to a fusion protein of venus and ECFP separated by a 20 amino acid linker sequence. Opsin fragments were fused to venus by replacing opsin in R-venus with the respective fragment using standard PCR and molecular biology procedures. Fragments opsin(1-146); opsin(147-348); opsin(1-240)**;** opsin(241-348); opsin(147-240) were used as previously published (Struthers, Yu et al. 1999; Yu and Oprian 1999).

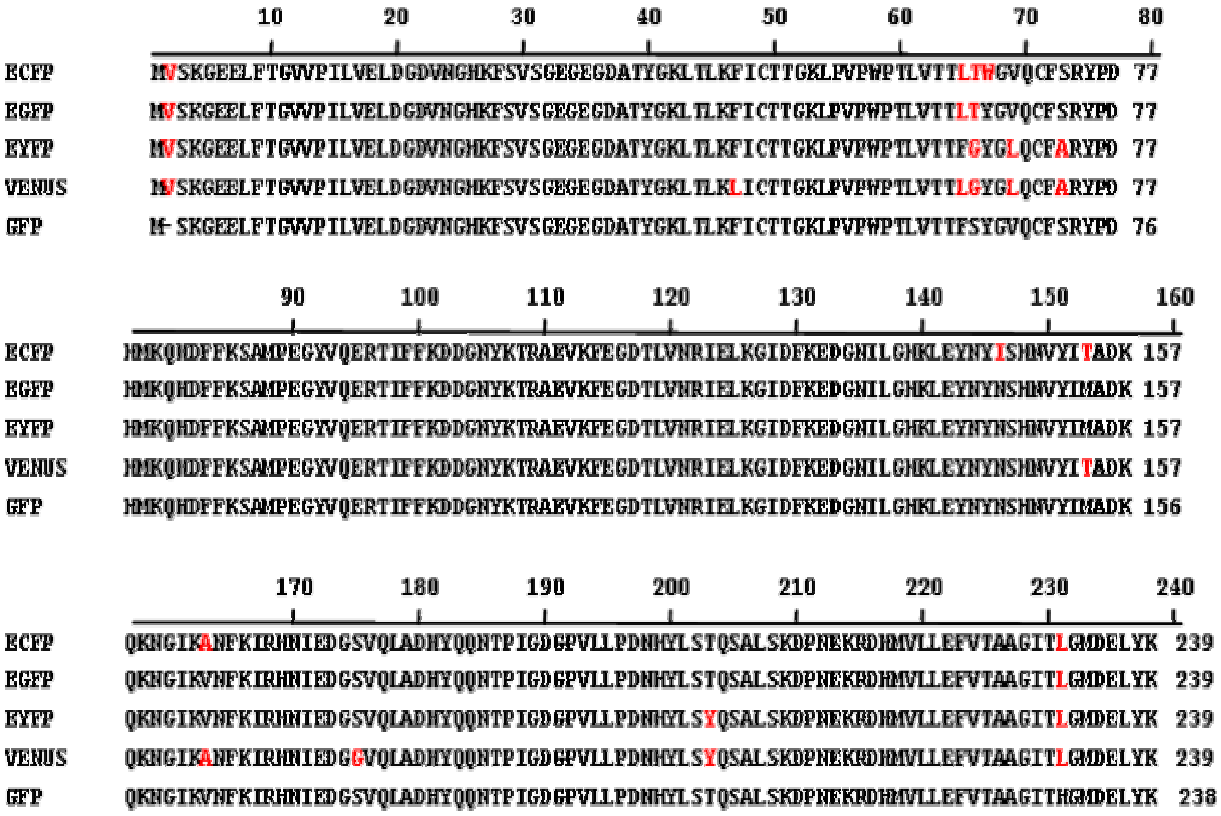

Figure 21: Amino acid alignment of GFP-derived fluorophores

Altered residues are marked in *red*, amino acid sequence as published in: ECFP (clontech), EGFP (clontech), EYFP (clontech), venus (Nagai, Ibata et al. 2002), and GFP (clontech).

6.1.2 FRET

In the last decade, fluorescence resonance energy transfer (FRET) has become an increasingly popular technique for studying protein-protein interaction *in vivo*, complementing a set of *in vitro* techniques like yeast-two hybrid and various pull down techniques. Especially since the development of GFP derived fluorophores suitable for FRET, it became a convenient technique for imaging protein interactions in living systems (Milligan, Ramsay et al. 2003; Hebert, Gales et al. 2006).

FRET is a phenomenon which has first been discovered by Theodor Förster (1946). He found that energy can be transferred without radiation between an excited donor molecule (D*) to an acceptor molecule (A).

$$D + h\nu_1 \rightarrow D^*$$

$$D^* + A \rightarrow A^* + D$$

$$A^* \rightarrow A + h\nu_2$$

For FRET to occur three conditions have to be fulfilled:

i) The emission spectra for the donor have to overlap with the absorption spectra of the acceptor.

ii) The emission dipole of the donor and absorption dipole of the acceptor must not be perpendicular to each other.

iii) The distance between donor and acceptor has to be below 10 nm.

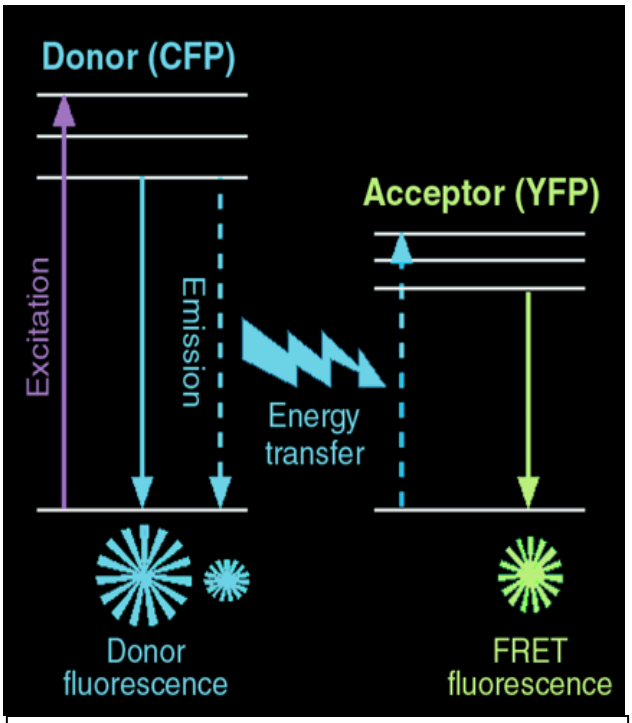

Figure 22: Fluorescene resonance energy transfer (FRET)

Figure adapted from (Siegel, Chan et al. 2000)

The donor is excited at a wavelength that ideally does not excite the acceptor. To get back to its basic energy level, S_0, the excited donor emits fluorescence at a wavelength, which compared to its excitation wavelength is generally shifted to longer wavelengths (Stokes shift). In close

presence of a suitable acceptor, the electromagnetic fields of both fluorophores can interact and the excitation energy can be transferred without radiation to the acceptor, which in turn emits fluorescence at an even longer wavelength (Figure 22).

The sensitivity of FRET as an indicator of proximity between different proteins of interest is due to the fact that the distance between donor and acceptor determines the efficiency of the energy transfer by the sixth power (r^6). Apart from the distance, the FRET efficiency is determined by the spectral overlap integral and the relative orientation of the fluorophores. The spectral overlap integral of any given donor/acceptor pair is constant and if the orientation in a first approximation is considered to be random, the only remaining variant is the distance (Siegel, Chan et al. 2000).

$$E = R_0^6 / \left(R_0^6 + r^6\right)$$

E = FRET efficiency

r = actual radius between donor and acceptor

R_0 = radius where FRET efficiency is ½ E_{max}

(for ECFP/EYFP R_0 = 49-52 Å if randomly orientated)

The FRET efficiency is quantified by mainly four different strategies (Siegel, Chan et al. 2000):

1) Direct FRET: quantification of the difference in acceptor fluorescence emission in the presence and the absence of a donor while exciting with a donor specific wavelength. The advantage of this approach is its intuitive principle and with the choice of appropriate fluorophores an easy data analysis. The drawback is that with currently available GFP-derived fluorophores this strategy can lead to false positive results due to partial overlaps of both excitation and emission spectra of donor and acceptor (spectral cross-talk). Thus, this has to be taken into account during data analysis.
2) Indirect FRET: uses the effect of donor fluorescence quenching during FRET. First, the donor is excited in the presence of the acceptor and donor emission spectra are recorded. The acceptor is then removed from the sample by selectively bleaching it (destroying it), the donor is excited again, and a second emission spectrum is recorded. The difference of donor fluorescence emission can be quantified and expressed in FRET efficiency. The strength of this technique is its more precise estimate of FRET efficiency without the need of accounting for spectral cross-talk. However, a drawback of this method is its time consuming bleaching process, which makes it difficult to perform time-resolved measurements (< min) like e.g. protein interactions after addition of a ligand. Another problem to keep in mind is that bleaching can (depending on the fluorophores) induce

other changes apart from the desired irreversible decrease of acceptor emission. The photo physics of the fluorophores thus require control experiments of the bleaching induced effects in isolated donor and acceptor preparations.

3) FRET efficiencies can also be quantified by measuring changes in donor fluorescence lifetime (FLIM). If FRET occurs, the fluorescence lifetime of the donor is diminished. This difference in decay constants of donor fluorescence emission after short excitation pulses can be quantified. The advantage of this technique is its independence from acceptor related problems like spectral cross-talk (1) and long bleaching protocols (2). Its disadvantage is that for detection of small changes in fluorescence lifetime, a large population of donors has to be measured, which leads to problems of bleaching or decreased time-resolution due to repetitive measurements. Also, FLIM requires special pulsed excitation equipment, normally a pulsed laser with a fairly blue shifted spectrum, and highly time-resolved emission quantification equipment. Both are currently not widely available and expensive.
4) Furthermore, FRET can also be measured using polarized excitation light and quantifying the amount of emission at different angels to the initial excitation. Normal fluorescence should be oriented parallel to excitation light, whereas possible fluorescence due to FRET will be independent of the initial angle. The advantage of this technique is that only one fluorophore is necessary (‘homo FRET’). Its disadvantage is the need for special polarization filter sets (Tramier 2003).

Here, FRET was quantified by acceptor bleaching as explained under (2), mainly because it is a feasible approach when using a regular widefield microscope and it circumvents problems related to spectral cross-talk.

The following acceptor bleaching protocol was applied to quantify FRET efficiencies:

1) Initial fluorescence emission levels of donor and acceptor were recorded ten times.

2) Venus was selectively bleached at 515 nm for 50 x 2 s, after each bleaching step, fluorescence emissions levels were measured.

At the end of the bleaching protocol, venus emission had decreased to about 10% of its initial value. For data analysis, only plasma membrane portions were taken into account by selecting them individually for each cell. To determine the maximal ECFP emission, ECFP emission was

plotted against the respective venus emission. The ECFP emission in the absence of venus fluorescence emission ($F_{venus} = 0$) could then be determined by linear regression analysis. FRET efficiency was calculated as followed:

$$E\% = \frac{\left(F_{ECFP\max} - F_{ECFP\min}\right)}{F_{ECFP\max}} * 100 = \left(1 - \frac{F_{ECFP\min}}{F_{ECFP\max}}\right) * 100$$

with E% = FRET efficiency,

$F_{ECFPmin}$ = ECFP emission before venus photobleaching, mean of ten single measurements before the bleaching protocol,

$F_{ECFPmax}$ = ECFP emission after venus photobleaching, linear regression analysis at $F_{venus} = 0$.

The measured FRET efficiency not only depends on the distance between acceptor and donor but also on the amount of monomeric donors and the amount of donor homo-oligomers (opsin-ECFP with itself). R-ECFP homo-oligomers falsely reduce the measured FRET efficiency due to the fact that they cannot be quenched by venus. They show constant ECFP emission before and after venus photobleaching, which increases the amount of $ECFP_{min}$, and therefore decreases the FRET efficiency. To circumvent the problem of falsely reduced FRET efficiency due to ECFP homo-oligomers, transfections were carried out with a plasmid DNA ratio (ECFP : venus) of 1:4. Before starting the photobleaching protocol, donor : acceptor ratios were determined by comparing emission values of R-venus and R-ECFP. For the final data analysis, only cells with a venus : ECFP ratio of > 1.5 were considered.

R-venus and R-ECFP were coexpressed in HEK293 cells as described (6.3.5). The amount of plasmid DNA and the DNA ratio (ECFP : venus) of 1:4 were kept constant for all transfection. For FRET competition experiments (8.2), the plasmid DNA mixture was constituted of 70% plasmids coding for the competing wildtype protein and 30% plasmids corresponding to the donor/acceptor mix. 24 h post transfection, coverslips were assembled into the custom-built measuring chamber and FRET buffer (128 mM NaCl, 6 mM KCl, 1 mM $MgCl_2$, 5.5 mM glucose, 10 mM HEPES, 1 mM $CaCl_2$, 0.2% BSA, pH 7.4-7.6) was carefully added onto the cells. FRET experiments were carried out using an inverted microscope with a monochromatic light source. The beam path was created by means of a dual reflectivity dichroic mirror, the

objective was a Plan-Apochromat 63x/1.4 objective (Zeiss). Fluorescence emission was filtered and recorded with a 12-bit cooled CCD camera. For ECFP: λ_{exc} = 415 nm, λ_{em} = 460-500 nm (band pass filter) and for venus: λ_{exc} = 515 nm, λ_{em} = 535-580 nm (band pass filter) were used.

6.1.3 Statistical analysis

In vivo FRET data was analyzed with Microsoft Excel by computing FRET efficiencies as means with standard deviation over all bleached cells of the respective experiment with an emission ratio of $\text{venus} : \text{ECFP} > 1.5$. To test for significant differences between resulting FRET efficiencies, Student's T-Test for unpaired, equal variance data was applied. Equal variance was tested before with the F-test. Changes were described as significant when $P < 0.05$.

6.2 Results

DNA for R-venus, R-ECFP and the ECFP-venus fusion proteins was cloned as described, sequenced and amplified. Fusion proteins were transiently overexpressed in COS-1 cells, regenerated with 11-*cis*-retinal, solubilized in DM and purified. Both fusion proteins show typical features of *wt* type rhodopsin: samples kept in the dark had an absorption maximum at 498 nm when fluorophore absorption was subtracted (Figure 23, green lines). After illumination, the absorption maxima shifted to 380 nm, a typical feature of *wt* rhodopsin in its Meta-II state (Figure 19, blue lines).

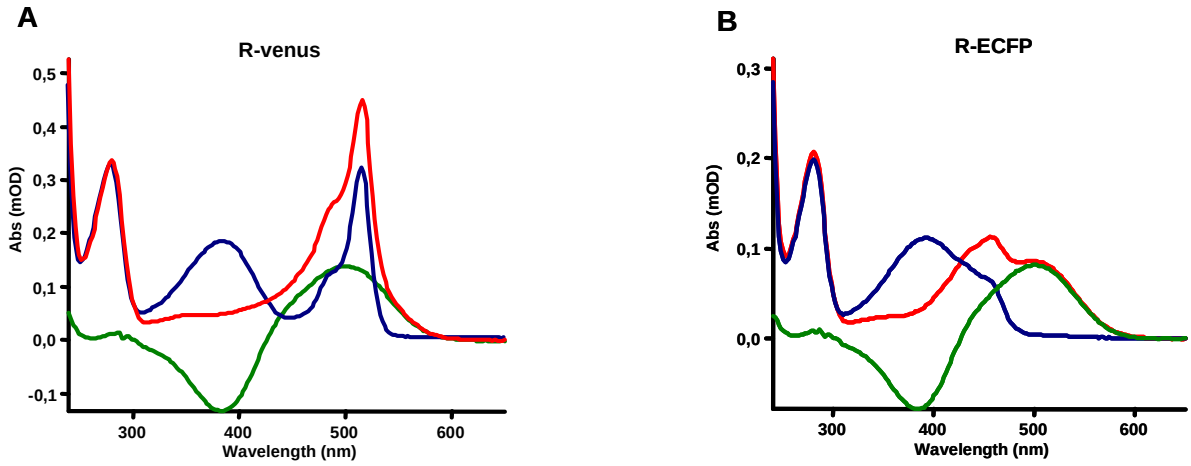

Figure 23: UV/Vis spectra of R-venus and R-ECFP

R-venus and R-ECFP were expressed in COS-1 cell, regenerated with 11-*cis*-retinal and purified as described under 4.3.1. *Red curves* are spectra taken in the dark, *blue curves* are spectra taken after illumination with orange light for 15 s, *green curve*s are difference spectra of dark-light spectra. The shift in absorption from 498 nm (dark state rhodopsin, red curve) to 380 nm (green curve) is a typical feature of *wt* rhodopsin. **A** R-venus shows an additional absorption peak at 515 nm (red and blue curve), which is the absorption maximum of venus. **B** R-ECFP shows maximal absorption at 478 nm (red curve), which is typical for ECFP.

For *in vivo* imaging, HEK293 were imaged 24 h post transfection. Cells expressing R-venus and/ or R-ECFP (Figure 24) showed strong fluorescence in the plasma membrane, furthermore weaker fluorescence in the ER, the Golgi apparatus and some inclusion bodies that might belong to the cellular degradation system. The correct targeting of fusion proteins to the plasma membrane, together with the UV/Vis spectra suggests a close to *wt* rhodopsin function for both constructs.

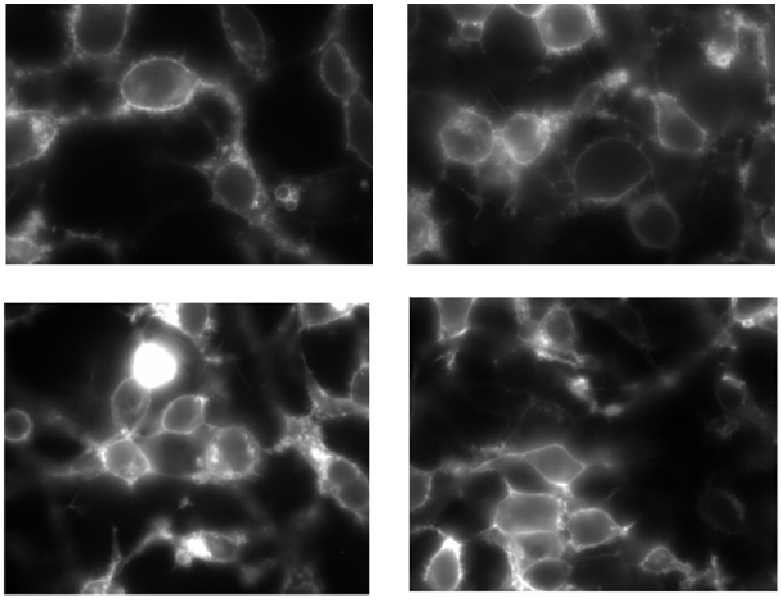

Figure 24: HEK293 cells coexpressing R-venus and R-ECFP

Four typical example pictures of HEK293 cells taken 24 h post transfection with R-venus and R-ECFP. Plasmid constructs, transfection procedure and imaging were as described under 6.1.

To determine the amount of FRET between opsin, cells were cotransfected with R-venus and R-ECFP with a plasmid DNA ratio of 4:1. Cells were imaged *in vivo* applying the acceptor bleaching protocol as described. For each bleaching experiment, all cells in the bleaching field with average expression of the fluorophores were analyzed. For data analysis, venus and ECFP emission of selected plasma membranes were plotted against time to test if the bleaching protocol produced sufficient reduction of acceptor fluorescence. The mean value of all selected cells in the bleaching field was used to calculate the FRET efficiency. To do so, ECFP fluorescence was plotted in dependence of venus emission (Figure 26). The data was fitted with a linear regression, yielding R-ECFP$_{max}$ at $F_{venus} = 0$. FRET efficiency (E%) was calculated with:

$$E\% = \frac{\left(F_{ECFP\,\max} - F_{ECFP\,\min}\right)}{F_{ECFP\,\max}} * 100 = \left(1 - \frac{F_{ECFP\,\min}}{F_{ECFP\,\max}}\right) * 100$$

where $F_{ECFPmin}$ = emission before venus photobleaching, mean of ten single measurements before the bleaching protocol,

$F_{ECFPmax}$ = ECFP emission after venus photobleaching, linear regression analysis at $F_{venus} = 0$.

FRET efficiency for R-venus/ R-ECFP in the plasma membrane of HEK293 cells was measured in nine independent bleaching experiments on different days. Each bleaching experiment contained three to seven cells that were analysed separately. Only cells with normal morphology, moderate expression of fluorophores, a donor : acceptor emission ratio > 1.5, and regular bleaching kinetics were considered. Data was pooled and averaged to give a mean FRET efficiency for each bleaching experiment. All bleaching experiments were averaged giving a FRET efficiency for opsin fusion proteins of **$E\%_{(R\text{-}venus/R\text{-}ECFP)} = 30\% +/- 3.4\%$.**

FRET efficiency not only depends on specific donor/acceptor fusion protein interaction but also reflects - especially in membranes - the amount of coincidental donor/acceptor encounters. The probability of coincidental encounters increases with the amount of expressed proteins. To check to which extent the measured FRET efficiency is a result of coincidental encounters due to receptor crowding in the plasma membrane, FRET was measured in cells exhibiting low overall fluorescence levels (at the detection limit for FRET measurements). This was achieved by decreasing the amount of plasmid DNA and adding pcDNA3 vector (clontech) without an insert during the transfection. Presumably, the pcDNA3 vector uses up parts of the replication capacity of the transfected cells, resulting in a lower amount of fluorescing proteins. Cells were transfected with a transfection cocktail containing 30% plasmid coding for R-venus/R-ECFP (in a 4:1 ratio) and 70% pcDNA3. FRET efficiency of cells expressing R-ECFP and R-venus with pcDNA3 was slightly lower but without statistical relevance (T-test > 5%) (Figure 25). This suggests that the measured FRET efficiency is not due mainly to overexpression and coincidental encounters but it is a product of specific interactions of the apoprotein opsin.

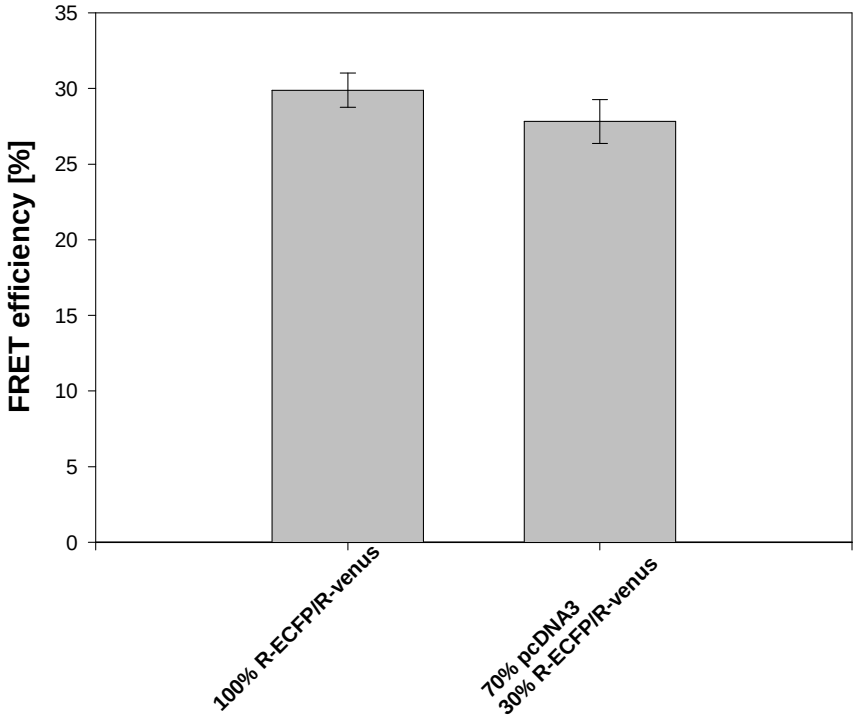

Figure 25: FRET efficiency of opsin

FRET efficiency with standard error for coexpression of opsin-ECFP and opsin-venus (R-ECFP/R-venus) on their own and with 70% pcDNA3.

Additional evidence for specific opsin-opsin interaction would be a negative FRET control. Two approaches are feasible for that purpose:

1) Direct approach: FRET between fluorescently labeled opsin and other, non-interacting labeled membrane proteins could be measured and compared. Even though this strategy seems very straightforward, the interpretation of the data is difficult due to the fact that FRET is dependent on distance and fluorophore orientation, which makes it difficult to compare FRET data of different sized membrane receptors with each other without knowing the precise tertiary structure of the fusion protein.

2) Indirect approach: Untagged membrane receptors could be coexpressed with the labeled opsin donor/acceptor pair. If the FRET efficiency stays constant while coexpressing other non-interacting membrane receptors, this indicates that FRET efficiencies report specific interactions of the apoprotein opsin with itself rather than coincidental encounters. Data from these

competition experiments can be more easily compared because the same donor/acceptor pair is used. This was the main reason for choosing the indirect approach as experimental strategy here.

The difference in FRET efficiency during competition experiments might not only be due to specific interaction but also to different expression levels of the competing membrane proteins. Since it was technically not possible to compare their expression levels by using fluorescently tagged membrane proteins for competition experiments, different expression levels cannot totally be ruled out. However, membrane proteins for competition experiments were selected according to their high expression levels when expressed as fluorophore tagged fusion proteins.
Coexpression of other membrane receptors with opsin were realized in the same 70% : 30% DNA ratio as described for the pcDNA3 vector. For each receptor combination, several bleaching experiments were performed and each bleaching result was analyzed as described above (Figure 26). Results were averaged, and the standard deviation and the standard error were calculated (Figure 27).

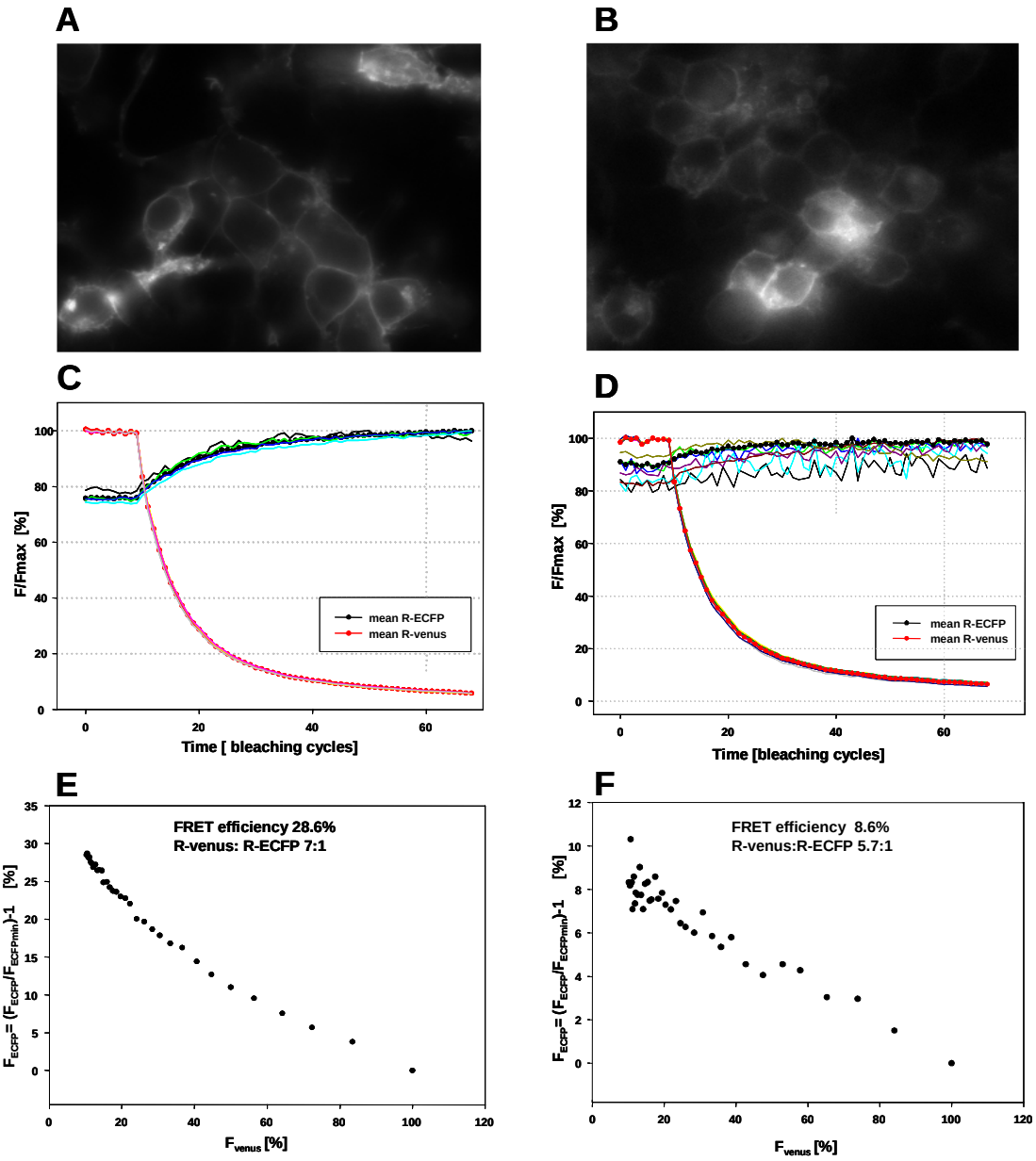

Figure 26: FRET in HEK293 cells coexpressing R-venus and R-ECFP

A, C, E: FRET measurements in HEK293 cells expressing R-venus, R-ECFP and 70% EGFR.

B, D, F: FRET measurements in HEK293 cells expressing R-venus, R-ECFP and 70% opsin.

C+D: Acceptor bleaching protocol: *black circles*: mean R-ECFP emission (dequenching), *red circles*: mean R-venus emission (irreversible destruction due to photo bleaching), *other fine lines*: single cells that were averaged to calculate mean R-venus and R-ECFP emission values.

E+F: ECFP emission plotted in dependence on venus emission, data was analyzed with linear regression to yield ECFP fluorescence in the absence of venus.

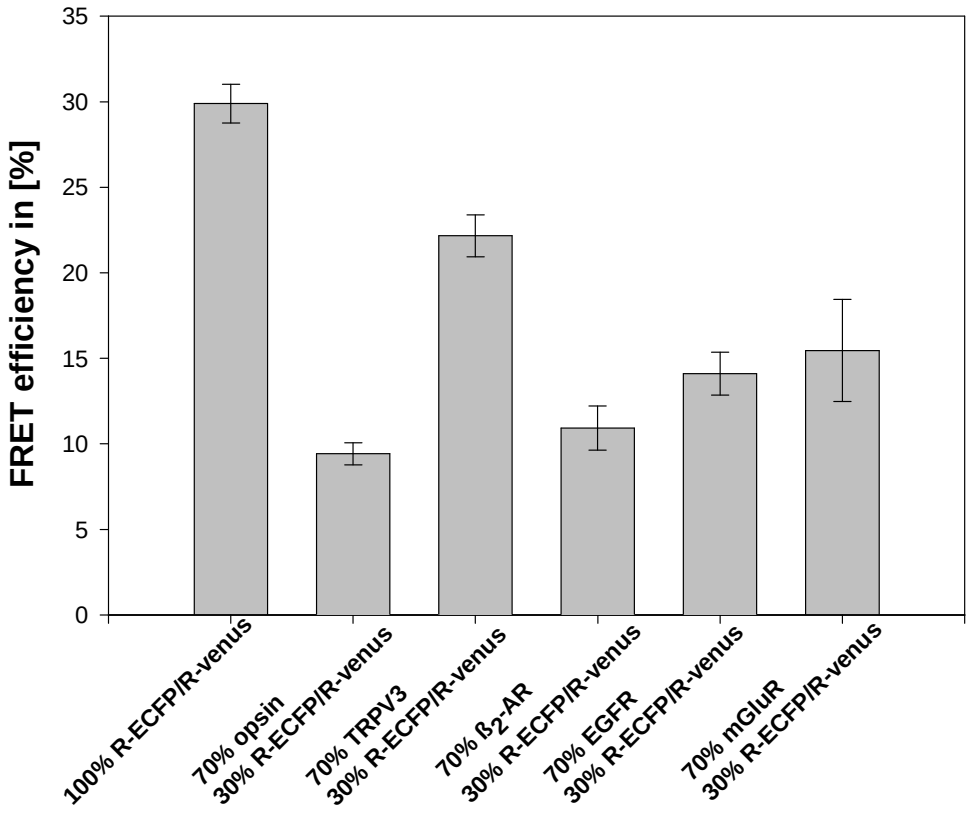

Figure 27: FRET efficiency of opsin for competition experiments with membrane proteins

FRET efficiency with standard error for coexpression of opsin-ECFP and opsin-venus (R-ECFP/R-venus) on their own and with 70% plasmid DNA coding for the named membrane proteins.

As a positive control, unlabeled opsin was used for competition experiments. Opsin should be able to compete with R-venus resulting in significantly decreased FRET levels. As expected, opsin decreased FRET efficiency to about 10%. Interestingly, there is no statistical significant difference between opsin and ß$_2$AR competition, which suggests that other GPCRs such as the ß$_2$-AR have a similar potential to interact with opsin. However, TRPV3, an ion channel from the TRP family, was significantly less able to decrease FRET efficiency to the extent opsin and the ß$_2$- AR did. Furthermore, EGFR, a tyrosine kinase, and mGluR, a class C GPCR, were used for competition experiments. Both of them did not differ significantly in their ability to decrease FRET efficiency in comparison to opsin as competitor. In the light of possible GPCR heterodimerization and structural similarities within the GPCR family, this is not so surprising for

the metabotropic glutamate receptor. However, the efficient competition with EGFR is unexpected as there is no known interaction between GPCRs and EGFR.

So far, helices IV and V (Liang, Fotiadis et al. 2003) as well as helices I, II and VIII (Salom, Lodowski et al. 2006) have been suggested as rhodopsin dimerization interface. The competition FRET approach was used here to further investigate the dimerization interface. Opsin fragments (Figure 28) were generated following published fragmentation sites (Struthers, Yu et al. 1999; Yu and Oprian 1999) and coexpressed with R-venus/R-ECFP to measure FRET. Opsin fragments were further fused to venus to check their expression levels as well as their targeting to the membrane (Figure 29).

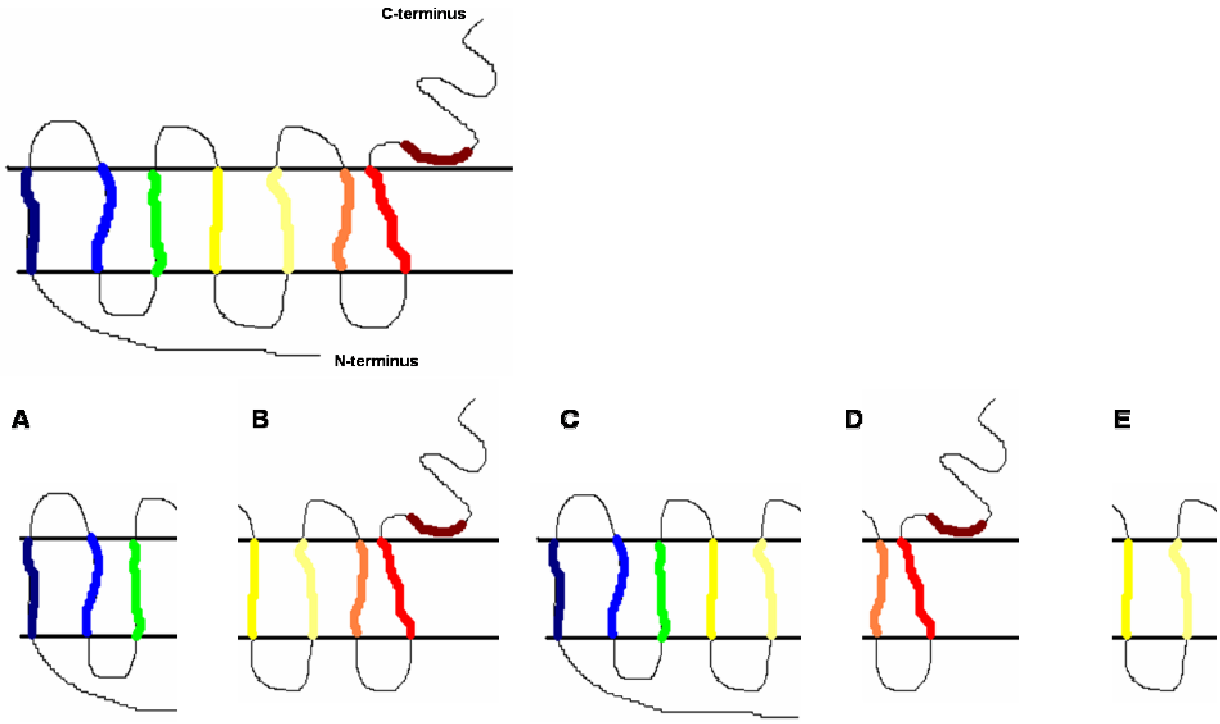

Figure 28: Opsin fragments for competition experiments

Top: Rhodopsin with its 7 transmembrane helices, the 8th helix is situated parallel to the membrane.
Bottom: Opsin fragments used in competition experiments are shown in A-E.
A: opsin(1-146); **B:** opsin(147-348); **C:** opsin(1-240)**; D:** opsin(241-348); **E:**opsin(147-240)

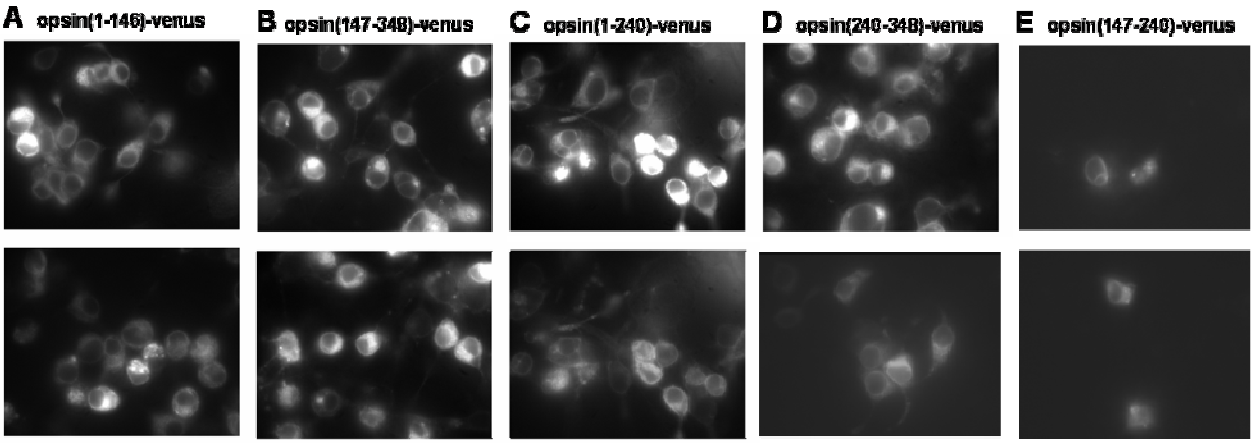

Figure 29: HEK293 cells expressing opsin fragments fused to venus

Typical pictures of HEK293 cells 24 h post transfection with plasmids coding for opsin fragments fused to venus. Plasmid constructs, transfection procedure and imaging were as described under 6.1.

Opsin(1-146)-venus, opsin(147-348)-venus, opsin(1-240)-venus, opsin(241-348)-venus and opsin(147-240)-venus were all cloned, sequenced and amplified for transfection experiments. Apart from opsin(147-240)-venus, all fragment fusion proteins could be equally well expressed and showed similar distribution within the cell (mainly plasma membrane and ER). Opsin(147-240)-venus showed overall reduced fluorescence, which also seemed to be localized mainly in the ER and the nuclear envelope. It is possible, however, that expression and targeting of opsin fragments fused to venus is different compared to untagged opsin fragments. One possible reason could be that folding and targeting in unlabeled opsin fragments might be less severely impaired than in opsin fragments fused to venus.

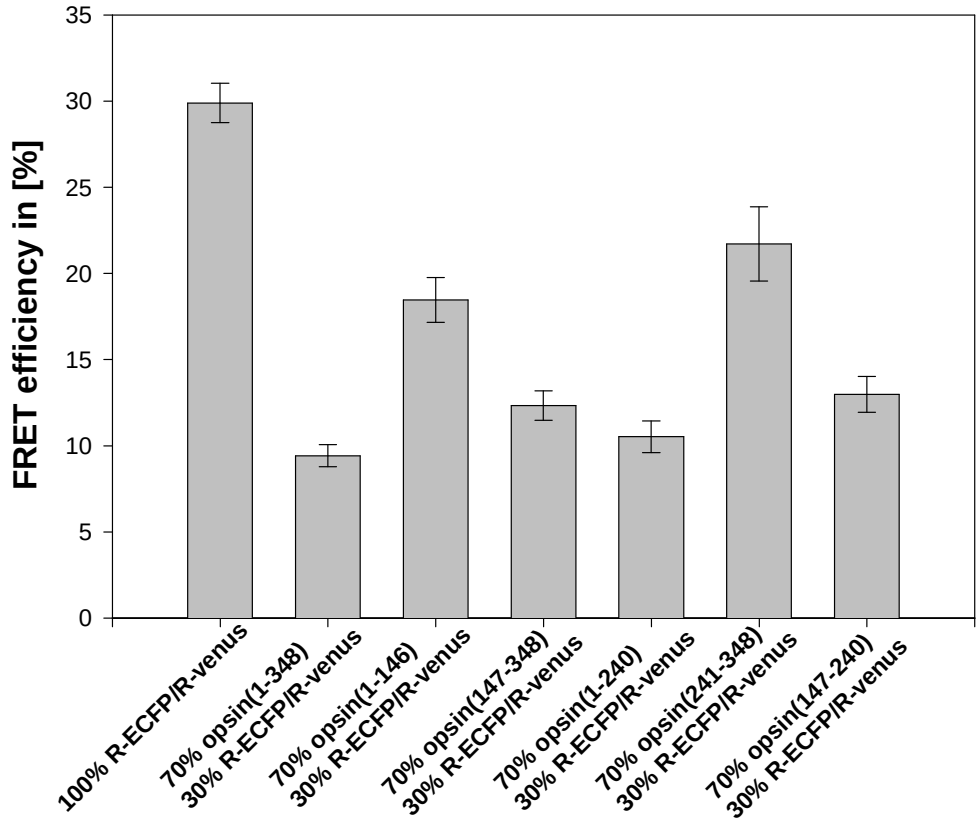

Figure 30: FRET efficiency of opsin for competition experiments with opsin fragments

FRET efficiency with standard error for coexpression of opsin-ECFP and opsin-venus (R-ECFP/R-venus) on their own and with 70% plasmid DNA coding for the named opsin fragments.

FRET results from opsin fragment competition experiments (Figure 30) showed that opsin(147-348) and opsin(1-240) are especially competent competitors, lowering FRET efficiency of R-venus/R-ECFP to 12% for opsin(147-348) and 11% for opsin(1-240). Opsin(1-146) and opsin(241-348) were significantly less competent in decreasing FRET efficiencies of R-venus/R-ECFP.

Both opsin(147-348) and opsin(1-240) contain helix IV and V. Therefore, the data is in good agreement with results from molecular modelling, which also suggested TM domains IV and V as dimerization interface of rhodopsin (Liang, Fotiadis et al. 2003).

FRET efficiency of competition experiments

	Mean	Standard deviation	Standard error of the mean	Number of bleaching experiments
R-venus/R-ECFP (100%)	30	3.4	1.14	9
pcDNA3 (70%) **R-venus/R-ECFP (30%)**	28	4.4	1.45	9
venus-ECFP	36	5.1		3
opsin (70%) **R-venus/R-ECFP (30%)**	9	2.0	0.64	10
opsin(1-146) (70%) **R-venus/R-ECFP (30%)**	18	6.1	1.30	22
opsin(147-348) (70%) **R-venus/R-ECFP (30%)**	12	3.9	0.85	21
opsin(1-240) (70%) **R-venus/R-ECFP (30%)**	11	3.4	0.91	14
opsin(241-348) (70%) **R-venus/R-ECFP (30%)**	22	6.8	2.15	10
opsin(141-240) (70%) **R-venus/R-ECFP (30%)**	13	4.9	1.04	22
TRPV3 (70%) **R-venus/R-ECFP (30%)**	22	3.9	1.23	10
ß$_2$AR (70%) **R-venus/R-ECFP (30%)**	11	4.5	1.29	12
EGFR (70%) **R-venus/R-ECFP (30%)**	14	5.0	1.25	16
mGluR (70%) **R-venus/R-ECFP (30%)**	15	6.7	2.98	5

6.3 Discussion

Overall, it can be said that coexpression of R-venus with R-ECFP in HEK293 yields a high FRET efficiency of about 30% in the plasma membrane. This is in good agreement with previously measured FRET in COS-1 cells (Kota, Reeves et al. 2006) and asolectin liposomes (Mansoor, Palczewski et al. 2006). The measured FRET efficiency is close to the FRET efficiency for when venus is directly fused to ECFP (36%). Taking into account that FRET is highly dependent on the distance of acceptor to donor (r^6), this suggests that dimerization efficiency of opsin is very high. In addition to that, the FRET efficiency does not show a strong dependency of expression levels of the fluorophore as shown by coexpressing pcDNA3 to lower fusion protein expression. The lack of strong concentration dependence of the measured FRET efficiencies suggests a specific receptor interaction rather than receptor crowding. However, unfortunately the concentration dependence could not be quantified. Furthermore, FRET efficiency can be competed efficiently by coexpression of untagged opsin, which is a clear indication that FRET does not occur due to donor/acceptor affinity. FRET efficiency can be significantly reduced with related membrane proteins such as the class A GPCR ß$_2$-AR and class C GPCR mGluR but also with the tyrosine kinase EGFR. This is an unexpected result, however, recent literature on EGFR/GPCR crosstalk during signal transduction might be an explication (Thomas, Bhola et al. 2006) (Fischer, Hart et al. 2003). So far though, none of these interactions were reported to be directly between EGFR and GPCR.
Nevertheless, coexpression of TRPV3 receptor as negative FRET control did not significantly decrease FRET efficiency even though it is well expressed and efficiently targeted to the plasma membrane of HEK293 cells (Hellwig 2005).
Competition experiments with opsin fragments showed that fragments containing helix IV/V decreased FRET efficiency almost as much as *wt* opsin, suggesting that helix IV or/and V might be important for dimerization. However, a general drawback of the FRET strategy is its poor control over expression levels of the competition proteins. Thus, it cannot be completely ruled out that at least parts of the change in FRET efficiency is due to different expression levels of the proteins.

It remains to be elucidated if rhodopsin shows the same FRET efficiency as its apoprotein opsin. Due to rhodopsin's light sensitivity and the low time-resolution of the acceptor bleaching

protocol, FRET measurements of R-venus/R-ECFP regenerated with *11-cis retinal* do not produce meaningful data. The use of light insensitive ligands did not show a significant change in FRET efficiency in comparison to opsin (data not shown). Since regeneration efficiency with light insensitive retinals is low and the amount of added retinal is limited due to its cell toxicity, it cannot be ruled out that a mixed population of regenerated opsin and apoprotein was measured.

Furthermore, it would be interesting to quantify the distance between two opsins. To be able to do so, it is necessary to differentiate between dimerization efficiency and the distance between two partners. Furthermore, the position of the fluorophores relative to each other is conveniently assumed to be random. This might be an erroneous assumption for oriented membrane proteins. Thus, this distance of donor and acceptor is not easily accessible from FRET experiments. However, the fact that directly linked fluorophores venus-ECFP showed only slightly higher amounts of FRET than opsin fusion proteins with each other, strongly suggests that opsin dimers might be closely packed and almost completely present as dimers.

7 PROPERTIES OF SOLUBILIZED RHODOPSIN

7.1 Fluorescence resonance energy transfer (FRET) experiments

7.1.1 Method

For FRET analysis, emission spectra of 0.55 µM coexpressed and purified R-venus and R-ECFP fusion proteins were measured under the same buffer and detergent conditions as G_t activation for *wt* rhodopsin (9.3). As a positive FRET control, a fusion protein between ECFP and venus was expressed, purified and measured under the same conditions as the R-venus / R-ECFP mixture.
All spectra were recorded with a SPEX fluorolog II spectrofluorometer. For ECFP and FRET spectra, the sample was excited at 420 nm while recording emission between 450 and 600 nm. Venus spectra were recorded between 520 and 600 nm while exciting at 510 nm. Fluorescence emission was recorded at scan steps of 1 nm. To determine FRET, R-ECFP spectra were compared to spectra of coexpressed R-ECFP and R-venus. Direct excitation of R-venus by the 420 nm excitation beam in the R-ECFP/R-venus sample was accounted for with the following procedure:
1) The emission spectrum of the R-venus only sample (excitation at 420 nm) was scaled to the amount of venus present in the R-ECFP/R-venus mixture by comparing maximal venus emission at 530 nm (excitation at 510 nm).
2) The scaled R-venus emission spectrum (excitation at 420 nm) was then subtracted from the emission spectrum of the R-ECFP/R-venus mixture (excitation at 420 nm). The difference spectrum of the corrected R-ECFP/R-venus spectrum and the R-ECFP spectrum (matched to the peak height at 480 nm) yields the emission due to FRET.
The same procedure was then applied to the spectra of the ECFP-venus fusion protein (positive control).

FRET was also measured in membrane samples. COS-1 cell membranes expressing R-venus, R-ECFP or an R-venus /R-ECFP mixture were purified as described under 4.3.4. The purified membrane samples were not regenerated with 11-*cis*-retinal, thus all measurements were carried out with opsin fusion proteins. The described FRET protocol was applied to the opsin fusion

protein samples and repeated after the addition of increasing amounts of DM (0.01% (w/v), 0.03%, 0.1% and 1%).

7.1.2 Results

For FRET in solubilized samples, R-ECFP and R-venus were coexpressed in COS-1 cells, solubilized and purified as described (9.1.1). The coexpressed samples had absorption spectra that were the sum of rhodopsin, venus and ECFP absorption spectra (Figure 23). When illuminated, the samples showed a shift in absorption to 380 nm (Figure 23), which is typically due to Meta II formation in *wt* rhodopsin. Its transducin activation capacity (see 6.4.1) was comparable to *wt* rhodopsin (data not shown). Taken together with *in vivo* experiments (6.2), there is no indication that R-venus and R-ECFP show compromised rhodopsin function. They seem to be produced, processed and transported to the cell membranes equally well as *wt* rhodopsin. This suggests an intact secondary and tertiary structure and thus also a quaternary structure comparable to *wt* rhodopsin.

After the described solubilization and purification process of coexpressed R-venus/R-ECFP, no emission peak at 530 nm was detectable when exciting at 420 nm (ECFP/FRET excitation conditions) (Figure 31 and 32). After accounting for direct excitation of R-venus at 420 nm, the spectra of the coexpressed sample were an almost perfect overlay to spectra of R-ECFP on its own (Figure 32, blue curve). However, for the positive control FRET experiment, the fusion protein ECFP-venus did show strong FRET fluorescence emission at 530 nm, even after accounting for direct excitation of venus at 420 nm (Figure 32, green curve).

Thus, there is no FRET detectable for purified R-venus/R-ECFP fusion proteins in 0.01% DM for rhodopsin concentrations up to 0.55 µM. It can therefore be concluded that under the chosen conditions, solubilized rhodopsin fusion proteins have no tendency to form dimeric/oligomeric structures and seem to be present as monomers. There is no indication that this should be otherwise for solubilized *wt* rhodopsin.

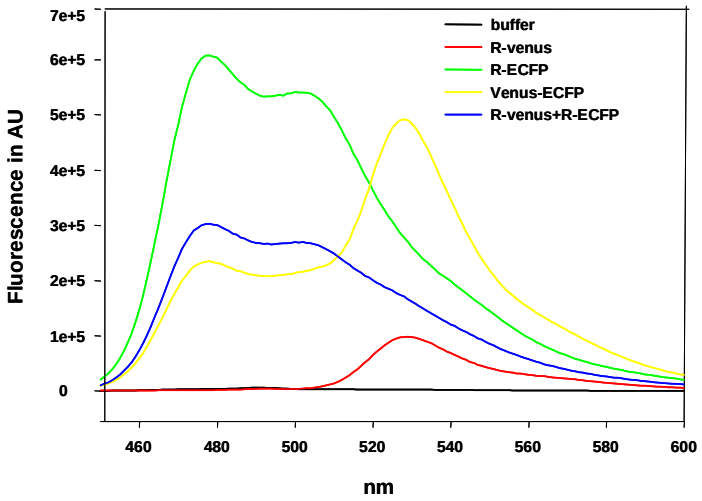

Figure 31: FRET measurements of solubilized R-ECFP / R-venus mixture in 0.01% DM

R-ECFP and R-venus were coexpressed, reconstituted with 11-*cis*-retinal and immunoaffinity purified as described in 4.3.1. Rhodopsin concentration was 0.55 µM with 0.01% (w/v) DM, 20 mM BTP, 130 mM NaCl, 1 mM $MgCl_2$, pH 7.5 at 20°C.

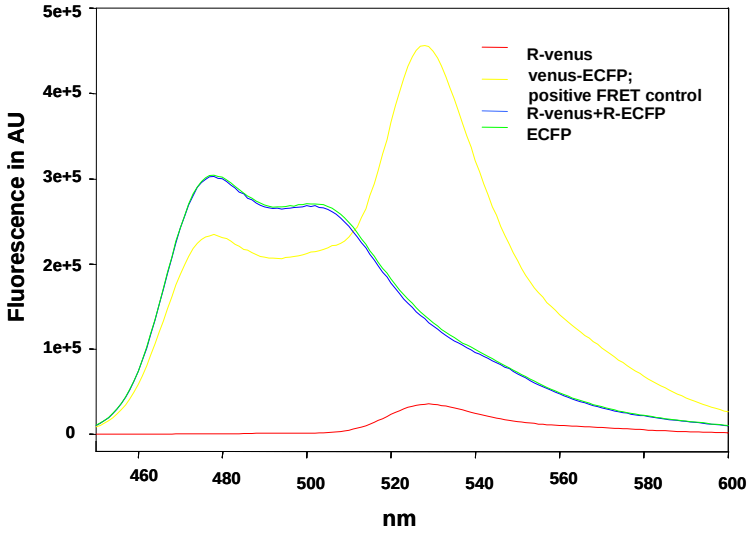

Figure 32: Normalized FRET spectra

Data from Figure 31 normalized as described under 7.1.1.

As a further positive control, membrane preparations of COS-1 cells were prepared as described under 4.3.4. In the case of membrane samples of COS-1 cells coexpressing R-venus and R-ECFP, a FRET signal at 530 nm was detectable, which disappeared gradually as increasing amounts of DM were added to the membrane sample (Figure 33 and 34). At the same time, ECFP emission was gradually dequenched as shown in Figure 35 (emission increase at 478 nm, red squares). At

1% DM, the emission spectra of coexpressed R-venus/R-ECFP were identical to R-ECFP control spectra, thus no FRET emission could be detected anymore at 530 nm. This suggests, especially taken together with FRET experiments *in vivo* (see 6.1-6.3), that DM leads to a disruption of the quaternary structure of opsin maintained in the plasma membrane and agrees with the notion that solubilized rhodopsin is of monomeric nature.

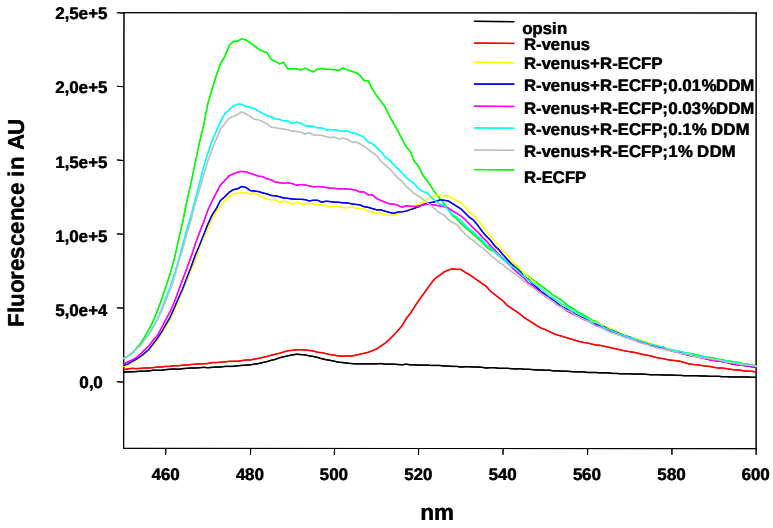

Figure 33: FRET emission spectra in COS-1 membranes

Raw data of emission spectra of membrane preparations of COS-1 cells coexpressing R-venus and R-ECFP; membrane preparations of R-venus, R-ECFP and opsin on their own were used as control emission spectra. Increasing amounts of DM (final concentration) were added to the samples as indicated.

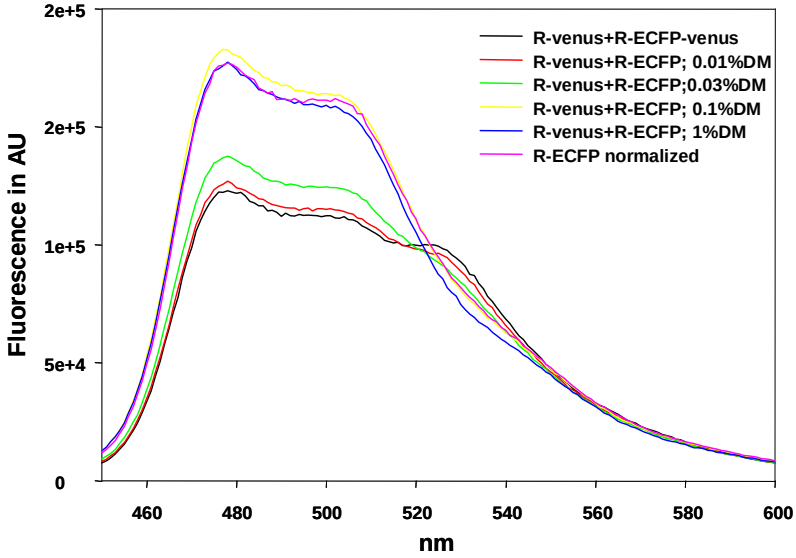

Figure 34: Normalized FRET emission spectra in COS-1 membranes

Emission spectra of Figure 33 normalized as described under 7.1.1.

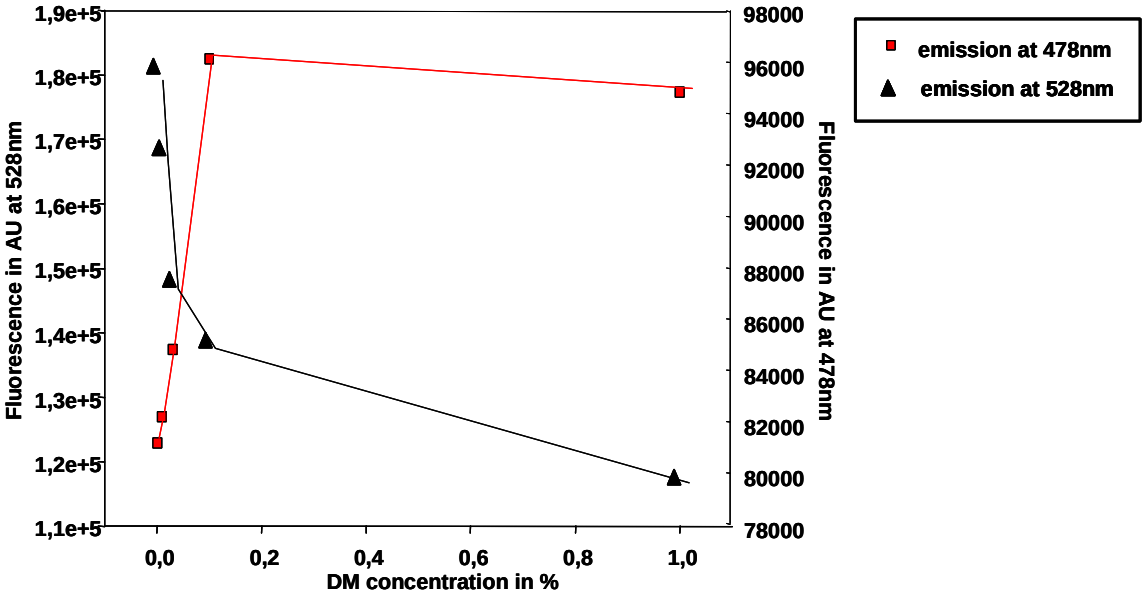

Figure 35: FRET decrease upon addition of DM to COS-1 cell membranes

Black triangles: venus emission at 528 nm while exciting at 420 nm in dependence on added DM (final concentration). *Red squares*: ECFP emission at 478 nm while exciting at 420 nm; data taken from normalized spectra as plotted in Figure 34.

7.1.3 Discussion

The FRET data acquired from membrane samples of COS-1 cells coexpressing R-venus and R-ECFP is in good agreement with *in vivo* FRET data from HEK293 cells as described in 6.1-6.3. Furthermore, it also agrees with data from COS-1 cells experiments by Kota et al. (Kota, Reeves et al. 2006), which found strong FRET emission at 530 nm when looking at whole COS-1 cells coexpressing opsin-YFP and opsin-CFP fusion proteins. However, their emission ratio YFP:CFP under FRET excitation conditions is higher than what could be measured here for COS-1 cell membrane samples. This might be due to different expression conditions but also to differences in sample preparation. Instead of membrane sample, Kota et al. used a solution of whole cells to measure FRET. In whole cell samples, it is impossible to distinguish FRET from the ER or Golgi from FRET in the plasma membrane. Depending on the amount of overexpression, this can lead to very strong FRET signals due to protein crowding in the ER and the Golgi.

The fluorescence spectra of solubilized opsin-ECFP/opsin-venus fusion proteins show no FRET in 0.01% DM up to rhodopsin concentrations of 0.55 µM. The data is in agreement with gel filtration experiments from Jastrzebska et al. (Jastrzebska, Maeda et al. 2004) that show that in the absence of a crosslinking agent, rhodopsin elutes as monomer during size exclusion

chromatography. However, it contradicts data from transmission microscopy (Jastrzebska, Fotiadis et al. 2006), which shows that in 3 mM DM rhodopsin is present as a mix of monomer and dimers. A possible explanation for this could be that rhodopsin samples for transmission microscopy were only solubilized and did not undergo the purification process described here (see 4.3.1). It might well be possible that a combination of solubilization and immunoaffinity purification is necessary to disrupt the dimeric/oligomeric quaternary structure of rhodopsin.

The data also disagrees with gel filtration and sucrose gradient sedimentation experiments published by Medina et al (Medina, Perdomo et al. 2004). They show evidence for a dimeric composition of rhodopsin for its dark as well as for its light-activated state by comparing the hydrodynamic properties (elution time) of solubilized rhodopsin to the properties of various soluble proteins of known molecular mass. However, these findings have been questioned by Chabre and le Maire (Chabre and le Maire 2005) because of the use of soluble proteins for size calibration. Due to the unknown hydrodynamic properties of the rhodopsin-detergent complex, this might yield a false size estimate.

7.2 Rhodopsin titration

7.2.1 Methods

Rhodopsin's ability to activate its cognate G protein was measured via the fluorescence dequenching of Gα upon GTP binding as described in 4.4.1. Rhodopsin concentration was varied from 0.1 nM to 500 nM while the G_t concentration was kept constant. G_t activation rates were measured under the following conditions: 5.8 µM G_t, 50 µM GTPγS, 1.5 mM GDP, 20 mM BTP, 130 mM NaCl, 1 mM $MgCl_2$, 0.01% DM, pH 7.5, 20°C in a final volume of 650 µl. All reagents were added to the measuring cuvette and allowed to adjust to 20°C while undergoing constant stirring for 4 minutes. To be able to measure G_t activation at high rhodopsin concentrations, 1.5 mM GDP (final concentration) was added to all measurements. GDP competes with GTP for binding at G_t, thus slowing down activation rates (Heck and Hofmann 2001). G_t activation rates measured in the presence of GDP can therefore not be compared with rates measured in the absence of the competitor GDP. However, since the GDP / G_t relation is kept constant within one set of experiments, rates can be compared to each other. Activation rates were calculated from the initial rise in fluorescence by linear regression analysis as described in (6.4.1).

7.2.2 Results

The initial slope of fluorescence increase was fitted with a linear regression as shown in Figure 36 (B and D). With the maximal amount of fluorescence increase (F_{total}) after addition of excess rhodopsin, the increase in fluorescence (F/t) was transferred into G_t activation rates (G_t*/t) with:

$$\frac{F}{t} \cdot \frac{G_{t(total)}}{F_{(total)}} = \frac{G_t^*}{t}$$ (see 4.4.1).

For low rhodopsin concentrations, the fit runs through zero (Figure 37, *left panel*). For higher rhodopsin concentrations (50 nM to 600 nM), the linear fit with y = mx+n yields a value for n different from 0 (Figure 37, *right panel*). Given that in the absence of rhodopsin, fluorescence levels were constant (which proves that no rhodopsin impurities are present in the G_t preparation), this is rather unexpected. The reason probably lies in a systematic underestimation of G_t activation rates due to the velocity of G_t activation, which reaches the detection limit of the used spectrophotometer at high rhodopsin concentrations (Figure 36 C and D). Also, the linear

range of the fluorescence increase decreases with growing enzyme concentration, making it increasingly difficult to analyze.

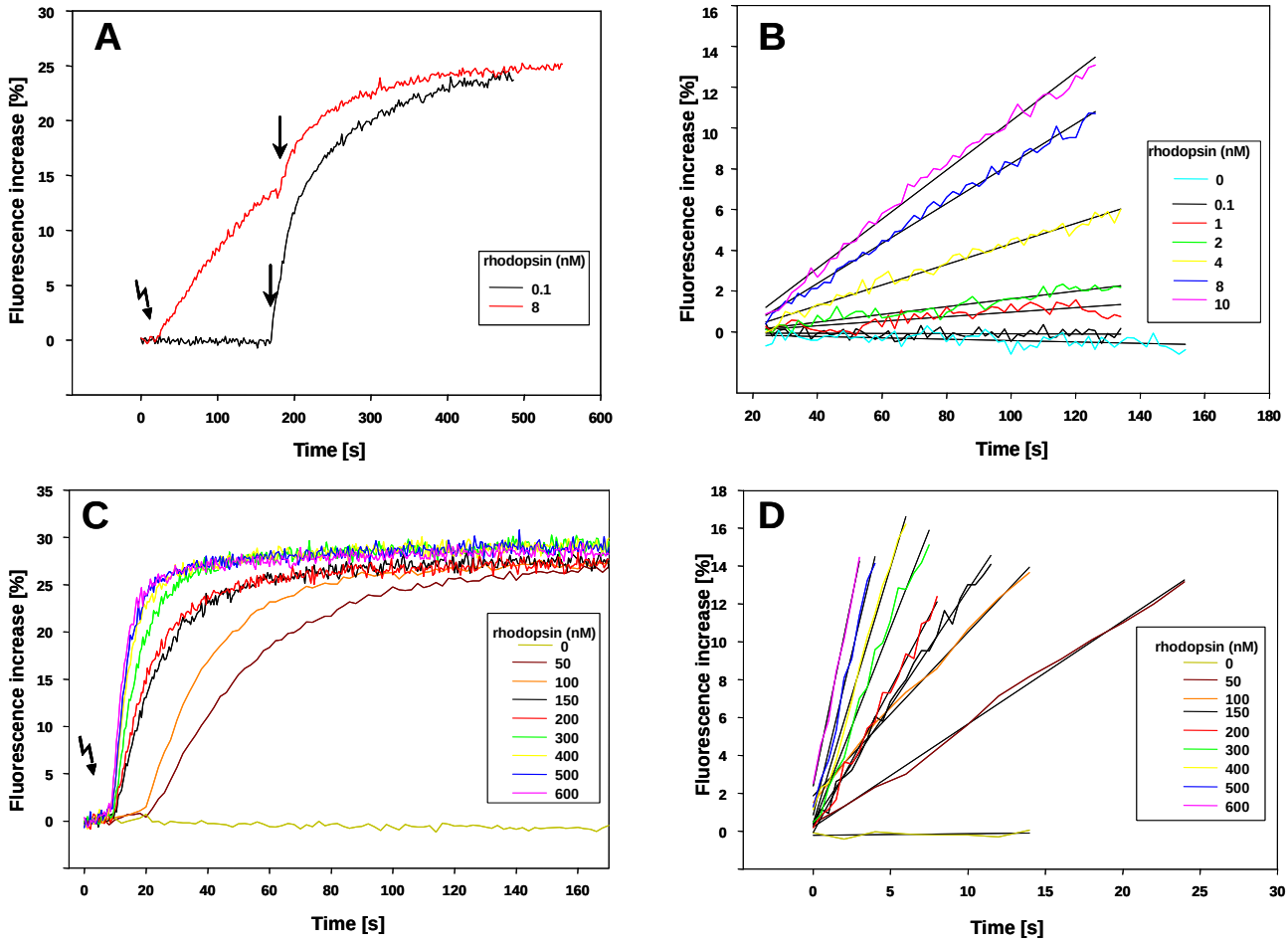

Figure 36: G_t activation upon binding of GTPγS at increasing rhodopsin concentrations

Rhodopsin concentration was varied as indicated in **A-D**, G_t concentration was kept constant at 5.85 µM with 1.5 mM GDP, 50 µM GTPγS, 20 mM BTP, 130 mM NaCl, 1 mM $MgCl_2$, 0.01% DM, pH 7.5, 20°C in a final volume of 650 µl

A and **C**: Fluorescence emission in % of basal fluorescence level plotted in dependence on time. *flash symbol:* rhodopsin activation is started by orange light, *arrow:* addition of 50 nM *wt* rhodopsin. **B** and **D**: linear regression analysis of initial fluorescence increase, legend refers to rhodopsin concentration.

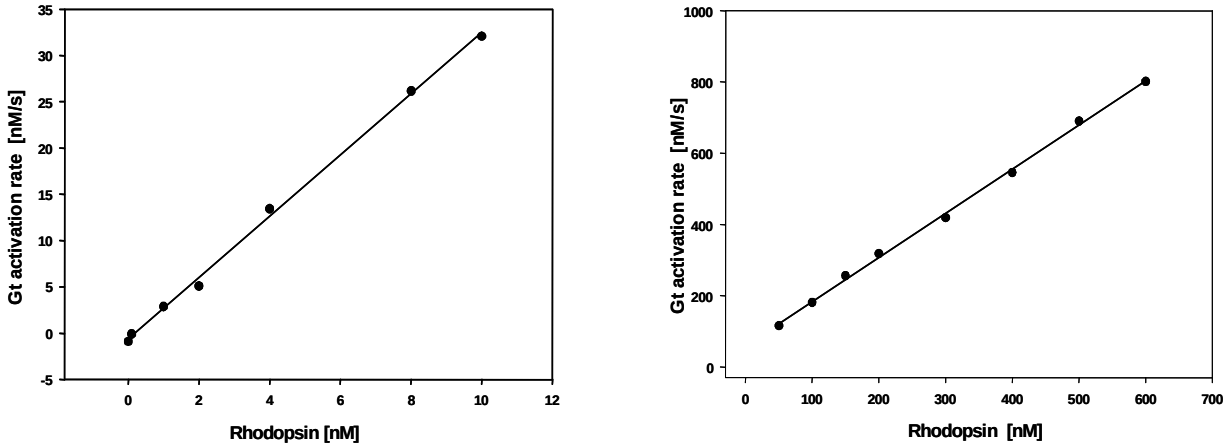

Figure 37: G_t activation rates in dependence on rhodopsin concentration

G_t concentration was kept constant at 5.85 µM with 1.5 mM GDP, 50 µM GTPγS, 20 mM BTP, 130 mM NaCl, 1 mM $MgCl_2$, 0.01% DM, pH 7.5, 20°C in a final volume of 650 µl. Gt activation rates were determined from linear regression analysis (Figure 36) as described under 4.4.1. **Left panel**: Gt activation rates for low rhodopsin concentrations (0.1-10 nM), **right panel**: Gt activation rates for high rhodopsin concentrations (50-600 nM).

However, the data shows that at constant G_t concentration, the initial rise in fluorescence emission –and thus G_t activation rates– grows linearly with rhodopsin concentration over a wide concentration range between 0.1 nM and 500 nM. This indicates that at least in the nanomolar range rhodopsin shows a constant G_t activation rate.

7.2.3 Discussion

The linear dependence of G_t activation on rhodopsin concentration is in good agreement with previously measured G_t activation rates for low nanomolar amounts of rhodopsin in the absence of GDP (Olaf Fritze, dissertation (2006)). The linear proportionality between activation rates and rhodopsin concentration allows the deduction of the catalytical capacity of a single rhodopsin. However, it cannot be deduced that the quaternary structure does not influence rhodopsin's ability to activate its G protein, since our FRET data indicates that rhodopsin in 0.01% DM is a monomer up to 0.55 µM.

7.3 Transducin activation assay

7.3.1 Method

Rhodopsin's ability to activate its cognate G protein was measured via the fluorescence dequenching of Gα upon GTP binding as described in (4.4.1). G_t concentrations were varied between 33 nM and 55 µM while keeping rhodopsin concentration constant at 1 nM. Activation rates were measured under the following experimental conditions: 200 µM GTPγS, 20 mM BTP, 130 mM NaCl, 2 mM DTT, 1 mM $MgCl_2$, 0.01% (w/v) DM, pH 7.1, 20°C in a final volume of 100 µl. All samples were mixed thoroughly, transferred to the measuring cuvette, and equilibrated for 4 min at 20°C. For each G_t concentration, G_t activation rates were determined twice. The whole set of experiments was repeated with different G_t and rhodopsin preparations. Data of both sets of separate experiments was used to calculate G_t activation rates via linear regression analysis of the initial slope as described under 4.4.1. To be able to precisely determine maximal activation rates, the exact amounts of functional G_t was measured by titrating it with known amounts of GTPγS (see 4.3.3). GTPγS concentration was determined by UV/Vis spectroscopy with ε_{253}= 13700 $M^{-1}cm^{-1}$.

7.3.2 Results

G_t activation rates were measured for two different G_t and rhodopsin preparations at G_t concentration between 33 nM and 55 µM (Figure 38 and 39). Interestingly, reaction velocity decreased at high µM G_t concentrations. This could be caused by agglomeration of G_t at high µM concentrations, which then cannot be activated by rhodopsin. This explanation seems plausible considering that with higher G_t concentration final fluorescence levels also decreased, which suggests that only a part of the G_t pool could be activated. For further data analysis, only G_t activation data up to a concentration of 11.7 µM was considered.

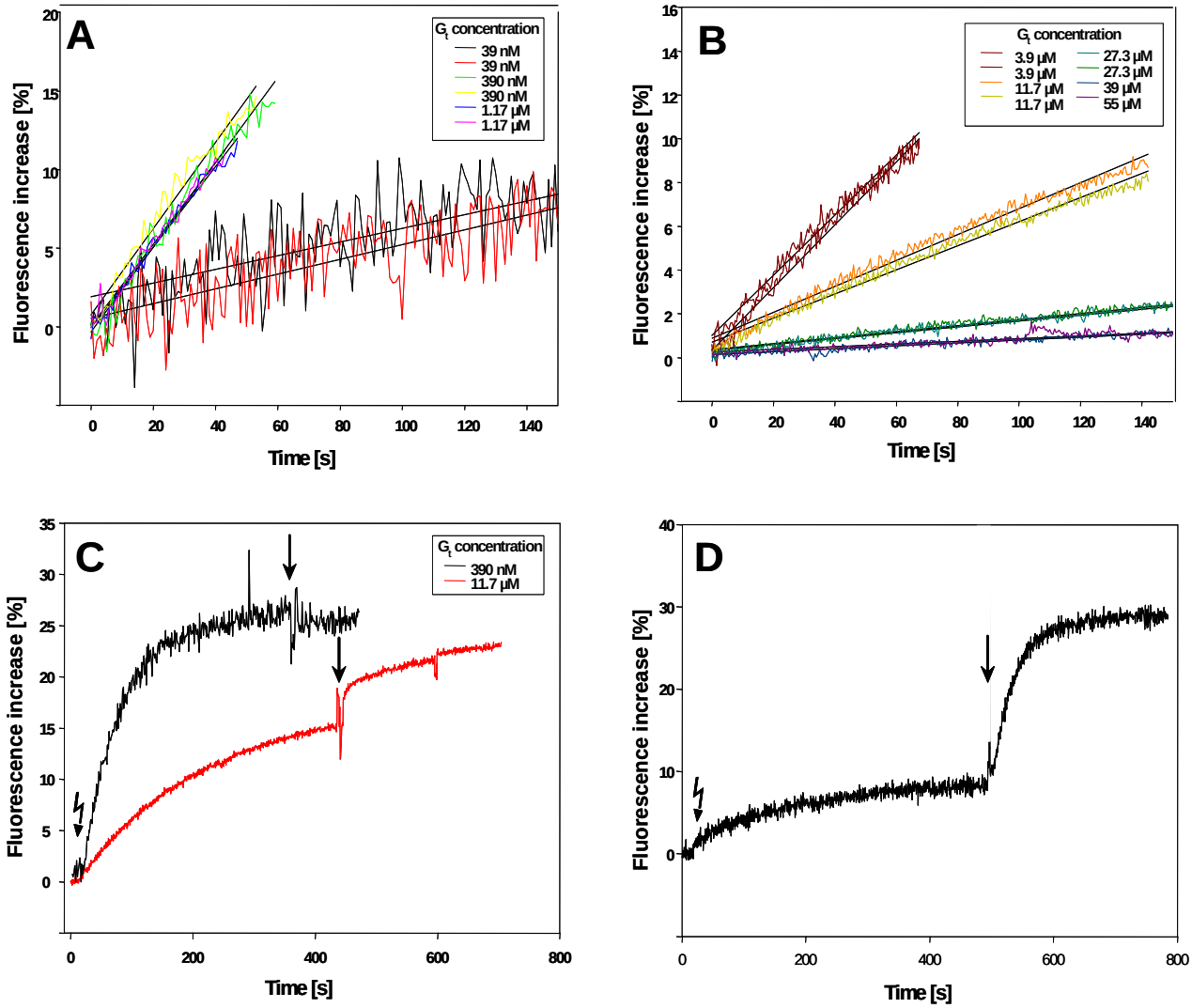

Figure 38: G_t activation upon binding of GTPγS at increasing G_t concentrations (1)

A and **B**: linear regression of initial slope of fluorescence increase, legend refers to G_t concentrations. **C**: examples of original traces (normalized to basal fluorescence level, dilution artefacts due to addition of *wt* rhodopsin were accounted for), *flash symbol*: reaction was started with orange light, *arrows*: addition of 50 nM *wt* rhodopsin; **D**: GTPγS titration to determine G_t concentration; flash symbol: reaction was started with orange light, *arrow*: excess amount of GTPγS was added to activate the whole G_t pool.

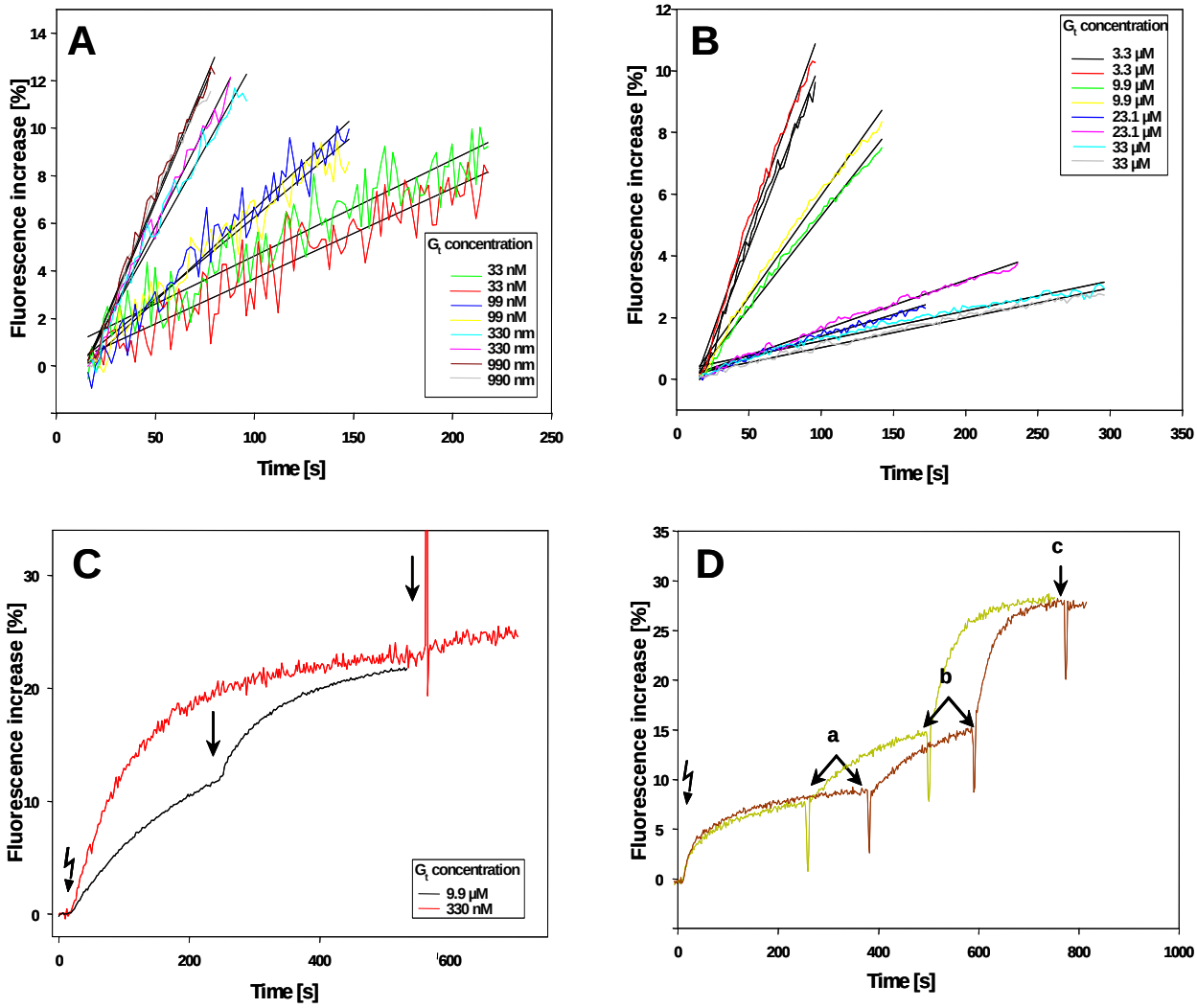

Figure 39: G_t activation assay upon binding of GTPγS at increasing G_t concentrations (2)

A and **B**: linear regression of initial slope of fluorescence increase, legend refers to G_t concentration. **C**: examples of original traces (normalized to basal fluorescence level, dilution artefacts due to addition of *wt* rhodopsin were accounted for), *flash symbol*: reaction was started with orange light, *arrows*: addition of 50 nM *wt* rhodopsin; **D**: GTPγS titration to determine G_t concentration; *flash symbol*: reaction was started with orange light, *arrows* **a**+**b**: additional GTPγS was added (**a**:100 nM, **b**: 200 nM, final concentration), *arrow* **c**: excess amount of GTPγS was added to activate the whole G_t pool.

Interactions of rhodopsin with its G protein transducin can be quantitatively described as enzyme-substrate interactions with a kinetic analysis according to Michaelis-Menten. The following assumptions have to be made to interpret the data with a Michaelis-Menten type of hyperbolic fit:

1) The catalyzed reaction has to be much faster than the reaction without catalysis ($k << k_{cat}$)
2) The enzymatic complex (R^*G_t) irreversibly leads to $G_t^*+R^*$
3) R^*, G_t and R^*G_t are in equilibrium
4) Rhodopsin as the enzyme is only present as R^* or R^*G_t

The catalytic reaction can then be described as:

$$[R^*]+[Gt] \underset{k_{-1}}{\overset{k_1}{\rightleftharpoons}} [R^*Gt] \overset{k_2}{\rightleftharpoons} [R^*]+[Gt^*]$$

The measured G_t activation rates (G_t/t) were plotted in dependence on G_t concentration and fitted with a hyberbolic function with:

$$V = \frac{k_{cat}[R^*][Gt]}{K_M + [Gt]}, \text{ with } K_M = \frac{k_2 + k_{-1}}{k_1}$$

$[G_t]$ = transducin concentration, k_{cat} = G_t/R·s and $K_M = [G_t]$ at 0.5 V_{max}, and V = reaction velocity. The fit yielded the characteristic hyperbolic curve with a positive asymptotic growth towards the maximal reaction velocity (V_{max}).

Parameters	**Value**	**standard error**
V_{max}	38	1.1
K_M	3.3	0.25

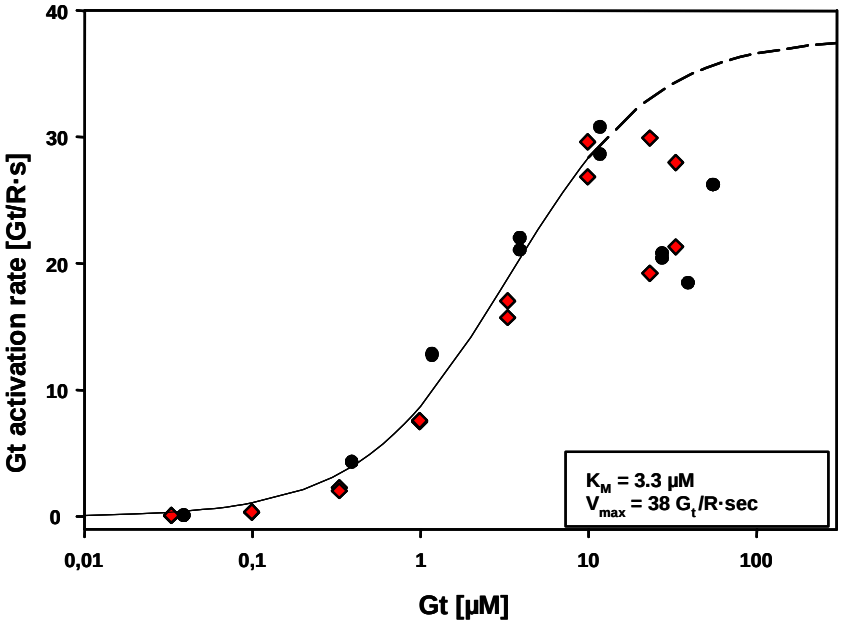

Figure 40: G_t activation rates in dependence on G_t concentration

G_t activation rates were derived from initial fluorescence slope analysis of two G_t titration data sets (Figure. 38 (*black circles*) and Figure 39 (*red squares*)).G_t activation rates were plotted in dependence of G_t concentration and analyzed with Michaelis Menten kinetics yielding a hyperbolic fit with a V_{max} of 38 G_t/R·s and a K_M of 3.3 µM.

7.3.3 Discussion

To characterize the absolute enzymatic activity, the maximal catalytic velocity of the enzyme is the adequate measure. The maximal reaction velocity of any enzyme is achieved when the substrate is present in constant, unlimited conditions and the formation of the enzyme-substrate complex merely depends on the amount of free enzyme. Therefore, the velocity of the product formation is only determined by the characteristics of the enzyme, in this case rhodopsin.

The K_M is often described as a measure of the affinity of the enzyme to its substrate. This is only correct if $k_2 << k_{-1}$, then $K_M = \frac{k_2 + k_{-1}}{k_1}$ can be simplified to $K_M = \frac{k_{-1}}{k_1}$ as the dissociation constant of the enzyme-substrate complex.

The performed Michaelis Menten fit yielded a k_{cat} of around 40 G_t/R·s and a Michaelis Menten constant K_M of 3.3 µM. To compare catalytic efficiency of different enzymes to each other, the specificity constant is often used as a parameter. The specificity constant of rhodopsin can here be calculated as $k_{cat}/K_M = 40 / 3 \cdot 10^{-6}\ M^{-1} \cdot s^{-1} = 1.3 \cdot 10^{7}\ M^{-1} \cdot s^{-1}$.The size of the specificity constant

is limited at its upper border by the diffusion of the reaction partner. The diffusion controlled limit was determined to be at around 10^8 $M^{-1}\cdot s^{-1}$ for reactions in solution. Many enzymes in nature have a specificity constant in that range (e.g. acetylcholinesterase: $1.6\cdot10^8$ $M^{-1}\cdot s^{-1}$, carboanhydrase: $8.3\cdot10^7$ $M^{-1}\cdot s^{-1}$). For enzymes with a specificity constant at the diffusion limit, the term 'catalytic perfection' is often used (Lehninger 2001). It was shown here that monomeric rhodopsin in solution works close to its theoretical, diffusional limit and can thus as well be called a perfect enzyme.

However, G_t activation rates in native rods were determined to be between 120-150 s^{-1}(Leskov, Klenchin et al. 2000) up to G_t activation rates of 600 s^{-1} (Heck and Hofmann 2001). This means that *in vivo*, rhodopsin's maximal activation velocity is 3-15 times faster than *in vitro*. It will be interesting to learn how this gain in function is achieved under physiological conditions. One possibility is that orientation of enzyme and substrate are optimized to make successful coupling quicker. Furthermore, it could also be an effect of different chemical conditions or due to changes in the quaternary structure of rhodopsin. However, it can be concluded that rhodopsin monomers are sufficient for efficiently catalyzing G protein activation.

8 CONCLUSIONS

In this thesis, several aspects concerning the quaternary structure of rhodopsin and its functional relevance were studied. In chapter 6, rhodopsin's quaternary structure was investigated *in vivo*. Upon coexpression of the fusion proteins R-venus and R-ECFP, high FRET efficiencies of 30% +/– 3% were measured in the plasma membrane portion of HEK293 cells. This shows that opsin fusion proteins are separated by a very short intermolecular distance (50-100 Å). Considering that the direct fusion protein of ECFP and venus yielded a FRET efficiency of 36%, this strongly suggests that opsin fusion proteins are overwhelmingly present as dimers/oligomers. As a control experiment, it was shown that FRET efficiency can be significantly lowered by coexpressing *wt* opsin but not by lowering the overall expression levels. This shows that FRET between R-venus/R-ECFP is not mainly a result of overexpression or due to the affinity of the fluorophores to each other. Coexpression of the β_2AR and, surprisingly, of EGFR also had the potential to reduce FRET efficiency. As a negative control, coexpression of the ion channel TRPV3 decreased FRET efficiency significantly less than *wt* opsin. The same competition assay was also used with opsin fragments to map possible opsin-opsin interaction domains. The resulting data is in good agreement with helices VI/V as dimerization interface. A possible caveat of the competition experiments is the poor control over expression levels of the competing proteins. Even though care was taken to select well expressed and transported membrane proteins, it cannot fully be ruled out that the effects of the competition experiments are partly due to different protein concentrations in the membrane. It remains to be further investigated if there are any physiological relevant, direct interactions between tyrosine kinase EGFR and class A GPCRs. It also remains to be elucidated which role the lipid environment plays for the quaternary structure of rhodopsin as it is known that the disc membranes of rods exhibit a cholesterol gradient.

Apart from FRET, BiFC was used to investigate rhodopsin's propensity to dimerize. Positive BiFC (chaper 5) was not only observed upon coexpression of complementing opsin BiFC constructs but also with several different control proteins. To summarize, it can be said that BiFC does not represent an unambiguous tool for monitoring specific interaction of membrane proteins. This might be due to the restriction of membrane proteins to 2-dimensional compartments. However, even unrelated, soluble proteins such as the MBP showed positive

BiFC with opsin. Nevertheless, BiFC could be a potentially interesting tool for shuttling proteins to different compartments of the cell as well as for coupling proteins to each other.

Much of our understanding of rhodopsin is derived from *in vitro* experiments using purified and solubilized rhodopsin samples. Therefore, in the last part of this thesis (chapter 7), rhodopsin's propensity to dimerize and its catalytic activity were studied in solubilized and purified rhodopsin samples. Using FRET, it could be shown that rhodopsin solubilized with a standard concentration of dodecyl maltoside (0.01%) is present as a monomer. Furthermore, purified membrane samples of COS-1 cells expressing R-venus/R-ECFP showed that FRET is successively lost upon addition of increasing amounts of detergent.
In a second step, rhodopsin's enzymatic capacity as a monomer was investigated. Its maximal G_t activation capacity was determined to be around 40 G_t/R·s, with a Michaelis Menten constant K_M of 3.3 µM. This means that monomeric rhodopsin is able to efficiently activate its G protein transducin. Moreover, its specificity constant of $1.3 \cdot 10^7$ $M^{-1} \cdot s^{-1}$ shows that monomeric rhodopsin works at the diffusional border. This evidence of monomeric rhodopsin as a highly efficient enzyme is in good agreement with a very recent paper published by Bayburt et al. (Bayburt 2007). The authors reconstituted rhodopsin in Nanodiscs of 10 nm diameter. The purified Nanodiscs had a stoichiometry of one or two rhodopsin per Nanodisc. In this preparation, the authors could also show that monomeric rhodopsin activates its G protein transducin.

However, it remains to be understood how and if rhodopsin's quaternary structure is of any relevance for achieving the high G_t activation rates of 120 – 600 s^{-1} (Leskov, Klenchin et al. 2000, Heck and Hofmann 2001) *in vivo*.

9 LITERATURE

Ausubel et al (1995). "3rd edition, Short protocols in molecular biology".

Bartl, F.J. et al. (2005) "Partial Agonism in a G Protein-coupled Receptor: Role of the Retinal Ring Structure in Rhodopsin Activation." J. Biol. Chem. **280**, 34259-67.

Bayburt T.H., Leitz A.J. (2007) "Transducin activation by nanoscale lipid bylayers containing one or two rhodopsins." J. Biol. Chem..[Epub ahead of print] PMID: 17395586

Beck E., Bremer E. (1980) "Nucleotide sequence of the gene ompA coding for the outer membrane protein II of Escherichia coli K-12." Nucleic Acids Res. 8:3011-3024.

Berg, O. G. and P. H. von Hippel (1985). "Diffusion-controlled macromolecular interactions." Annu Rev Biophys Biophys Chem **14**: 131-60.

Bock, R.M., Ling, N.S., Morell, S.A. & Lipton, S.H. (1956). "Ultraviolet absorption spectra of adenosine-5'-triphosphate and related 5'-ribonucleotides." Arch. Biochem. Biophys. **62**, 253-64.

Bulenger, S., S. Marullo, et al. (2005). "Emerging role of homo- and heterodimerization in G protein-coupled receptor biosynthesis and maturation." Trends Pharmacol Sci **26**(3): 131-7.

Bradford, M. M. (1976) "A Rapid and Sensitive Method for the Quantitation of Microgram Quantities of Protein Utilizing the Principle of Protein-Dye Binding." Anal. Biochem. **72**:248-254.)

Brueggemann, L.I. & Sullivan, J.M. (2002). "HEK293S cells have functional retinoid processing machinery." J. Gen. Physiol. **119**, 593-612.

Chabre, M. (1975). "X-ray diffraction studies of retinal rods. I. Structure of the disc membrane, effect of illumination." Biochim Biophys Acta **382**(3): 322-35.

Chabre, M. and A. Cavaggioni (1975). "X-ray diffraction studies of retinal rods. II. Light effect on the osmotic properties." Biochim Biophys Acta **382**(3): 336-43.

Chabre, M. and M. le Maire (2005). "Monomeric G protein-coupled receptor as a functional unit." Biochemistry **44**(27): 9395-403.

Cole, K. C., H. W. McLaughlin, et al. (2007). "Use of bimolecular fluorescence complementation to study in vivo interactions between Saccharomyces cerevisiae Cdc42p and Rdi1p." Eukaryot Cell.

Cone, R. A. (1972). "Rotational diffusion of rhodopsin in the visual receptor membrane." Nat. New Biol. **236**(63): 39-43.

Ernst, O. P., C. Bieri, et al. (2000). "Intrinsic biophysical monitors of transducin activation: fluorescence, UV-visible spectroscopy, light scattering, and evanescent field techniques." Methods in Enzymology **315**: 471-489.

Filipek, S. B., K. A. Krzysko, et al. (2004). "A concept for G protein activation by G protein-coupled receptor dimers: the transducin/rhodopsin interface." Photobiochem. Photobiol. Sci.

Fischer, O. M., S. Hart, et al. (2003). "EGFR signal transactivation in cancer cells." Biochem Soc Trans **31**(Pt 6): 1203-8.

Fotiadis, D., B. Jastrzebska, et al. (2006). "Structure of the rhodopsin dimer: a working model for G protein-coupled receptors." Curr Opin Struct Biol **16**(2): 252-9.

Fotiadis, D., B. Jastrzebska, et al. (2006). "Structure of the rhodopsin dimer: a working model for G protein-coupled receptors." Curr Opin Struct Biol.

Fotiadis, D., Y. Liang, et al. (2003). "Atomic-force microscopy: Rhodopsin dimers in native disc membranes." Nature **421**(6919): 127-8.

Franke, R.R., Sakmar, T.P., Oprian, D.D. & Khorana, H.G. (1988). "A single amino acid substitution in rhodopsin (lysine 248----leucine) prevents activation of transducin." J. Biol. Chem. **263**, 2119-22.

Fredriksson, R., M. C. Lagerstrom, et al. (2003). "The G protein-coupled receptors in the human genome form five main families. Phylogenetic analysis, paralogon groups, and fingerprints." Mol Pharmacol **63**(6): 1256-72.

Fritze, O., S. Filipek, et al. (2003). "Role of the conserved NPxxY(x)5,6F motif in the rhodopsin ground state and during activation." Proc Natl Acad Sci U S A **100**(5): 2290-2295.

Gluzman, Y. (1981). "SV40-transformed simian cells support the replication of early SV40 mutants." Cell **23**(1): 175-82.

Graham, F. L., J. Smiley, et al. (1977). "Characteristics of a human cell line transformed by DNA from human adenovirus type 5." J Gen Virol **36**(1): 59-74.

Griffin, T. A., D. Nandi, et al. (1998). "Immunoproteasome assembly: cooperative incorporation of interferon gamma (IFN-gamma)-inducible subunits." J Exp Med **187**(1): 97-104.

Hague, C., M. A. Uberti, et al. (2004). "Cell surface expression of alpha1D-adrenergic receptors is controlled by heterodimerization with alpha1B-adrenergic receptors." J Biol Chem **279**(15): 15541-9.

Han, M. and T. P. Sakmar (2000). "Assays for activation of recombinant expressed opsins by all-trans-retinals." Methods in Enzymology **315**: 251-267.

Hargrave, P. A., H. E. Hamm, et al. (1993). "Interaction of rhodopsin with the G protein, transducin." Bioessays **15**(1): 43-50.

Hebert, T. E., C. Gales, et al. (2006). "Detecting and imaging protein-protein interactions during G protein-mediated signal transduction in vivo and in situ by using fluorescence-based techniques." Cell Biochem Biophys **45**(1): 85-109.

Heck, M. and K. P. Hofmann (1993). "G protein-effector coupling: a real-time light-scattering assay for transducin-phosphodiesterase interaction." Biochemistry **32**(32): 8220-8227.

Heck, M. and K. P. Hofmann (2001). "Maximal rate and nucleotide dependence of rhodopsin catalyzed transducin activation: Initial rate analysis based on a double displacement mechanism." Journal of Biological Chemistry **276**(13): 10000-10009.

Hellwig N, Albrecht N, Harteneck C, Schultz G, Schaefer M. (2005). "Homo- and heteromeric assembly of TRPV channel subunits. " J Cell Sci.118(Pt 5):917-28.

Herrmann, R., M. Heck, et al. (2004). "Sequence of interactions in receptor-G protein coupling." J Biol Chem **279**: 24283-24290.

Higashijima, T., K. Ferguson, et al. (1987). "The effect of GTP and Mg2+ on the GTPase activity and the fluorescent properties of Go." J. Biol. Chem. **262**(2): 757-761.

Hofmann, K. P. (1993). Rhodopsin/G protein interaction. GTPases in Biology. B. Dickey and L. Birnbaumer. Berlin, Springer. **108/II:** 267-290.

Hu, C. D., Y. Chinenov, et al. (2002). "Visualization of interactions among bZIP and Rel family proteins in living cells using bimolecular fluorescence complementation." Mol Cell **9**(4): 789-98.

Hu, C. D. and T. K. Kerppola (2003). "Simultaneous visualization of multiple protein interactions in living cells using multicolor fluorescence complementation analysis." Nat Biotechnol **21**(5): 539-45.

Hynes, T. R., L. Tang, et al. (2004). "Visualization of G protein betagamma dimers using bimolecular fluorescence complementation demonstrates roles for both beta and gamma in subcellular targeting." J Biol Chem **279**(29): 30279-86.

Jacoby, E., R. Bouhelal, et al. (2006). "The 7 TM G protein-coupled receptor target family." ChemMedChem **1**(8): 761-82.

Jastrzebska, B., D. Fotiadis, et al. (2006). "Functional and structural characterization of rhodopsin oligomers." J Biol Chem.

Jastrzebska, B., T. Maeda, et al. (2004). "Functional characterization of rhodopsin monomers and dimers in detergents." J Biol Chem **279**: 54663-54675.

Kerppola, T.K. (2006). "Visualization of molecular interactions by fluorescence complementation." Nat. Methods 3(12):969-71.

Kobilka B.K. et al. (1987) "cDNA for the human beta 2-adrenergic receptor: a protein with multiple membrane-spanning domains and encoded by a gene whose chromosomal location is shared with that of the receptor for platelet-derived growth factor." Pro. Natl. Acad. Sci. U.S.A. 84:46-50.

Kota, P., P. J. Reeves, et al. (2006). "Opsin is present as dimers in COS1 cells: Identification of amino acids at the dimeric interface." Proc Natl Acad Sci U S A.

Kropf, A., B. P. Whittenberger, et al. (1973). "The spectral properties of some visual pigment analogs." Experimental Eye Research **17**(6): 591-606.

Kühn, H. (1982). "Light-regulated binding of proteins to photoreceptor membranes and its use for the purification of several rod cell proteins." Methods in Enzymology **81**: 556-564.

Lambright, D. G., J. Sondek, et al. (1996). "The 2.0 A crystal structure of a heterotrimeric G protein." Nature **379**(6563): 311-9.

Lee, S.P. et al. (2004) "Dopamine D1 and D2 receptor co-activation generates a novel phospholipase C-mediated calcium signal." J. Biol. Chem. 279, 35671–3567

Leskov, I. B., V. A. Klenchin, et al. (2000). "The gain of rod phototransduction: reconciliation of biochemical and electrophysiological measurements." Neuron **27**(3): 525-537.

Liang, Y., D. Fotiadis, et al. (2003). "Organization of the G Protein-coupled Receptors Rhodopsin and Opsin in Native Membranes." J. Biol. Chem. **278**: 21655-21662.

Lin C.R. et al. (1984) "Expression cloning of human EGF receptor complementary DNA: gene amplification and three related messenger RNA products in A431 cells." Science 224:843-848

Mansoor, S. E., K. Palczewski, et al. (2006). "Rhodopsin self-associates in asolectin liposomes 10.1073/pnas.0511010103." PNAS.

Marshall, F. H., J. White, et al. (1999). "GABA(B) receptors function as heterodimers." Biochem Soc Trans **27**(4): 530-5.

McCutchan, J. H. and J. S. Pagano (1968). "Enchancement of the infectivity of simian virus 40 deoxyribonucleic acid with diethylaminoethyl-dextran." J Natl Cancer Inst **41**(2): 351-7.

Medina, R., D. Perdomo, et al. (2004). "The Hydrodynamic Properties of Dark- and Light-activated States of n-Dodecyl {beta}-D-Maltoside-solubilized Bovine Rhodopsin Support the Dimeric Structure of Both Conformations." J. Biol. Chem. **279**(38): 39565-39573.

Milligan, G. (2006). "G protein-coupled receptor heterodimers: pharmacology, function and relevance to drug discovery." Drug Discov Today **11**(11-12): 541-9.

Milligan, G. and E. Kostenis (2006). "Heterotrimeric G proteins: a short history." Br J Pharmacol **147 Suppl 1**: S46-55.

Milligan, G., D. Ramsay, et al. (2003). "GPCR dimerisation." Life Sci **74**(2-3): 181-8.

Nagai, T., K. Ibata, et al. (2002). "A variant of yellow fluorescent protein with fast and efficient maturation for cell-biological applications." Nat Biotechnol **20**(1): 87-90.

Nelson, D., M. Cox (2001). "Lehninger Biochemie." Springer Verlag, Berlin Heidelberg New York

Oprian, D. D., R. S. Molday, et al. (1987). "Expression of a synthetic bovine rhodopsin gene in monkey kidney cells." Proceedings of the National Academy of Sciences of the United States of America **84**(24): 8874-8878.

Oprian, D.D. (1993). in Methods in Neurosciences, Vol. 15, Photoreceptor cells (ed. Hargrave, P.A.) pp. 301-306 (Academic Press, Inc., San Diego).

Palczweski, K. (2006). "G protein-coupled receptor rhodopsin" Annu Rev Biochem **75**:743-67.

Palczewski, K., T. Kumasaka, et al. (2000). "Crystal structure of rhodopsin: A G protein-coupled receptor." Science **289**(5480): 739-745.

Papermaster, D. S. (1982). "Preparation of retinal rod outer segments." Methods in Enzymology **81**: 48-52.

Park, P. S.-H. and K. Palczewski (2005). "Diversifying the repertoire of G protein-coupled receptors through oligomerization." PNAS **102**(25): 8793-8794.

Peier A.M. et al. (2002) "A heat-sensitive TRP channel expressed in keratinocytes." Science 296:2046-2049.

Phillips, W. J. and R. A. Cerione (1988). "The intrinsic fluorescence of the alpha subunit of transducin. Measurement of receptor-dependent guanine nucleotide exchange." Journal of Biological Chemistry **263**(30): 15498-15505.

Poo, M. and R. A. Cone (1974). "Lateral diffusion of rhodopsin in the photoreceptor membrane." Nature **247**(441): 438-441.

Quiocho, F. A. et al. (1997). "Extensive features of tight oligosaccharide binding revealed in high-resolution structure of the maltodextrin transport/chemosensory receptor." Structure 5(8):997-1015

Rajan, R.S. & Kopito, R.R. (2005). "Suppression of wild-type rhodopsin maturation by mutants linked to autosomal dominant retinitis pigmentosa." J. Biol. Chem. **280**, 1284-91.

Rosevear, P., T. VanAken, et al. (1980). "Alkyl glycoside detergents: a simpler synthesis and their effects on kinetic and physical properties of cytochrome c oxidase." Biochemistry **19**(17): 4108-15.

Salom, D., D. T. Lodowski, et al. (2006). "Crystal structure of a photoactivated deprotonated intermediate of rhodopsin." Proc Natl Acad Sci U S A **103**(44): 16123-8.

Schioth, H. B. and R. Fredriksson (2005). "The GRAFS classification system of G protein coupled receptors in comparative perspective." Gen Comp Endocrinol **142**(1-2): 94-101.

Siegel, R. M., F. K. Chan, et al. (2000). "Measurement of molecular interactions in living cells by fluorescence resonance energy transfer between variants of the green fluorescent protein." Sci STKE **2000**(38): PL1.

Sondek, J., A. Bohm, et al. (1996). "Crystal structure of a G protein beta gamma dimer at 2.1A resolution." Nature **379**(6563): 369-74.

Struthers, M., H. Yu, et al. (1999). "Tertiary interactions between the fifth and sixth transmembrane segments of rhodopsin." Biochemistry **38**(20): 6597-603.

Thomas, S. M., N. E. Bhola, et al. (2006). "Cross-talk between G protein-coupled receptor and epidermal growth factor receptor signaling pathways contributes to growth and invasion of head and neck squamous cell carcinoma." Cancer Res **66**(24): 11831-9.

Tramier, M., Piolot, T. et al. (2003). "Homo-FRET versus hetero-FRET to probe homodimers in living cells. " Methods Enzymol. 360:580-97.

Walter, M., C. Chaban, et al. (2004). "Visualization of protein interactions in living plant cells using bimolecular fluorescence complementation." Plant J **40**(3): 428-38.

Wang, Y. and K. S. Kim (2002). "Role of OmpA and IbeB in Escherichia coli K1 invasion of brain microvascular endothelial cells in vitro and in vivo." Pediatr Res **51**(5): 559-63.

Xie, G., A. K. Gross, et al. (2003). "An opsin mutant with increased thermal stability." Biochemistry **42**(7): 1995-2001.

Xu, H., I. S. Ramsey, et al. (2002). "TRPV3 is a calcium-permeable temperature-sensitive cation channel." Nature **418**(6894): 181-6.

Yu, H. and D. D. Oprian (1999). "Tertiary interactions between transmembrane segments 3 and 5 near the cytoplasmic side of rhodopsin." Biochemistry **38**(37): 12033-40.

Zhang, Y., M. E. Devries, et al. (2006). "Structure modeling of all identified G protein-coupled receptors in the human genome." PLoS Comput Biol **2**(2): e13.

ACKNOWLEDGEMENTS

I would like to thank Prof. Dr. K. P. Hofmann and PD Dr. O. Ernst for giving me the possibility to realize my medical thesis in their laboratory. I am very grateful for their support, their ideas and their knowledgeable discussions about rhodopsin that greatly brought forward my thesis and my understanding about rhodopsin and science in general.

I would further like to thank Dr. Martin Heck for numerous and greatly helpful pieces of advice, and the productive discussions about kinetics of G protein/rhodopsin interaction for chapter 9. I also would like to thank Prof. Dr. Michael Schäfer and Philipp Voigt (Institut für klinische Pharmakologie, FU) for the possibility of using the confocal microscope and FRET equipment, for providing me with some of the DNA of the control constructs of chapter 8, their help with realizing my experiments and the productive discussion of my FRET data.

I especially like to thank Helena Seibel, Christine Koch, Jana Engelmann, Ingrid Semjonow, Anja Koch, and Katja Engel for their help with DNA, rhodopsin and G protein preparations and their generous and friendly support throughout my thesis work.

I also especially like to thank Dr. Olaf Fritze for sharing his expertise on rhodopsin work and computers and Bernhard Knierim for helpful discussions and comments when editing my thesis. Furthermore, I'd like to thank all employees of the IMPB, especially Dr. Eglof Ritter, Dr. Petra Henklein, Kerstin Zimmermann, Katja Waterstradt, Sebastian Rausch, Andreas von Usedom, Dr. Alexander Pulvermüller and PD Dr. Franz Bartl for sharing their knowledge, a nice and cooperative lab atmosphere and general support. I'd like to thank Carola Mascow, Renate Raddatz, Martina Wittling and Magrit Neumann for their help with bureaucratic procedures. Further thanks go to the DFG and the Graduiertenkolleg 'Signal recognition and transduction' for financial support. I also like to thank my thesis' reviewers.

Finally, I would also like to thank my boyfriend Ewout van Ginneken, my parents, my brothers and my friends for their caring support throughout my thesis work.

„Mein Lebenslauf wird aus Datenschutzgründen in der elektronischen Version meiner Arbeit nicht mit veröffentlicht.“

EIDESSTAATLICHE ERKLÄRUNG

Ich, Verena Gramse, erkläre, dass ich die vorgelegte Dissertationsschrift mit dem Thema ‚The quaternary structure of rhodopsin and its implications for rhodopsin function.' selbst verfasst und keine anderen als die angegebenen Quellen und Hilfsmittel benutzt, ohne die (unzulässige) Hilfe Dritter verfasst und auch in Teilen keine Kopien anderer Arbeiten dargestellt habe.

Berlin, den 30.4.2007